Spherical Aromaticity: Recent Work on Fullerenes, Polyhedral Boranes, and Related Structures†

Zhongfang Chen* and R. Bruce King

Department of Chemistry and Center for Computational Chemistry, University of Georgia, Athens, Georgia 30602-2525

Contents

1. Introduction

Aromaticity,[1] one of the most important concepts in chemistry, is confined not only to planar two-dimensional (2D) molecules but also can be extended to diverse structures of other types. Thus, aromatic systems include not only benzenoid hydrocarbons with $4N + 2$ π-electrons but also fully conjugated heterocycles,[2] [*n*]trannulenes,[3] pericyclic transition states,[4] Möbius cycles,[5] and triplet annulenes[6] with $4N$ π-electrons as well as metallacycles,[7] three-dimensional (3D) transition metal (half-) sandwiches such as ferrocenes,[8] and even the carbon free sandwich complex $[(P_5)_2Ti]^{2-}$,[9] and some 3D and planar boron-based clusters.[10] Various metal clusters have also been considered to be aromatic,[11] such as Hg_4^{6-} found in amalgams used since ancient times,[12] $Ga_3R_3^{2-}$,[13] and Al_4Li^-.[14] Some systems without π-electrons such as hydrogen clusters,[15] the planar bimetallic cluster Au_5Zn^+,[16] and the tetrahedral gold cluster Au_{20}[17] are also considered to be aromatic. The claimed antiaromatic $Al_4Li_3^-$ has also been produced in gas phase,[18] although its aromatic nature is still in debate.[19] Surely, we should not miss fullerenes[20] and carbon nanotubes.[21]

The recognition of aromaticity in three dimensions goes back more than 40 years. Thus, in 1959, Lipscomb[22] proposed the term "superaromaticity" to explain the 3D aromaticity of $B_{12}H_{12}^{2-}$. Yoneda[23] used this term in 1977 in a short review article in Japanese. According to this article, the Second International Symposium of Nonbenzenoid Aromatics (ISNA-II) was held at Lindau in 1974. In the concluding remarks of this symposium, Prof. R. Breslow stressed the importance of the extensive study of 3D aromaticity (no references were cited). An explicit suggestion of 3D aromaticity in deltahedral boranes was made by Aihara[24] in 1978, who used a graph-

Zhongfang Chen was born in Liaoyang, P. R. China, in 1971. He earned his B. Sc. (organic chemistry, in 1994), M. Sc. (physical chemistry, with Xuezhuang Zhao, in 1997), and Ph. D. (physical chemistry, with Xuezhuang Zhao and Auchin Tang, in 2000) at Nankai University, Tianjin, P. R. China. In late 1999, he began to work in Germany with Andreas Hirsch (Universität Erlangen-Nürnberg) and Walter Thiel (Max-Planck-Institut für Kohlenforschung in Mülheim/Ruhr) as a postdoc, under the support of Alexander von Humboldt foundation and Max-Planck society. He joined Paul v. R. Schleyer's group in late 2002, but physically remained in Erlangen until his move to the University of Georgia (Athens, GA) in October of 2003. His early research was on the synthesis of fullerenes and their derivatives. Tempted by the charm of modern computational chemistry, in 1997, he switched to apply these powerful tools to characterize the experimentally synthesized structures, to design new materials with novel chemical bonding and potential applications, and to investigate rules and trends in chemistry. His main research areas are fullerenes, nanotubes, aromaticity of spherical molecules and clusters, and molecules with novel chemical bonding. He enjoys his extensive collaborations with peer experimentalists and theoreticians. So far, he has given over 30 lectures and has around 70 publications.

R. Bruce King was born in Rochester, New Hampshire, in 1938, attended Oberlin College (B. A. 1957), and was an NSF Predoctoral Fellow with Prof. F. G. A. Stone at Harvard University (Ph.D. 1961). After a year at du Pont and 4.5 years at the Mellon Institute, he joined the faculty of the University of Georgia where he is now Regents' Professor of Chemistry. His research interests have ranged from synthetic organometallic and organophosphorus chemistry to applications of topology and graph theory in inorganic chemistry. He is currently involved in a collaborative research project on aromaticity with colleagues at both the University of Georgia and the Babeş-Bolyai University in Romania. Prof. King was the American Regional Editor of the *Journal of Organometallic Chemistry* from 1981 to 1998. He is also Editor-in-Chief of the *Encyclopedia of Inorganic Chemistry* first published in 1994, with a new edition currently in press. He is the recipient of American Chemical Society Awards in Pure Chemistry (1971) and Inorganic Chemistry (1991). During the past 15 years, he has authored books entitled *Applications of Graph Theory and Topology in Inorganic Cluster and Coordination Chemistry* (1993), *Inorganic Main Group Element Chemistry* (1994), and *Beyond the Quartic Equation* (1996). Prof. King's hobbies include contract bridge, music, and travel; he has attained the status of Life Master with the American Contract Bridge League.

theoretical method to find significant positive resonance energies for deltahedral $B_nH_n^{2-}$ ($6 \leq n \leq 12$) with the experimentally stable $B_{12}H_{12}^{2-}$ having the highest resonance energy.

Aromaticity can be characterized by abnormal stability, reactivity, and structural and magnetic properties. However, it is impossible to obtain anything experimentally similar to a resonance energy for a fullerene. Furthermore, reactivity criteria cannot be used for fullerenes, since there are no external hydrogens to substitute. The structure index is also not applicable. For example, B3LYP and CCSD(T) computations show that the ground state of the well-known "magic" Si_6 cluster does not adopt the distorted octahedron of D_{4h} symmetry, as formerly established by second-order Møller–Plesset perturbation theory. Instead, two almost isoenergetic structures of lower symmetry are preferred for Si_6 (Figure 1).[25] Thus, using the lowest energy structure to judge its aromaticity, Si_6 should be put into the antiaromatic category solely based on its distorted structure, which is in contrast to chemical intuition.

Among the magnetic criteria, the nucleus-independent chemical shift (NICS) introduced by Schleyer and co-workers[26,27] has proven to be a simple and efficient aromaticity probe. NICS indices correspond to the negative value of the magnetic shielding computed at chosen points in the vicinity of molecules. These are typically computed at ring centers (nonweighted mean of the heavy atoms), at

points above, and even as grids in and around the molecule. Significantly negative (i.e., magnetically shielded) NICS values in interior positions of rings or cages indicate the presence of induced diatropic ring currents or "aromaticity," whereas positive values (i.e., deshielded) at each points denote paratropic ring currents and "antiaromaticity". In fullerenes, the NICS values can be assessed experimentally by the equivalent endohedral ^{3}He chemical shifts in fullerenes and their derivatives[28] and can be computed easily using modern quantum chemical methods.[29] For example, Si_6 is characterized as aromatic regardless of the distorted structures as indicated by the diatropic NICS values (represented by the red dots) in the center of the Si_6 cage (red circles in Figure 1).
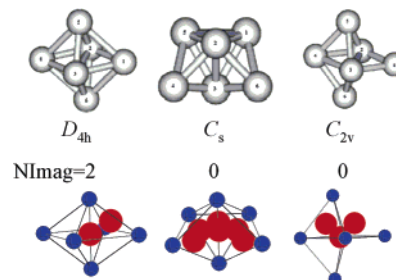

Figure 1. Optimized structures and NICS grid plots for Si_6. The red dots denote negative NICS values (aromaticity). Reprinted with permission from ref 25 (http://link.aps.org/abstract/PRA/v64/p23202). Copyright 2001 APS.

The aromaticity or antiaromaticity of 2D annulenes and heteroannulenes obeys the well-known Hückel rule.[30] Because of their closed valence shell structures, annulenes having $4N + 2$ π-electrons tend to exhibit high stability and symmetrical planar structures with strong diamagnetic ring currents, while singlet annulenes with $4N$ π-electrons exhibit distorted structures and high reactivity, low stability, and very pronounced paratropic character. However, the Hückel rule cannot be used for spherical systems such as fullerenes.

In the previous thematic issue of *Chemical Reviews*, Bühl and Hirsch[31] comprehensively reviewed the spherical aromaticity of fullerenes. The subsequent 4 years have seen rapid development in this area. More importantly, the spherical aromaticity concept[32] has been extended to inorganic cages, homoaromatic systems, and 3D σ-systems and has been employed successfully to design novel materials such as spherical homoaromatic Si_8^{2-} (T_d) and Ge_8^{2-} (T_d) (see section 5). This review summarizes the most significant progress in this area in recent years, particularly the last 4 years since publication of the thematic issue.

2. Chemical Bonding Models for Fullerenes, Polyhedral Boranes, and Related Polyhedral Molecules

2.1. Sphericity of Fullerenes

The well-known resemblance of the famous fullerene C_{60} to a soccer ball and thus to a sphere suggests the approximation of the molecular orbitals (MOs) of fullerenes using spherical harmonics, which are familiar to chemists as generating the angular components of atomic orbitals (AOs) of various types. This connection between chemical bonding in approximately spherical molecules and atomic structure theory has been recently discussed by Reiher and Hirsch in great detail.[33] This is also related to the analogy noted by Aihara and co-workers between the π-MOs in fullerenes and the free electron model.[34]

The spherical harmonic wave functions, Ψ, used in this approach, arise from solution of the following second-order differential equation in which the potential energy V is spherically symmetric:[35]

$$\frac{\partial^2 \Psi}{\partial x^2} + \frac{\partial^2 \Psi}{\partial y^2} + \frac{\partial^2 \Psi}{\partial z^2} + \frac{8\pi^2 m}{h^2}(E - V)\Psi =$$

$$\nabla^2 \Psi + \frac{8\pi^2 m}{h^2}(E - V)\Psi = 0 \quad (1)$$

These wave functions may be factored into the product:

$$\Psi(r,\theta,\phi) = R(r) \cdot \Theta(\theta) \cdot \Phi(\phi) \quad (2)$$

in which the factors R, Θ, and Φ are functions solely of r, θ, and ϕ, respectively, which are related to the Cartesian coordinates x, y, and z by the following equations:

$$x = r \sin\theta \cos\phi \quad (3a)$$

$$y = r \sin\theta \sin\phi \quad (3b)$$

$$z = r \cos\theta \quad (3c)$$

Because the value of the radial component $R(r)$ of Ψ is completely independent of the angular coordinates θ and ϕ, it is independent of direction (i.e., isotropic) and therefore remains unaltered by any symmetry operations. For this reason, all of the symmetry properties of a spherical harmonic Ψ are contained in its angular component $\Theta(\theta) \cdot \Phi(\phi)$, which is defined by the scalar spherical harmonics $Y_{LM}(\theta,\phi)$, i.e.,

$$\Theta(\theta) \cdot \Phi(\phi) = Y_{LM}(\theta,\phi) \quad (4)$$

Each of the three factors of Ψ (eq 2) generates a quantum number. Thus, the factors $R(r)$, $\Theta(\theta)$, and $\Phi(\phi)$ generate the quantum numbers N, L, and M, respectively, where capital letters are used to differentiate the spherical harmonic designations of MOs from the commonly used spherical harmonic designations of AOs. The principal quantum number N, derived from the radial component $R(r)$, relates to the distance from the center of the sphere. The azimuthal quantum number L, derived from the factor $\Theta(\theta)$ in eq 2, relates to the number of nodes in the angular component $\Theta(\theta) \cdot \Phi(\phi)$. In this connection, a node is a plane corresponding to a zero value of $\Theta(\theta) \cdot \Phi(\phi)$ or Ψ, i.e., where the sign of $\Theta(\theta) \cdot \Phi(\phi)$ changes from positive to negative MOs of spherical molecules. Orbitals where $L = 0, 1, 2, 3, 4, 5$, etc., are conventionally designated as S, P, D, F, G, H, etc., orbitals, respectively, by analogy with standard
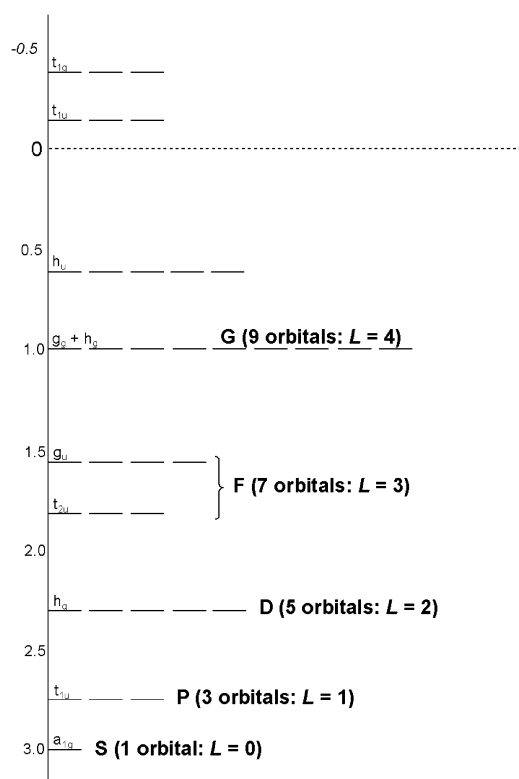

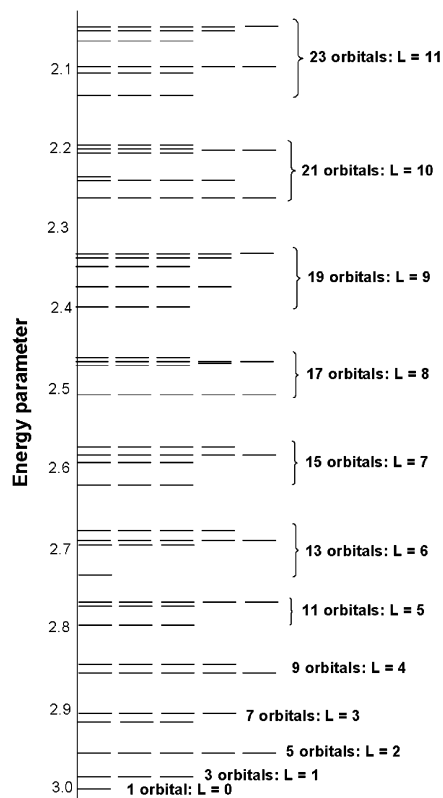**Figure 2.** Spherical harmonics of C_{60} (I_h).

Figure 3. Lowest lying MOs of C_{960} (I_h).

designations of AOs and their quantum numbers. For a given value of the azimuthal quantum number L, the magnetic quantum number M, derived from the factor $\Phi(\phi)$ in eq 2, indicates the tilt of the plane of orbital motion with respect to some reference direction[36] (typically the z-axis). The quantum number M may take on all $2L + 1$ different values from $+L$ to $-L$. There are therefore necessarily $2L + 1$ distinct orthogonal orbitals for a given value of l corresponding to 1, 3, 5, 7, 9, 11,... distinct S, P, D, F, G, H,... orbitals, respectively. Thus, a set of MO energy parameters satisfactorily approximated by spherical harmonics is partitioned into relatively closely spaced groups of 1, 3, 5, 7, 9, etc. MOs starting with the MO of lowest energy. Note that filling these spherical harmonic MOs with electron pairs starting from the low energy S orbital and ending with a filled grouping at $L_{max} = N$ leads to $2(N + 1)^2$ skeletal bonding electrons as found in a number of molecules exhibiting spherical aromaticity discussed later in this review.

The partitioning of fullerene MOs according to spherical harmonics is illustrated in Figure 2 for C_{60}. This spherical harmonic approximation is most closely followed for the MOs of lowest energy, namely, the most strongly bonding MOs. For C_{60}, clear groupings of 1, 3, 5, 7, and 9 MOs are observed corresponding to the S, P, D, F, and G MOs.

The spherical harmonic pattern for fullerene MOs is most dramatically illustrated in the extended Hückel calculations of Tang, Huang, Li, and Liu[37] for icosahedral (I_h) fullerenes in the homologous series C_{60n^2}, of which C_{60} (i.e., $n = 1$) is the first member. In this connection, Figure 3 shows the lowest lying MOs for the fourth member of this series, namely, C_{960} (i.e., C_{60n^2} for $n = 4$).[38] Here, all of the groupings of $2L + 1$ MOs can be seen up to the 23-orbital grouping for $L = 11$ (i.e., the N orbitals in the S, P, D, F, G,... designation scheme).

The need for spherical harmonics to approximate fullerene MOs makes of interest methods for visualizing the spherical harmonics of higher L values than those of interest for AOs. The shapes of the s, p, and d orbitals ($l = 0$, 1, and 2, respectively) are well-known to chemists, and those of the f orbitals ($l = 3$) are readily available in relevant books and articles. However, AOs for $l \geq 4$ (i.e., g orbitals and beyond) are irrelevant to chemistry because the Periodic Table runs out of elements before such orbitals are needed to describe chemistry. This is not the case with the spherical harmonic description of the MOs of fullerenes and other spherical molecules where MOs approximated by $L \geq 4$ may be needed. In this connection, an orbital graph[39] is useful for describing the pattern of the lobes of MOs approximated by spherical harmonics for any value of L. In such an orbital graph, the vertices correspond to the lobes of the AOs and the edges to nodes between adjacent lobes of opposite sign. An orbital graph is necessarily a signed bipartite graph in which each vertex is labeled with the sign of the corresponding lobe and only vertices of opposite sign can be connected by an edge. Bipartite graphs are recognized by organic chemists as alternant graphs in which the starred vertices correspond to the plus vertices of the orbital graphs and the unstarred vertices to the minus vertices (or vice versa, of course).

Figure 4 depicts the orbital graphs for the five types of the standard set of nine G orbitals with different absolute values for the quantum number M.
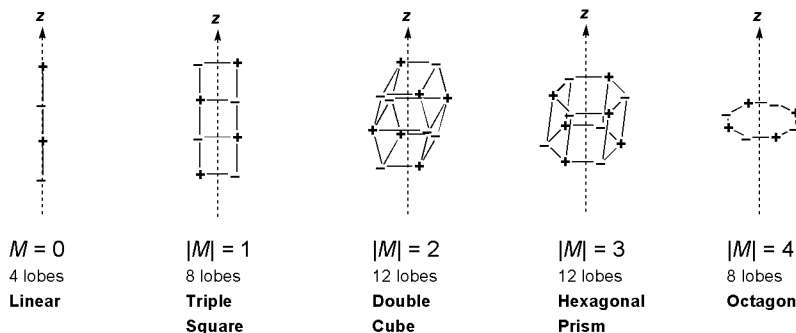

Figure 4. Orbital graphs for the five types of the standard set of nine G orbitals with different absolute values for the quantum number M.

The orbital graphs for MOs with even higher L values (e.g., the H orbitals and beyond) follow a similar pattern.

2.2. Spherical Harmonics in Boranes

The most stable boranes are those with the stoichiometry $B_nH_n^{2-}$ ($6 \leq n \leq 12$) and the isoelectronic carboranes $CB_{n-1}H_n^-$ and $C_2B_{n-2}H_n$. The structures of these boranes are based on the "most spherical" deltahedra (Figure 5) in which all faces are triangles and all vertices have degrees 4 or 5 except for the topologically required single degree 6 vertex in the 11 vertex deltahedron. In this connection, the degree of a vertex is the number of edges meeting at a vertex.

Even though the borane deltahedra have far fewer vertices than the fullerene polyhedra, their MOs, like those of fullerenes, can be approximated by spherical harmonics. This is the basis for the tensor surface harmonic (TSH) theory developed by Stone and Alderton,[40−43] in 1980 thereby predating the discovery of fullerenes by several years. The motivation for this work was to understand the chemical bonding in boranes and metal clusters. In TSH theory, the borane (or metal cluster) deltahedron is treated as an assembly of atoms with nuclei arranged on the surface of a single sphere with the atom positions described by the standard angular coordinates θ and ϕ related to latitude and longitude. The wave functions for such a system are then obtained by treating the magnitude of the spherical harmonic function at an atom site as the coefficient in an LCAO MO. This considers the actual structure of the borane deltahedron in a perfectly general way except that variations in radial position are ignored. The orbitals constructed by this procedure are assumed to retain approximately the symmetry characteristics of the spherical harmonics from which they are derived. Thus, there is assumed to be no mixing between orbitals that differ in the quantum numbers L and/
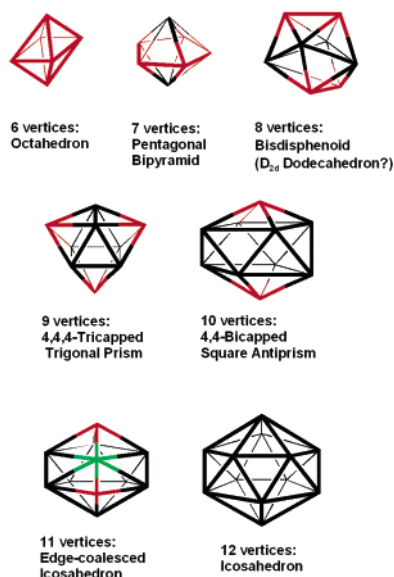
Figure 5. "Most spherical" deltahedra. Vertices of degrees 4, 5, and 6 are indicted in red, black, and green, respectively.
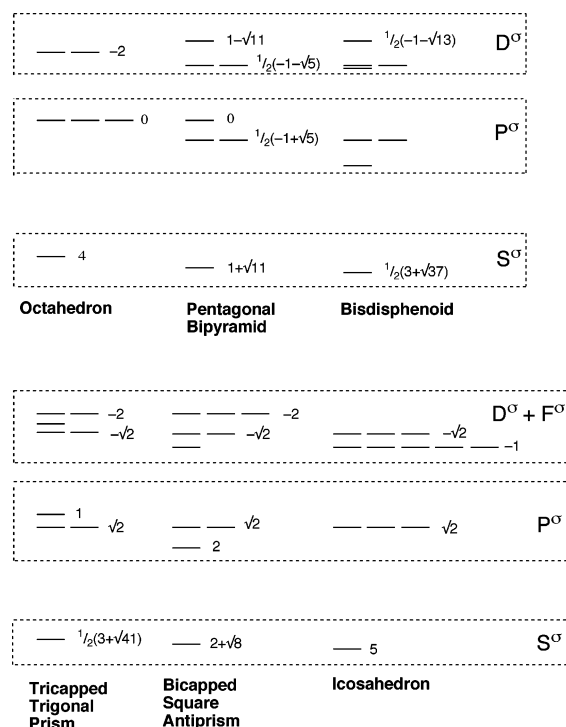
Figure 6. Skeletal bonding orbitals of six of the deltahedra in Figure 5 as the scalar spherical harmonics, S^σ, P^σ, D^σ, and F^σ.

or M and that a set of orbitals with a given L share the same energy. This leads to a classification of the MOs of the deltahedral boranes and their energies in terms of their L quantum numbers, designated by the capital letters S, P, D, F, ..., etc., similar to those used for the fullerenes discussed above. Because of the resulting $(2L + 1)$-fold degeneracy in this approximation, this simplifies matters considerably.

The four AOs on each of the vertex atoms in the deltahedral boranes $B_nH_n^{2-}$ ($6 \leq n \leq 12$) can be partitioned as follows: (i) An external orbital oriented toward the external hydrogen atom or related monovalent group (nominally an sp hybrid); (ii) a radial orbital pointing toward the center of the deltahedron (the other sp hybrid); and (iii) two equivalent orthogonal tangential orbitals tangent to the surface of the deltahedron (the remaining two p orbitals).

Multicenter overlap of the radial orbitals at the center of a deltahedron having n vertices leads in TSH theory to core bonding and antibonding MOs described by the scalar spherical harmonics $\Theta(\theta) \cdot \Phi(\phi) = Y_{LM}(\theta)(\phi)$. Such orbitals correspond successively to a single anodal S^σ orbital (Y_{00}), the three uninodal P^σ orbitals (Y_{10}, Y_{11c}, and Y_{11s}), the five binodal D^σ orbitals (Y_{20}, Y_{21c}, Y_{21s}, Y_{22c}, and Y_{22s}), the seven trinodal F^σ orbitals (Y_{30}, Y_{31c}, Y_{31s}, Y_{32c}, Y_{32s}, Y_{33c}, and Y_{33s}), etc. of increasing energy. The energy levels of these orbitals for the skeletal bonding in the seven deltahedra (Figure 5) are depicted in Figure 6 with their S, P, D, and F labels. In the deltahedra found in boranes, the S^σ and P^σ MOs appear in well-separated groups whereas the clearly antibonding D^σ and F^σ MOs are not as clearly separated.

The π-type tangential orbitals lead to surface bonding described by the vector surface harmonics. Two vector surface harmonic functions can be gener-

ated from each $Y_{LM} (\theta,\phi)$ as follows:

$$V_{LM} = \nabla Y_{LM} \tag{5a}$$

$$\bar{V}_{LM} = \mathbf{r} \times \nabla Y_{LM} \tag{5b}$$

In eq 5a,b, ∇ is the following vector operator:

$$\nabla = \left(\frac{\partial}{\partial\theta}, \frac{1}{\sin\theta}\frac{\partial}{\partial\phi}\right) \tag{6}$$

In addition, $\times$ is the vector cross-product, the $\bar{V}_{LM}$ of eq 5b is the parity inverse of the V_{LM} of eq 5a, corresponding to a rotation of each atomic π-function by 90° about the radial vector $\mathbf{r}$. This 90° rotation corresponds to the geometrical relationship between the two twin tangential orbitals on a given vertex atom. The V_{LM} and $\bar{V}_{LM}$ correspond to the equal numbers of bonding and antibonding surface orbitals in a globally delocalized deltahedral cluster leading to three P^π, five D^π, seven F^π, etc. bonding/antibonding orbital pairs of increasing energy and nodality. Because Y_{00} is a constant, $\nabla Y_{00} = 0$ so that there are no S^π or $\bar{S}^\pi$ orbitals.

The core and surface orbitals defined above by TSH theory can be related to the skeletal bonding in deltahedral boranes as follows: (i) the lowest energy fully symmetric core orbital (A_{1g}, A_g, A_1, or A_1' depending upon the point group of the deltahedron) corresponds to the S^σ orbital in TSH theory. Because there are no S^π or $\bar{S}^\pi$ surface orbitals, this lowest energy core orbital cannot mix with any surface orbitals, so that it cannot become antibonding through core−surface mixing. (ii) The three core orbitals of next lowest energy correspond to P^σ orbitals in TSH theory. These orbitals can mix with the P^π surface orbitals so that the P^σ core orbitals become antibonding with corresponding lowering of the bonding energies of the P^π surface orbitals below the energies of the other surface orbitals.

2.3. Duality of Fullerenes and Deltahedral Boranes

Fullerene polyhedra and borane deltahedra have an interesting dual relationship. In this connection, a given polyhedron P can be converted into its dual P* by locating the centers of the faces of P* at the vertices of P and the vertices of P* above the centers of the faces of P. Two vertices in the dual P* are connected by an edge when the corresponding faces in P share an edge. An example of the process of dualization is the conversion of a cube to a regular octahedron (Figure 7).

The process of dualization has the following properties as illustrated by the octahedron/cube dual pair: (i) The numbers of vertices and edges in a pair of dual polyhedra P and P* satisfy the relationships $v* = f$, $e* = e$, and $f* = v$. Thus, for the cube/octahedron dual pair (Figure 7), $v* = f = 8$, $e* = e = 12$, and $f* = v = 6$. (ii) Dual polyhedra have the same symmetry elements and thus belong to the same symmetry point group. Thus, both the cube and the octahedron have the O_h symmetry point group. (iii) Dualization of the dual of a polyhedron leads to the original polyhedron. (iv) The degrees of the vertices
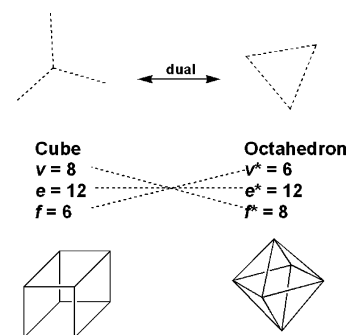
Figure 7. Process of dualization is the conversion of a cube to a regular octahedron.

of a polyhedron correspond to the number of edges in the corresponding face polygons in its dual. Thus, the degree 3 vertices in the cube become triangular faces in the octahedron.

The duals of fullerene polyhedra are seen to be deltahedra. Thus, fullerene polyhedra necessarily have all vertices of degree 3. These become triangular faces upon dualization. The dual of the truncated icosahedron of C_{60} ($v = 60$, $e = 90$, and $f = 32$) is the experimentally unknown macroicosahedral deltahedral borane $B_{32}H_{32}^{2-}$ ($v = 32$, $e = 90$, and $f = 60$), which is the first possible deltahedron after $B_{12}H_{12}^{2-}$ to have icosahedral (I_h) symmetry. This structure for $B_{32}H_{32}^{2-}$ was first proposed by Lipscomb and co-workers in 1978.[44] A qualitative extended Hückel treatment of $B_{32}H_{32}^{2-}$ by Fowler and co-workers[45] indicated an accidental degeneracy at the nonbonding level from which charges of +4, −2, or −8 might be deduced. Later ab initio calculations[46] using an STO-3G basis set suggested that $B_{32}H_{32}^{z-}$ is most stable as a dianion similar to the smaller deltahedral boranes.

2.4. Skyrmion Model for Fullerenes and Deltahedral Boranes

The spherical harmonic models for the MOs in fullerenes and deltahedral boranes discussed above are based on analogies between their spherical structures and the spherical atom. An alternative model for the structures of these polyhedral molecules is based on the analogy between their spherical structures and the skyrmions used to describe an approximately spherical nucleus. Thus, in a nucleus,[47] the skyrmion configuration leads to a polyhedral baryon density isosurface, where baryons correspond to the protons and neutrons in a nucleus. For B baryons, this density isosurface of the skyrmion configuration is an almost spherical trivalent polyhedron having $4(B - 2)$ vertices, $2(B - 1)$ faces, and $6(B - 2)$ edges. For a sufficiently large baryon number B, the resulting skyrmion configuration corresponds to fullerene polyhedra, as first noted by Battye and Sutcliffe.[48,49] Thus, the truncated icosahedron of C_{60} corresponds to a skyrmion configuration of 17 baryons. Furthermore, these authors have shown that the trivalent polyhedra for all skyrmion configurations for B baryons where $7 \le B \le 22$ except for $B = 9$ and 13 have 12 pentagonal faces and $2(B - 7)$ hexagonal faces exactly like favored fullerene polyhedra. A skyrmion field was also generated,
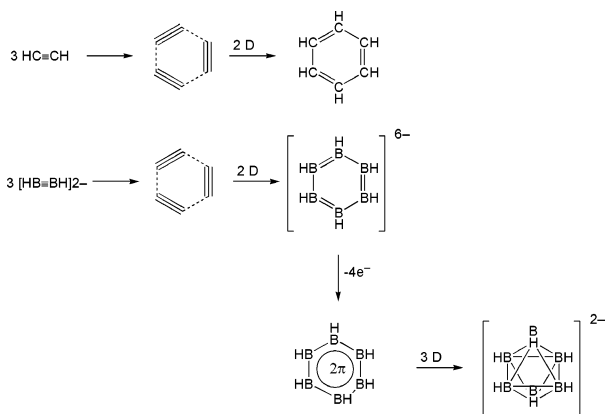
Figure 8. (a) Construction of hexagonal benzene by trimerization of HC≡CH units. (b) Construction of $B_6H_6^{2-}$ by trimerization of $[HB≡BH]^{2-}$ units followed by oxidation.

which led to the infinite hexagonal lattice of graphite.[48]

The dual relationship between the fullerene polyhedra and the borane deltahedron noted above suggests the possible application of the skyrmion model to the deltahedral boranes.[50,51] However, use of this skyrmion model for the skeletal chemical bonding in a borane deltahedron requires identification of the units within a borane deltahedron corresponding to the mesons and baryons of the skyrmion model. In this connection, consider the construction of deltahedral boranes by oligomerization of acetylenic $[HB≡BH]^{2-}$ units, which are regarded as analogues of the mesons. The chemical interactions between the $[HB≡BH]^{2-}$ units in the construction of the borane deltahedron thus become the analogues of the baryons. This approach for the studying of chemical bonding in deltahedral boranes has the following benefits: (i) The experimentally observed geometries for $B_nH_n^{2-}$ ($n = 6, 8, 10, 12$) arise directly from the skyrmion model as their duals. (ii) The analogy between the 2D aromaticity in benzene and the 3D aromaticity in deltahedral boranes is readily apparent from the model.

The ideas behind the skyrmion model for aromaticity can first be illustrated by construction of the 2D benzene by the cyclization of three one-dimensional (linear) acetylene units HC≡CH (Figure 8a). This cyclization process requires formation of three new carbon−carbon bonds, with concurrent reduction of the formal carbon−carbon bond order in the original acetylene units from three to two. The formation of the three new carbon−carbon bonds in benzene during the cyclization of the three acetylene units introduces the second dimension into the benzene structure. Thus, in benzene, the HC≡CH building blocks are the "mesons" and the three new interactions between the HC≡CH units are the "baryons" so that benzene is the analogue of a 2D "nucleus" with three 2D "baryons" (i.e., 2D protons or neutrons).

Now consider a similar construction of the octahedral borane $B_6H_6^{2-}$ from three acetylene-like $[HB≡BH]^{2-}$ units implying the necessary four-electron oxidation to convert the hypothetical $B_6H_6^{6-}$ isoelectronic with benzene to the actual octahedral $B_6H_6^{2-}$ (Figure 8b). The first stage of this process is

exactly analogous to the construction of benzene from three HC≡CH units and introduces a second dimension into the B_6H_6 structure with three new boron−boron interactions leading ultimately to the surface bonding in octahedral $B_6H_6^{2-}$. However, oxidation of the hypothetical hexagonal $B_6H_6^{6-}$ to $B_6H_6^{2-}$ provides the opportunity for a second type of interaction between the three HB≡BH "mesons," namely, the six-center two-electron core interaction leading to oxidative folding to provide the third dimension of the $B_6H_6^{2-}$ octahedron. The trimerization of $[HB≡BH]^{2-}$ to give hexagonal $B_6H_6^{6-}$ provides three baryons, and the oxidative folding of hexagonal $B_6H_6^{6-}$ to octahedral $B_6H_6^{2-}$ provides a fourth baryon. Octahedral $B_6H_6^{2-}$ is thus an analogue of a 3D "nucleus" with four baryons, e.g., the very stable ^{4}He.

An analogous two-stage process can be used to construct the other deltahedral $B_nH_n^{2-}$ ($n = 8, 10, 12$) from $n/2$ $[HB≡BH]^{2-}$ units. This introduces $n/2$ new boron−boron interactions in the first (surface-bonding) stage and one additional n-center two-electron bond in the second (core-bonding) stage corresponding to a $1/2(n + 2)$ baryon "nucleus." Because the baryons in this model are considered to be chemical bonds in which electrons are shared between two or more nuclei, it appears reasonable for the baryon densities determined by the skyrmion model[47] to correspond to the bonding electron densities in conventional skeletal bonding models. This leads naturally to the distribution of electron density on the vertices of the duals of the borane deltahedra as depicted by the corresponding baryon density isosurfaces. Electron density on the vertices of the duals of the borane deltahedra corresponds to the three-center two-electron B−B−B bonds in the triangular faces of the deltahedra used as building blocks for Kekulé-like localized bonding models[52] for the deltahedral boranes.

3. Aromaticity of Fullerenes

3.1. Aromaticity of C_{60}, C_{70}, and Their Hexaanions

3.1.1. Endohedral Probes: ^{3}He NMR Chemical Shifts and NICSs

Helium-3 NMR chemical shifts continue to serve as a sensitive method to characterize the structures and the aromaticity of fullerenes and their derivatives. The encapsulated ^{3}He nucleus reflects the substantial differences among fullerenes in different oxidation states in addition to structures, stability, and reactivity on the cage surface. For example, weakly aromatic C_{60} has a moderately upfield shifted δ ^{3}He of −6.4 ppm,[28a] while the corresponding hexaanion C_{60}^{6-} is highly aromatic with δ ^{3}He = −48.7 ppm.[28d] In contrast, δ ^{3}He changes from −28.8 ppm for the aromatic C_{70} to 8.2 ppm for the weakly antiaromatic C_{70}^{6-}.[28a,d]

The large cavities of some fullerenes make them possible to accommodate more than one helium atom. In 1998, Rabinovitz et al.[53] successfully produced the dihelium compound, He₂@C_{70}, by using a high-temperature, high-pressure procedure for incorporating the ^{3}He. The chemical shift of ^{3}He₂@C_{70} is slightly

Table 1. Chemical Shifts of Endohedral ^{3}He in C_{60} and C_{70}

	δ ^{3}He@$C_n{}^a$	δ ^{3}He$_2$@$C_n{}^a$	Δ^b
C_{60}	−6.403	−6.403^c	0
$C_{60}{}^{6-}$	−49.266	−49.173	−0.093
C_{70}	−28.821	−28.807	−0.014
$C_{70}{}^{6-}$	+8.198	+8.044	+0.154

^{a} In ppm, relative to ^{3}He in THF-d_8. ^{b} $\Delta = \delta$ ^{3}He@C_n − δ ^{3}He$_2$@C_n. ^{c} Most probably, the ^{3}He$_2$ peak is under the main peak.

downfield relative to ^{3}He@C_{70} by ca. 0.014 ppm. However, in contrast to C_{70}, no He$_2$@C_{60} was observed by ^{3}He NMR or mass spectrometry at that time.

In 2002, Rabinovitz et al.[54] reduced the endohedral ^{3}He complexes to hexaanions and obtained both He$_2$@$C_{60}{}^{6-}$ and He$_2$@$C_{70}{}^{6-}$ (Table 1). The ample space in the cage provides the helium atoms with enough freedom of movement so that the chemical shift is a weighted average of the magnetic fields at the different positions sampled by the helium atoms. However, the motion of the two helium atoms inside a cage is restricted by repulsion keeping them roughly 1.5 Å apart and preventing them from getting to the center. Therefore, by comparing the ^{3}He chemical shift of a dihelium compound with that of a monohelium compound, the internal magnetic field of the fullerenes can be probed.

The magnetic field inside C_{60} is practically uniform throughout the interior cavity until reaching the walls, where there are local effects. Displacing the helium atom inside C_{60} leads to indistinguishable He chemical shift changes.[55] At the GIAO-B3LYP/6-31G*//B3LYP/6-31G* level of theory, the NICS at the cage center is −2.79 ppm, moving from the cage center toward a six-membered ring (6-MR), $\delta = -2.79$ at 0.75 Å and $\delta = -3.11$ at 1.5 Å; moving toward a five-membered ring (5-MR), the corresponding values are −2.78 and −2.26 ppm, respectively (Figure 9). The NICS values diverge at around 1.25 Å away from the cage center. The NICS that points further away toward the 6-MR becomes much more shielded so that the NICS at the surface 6-MR center is −2.45 ppm. However, the NICS that points toward the 5-MR becomes deshielded so that the NICS at the surface 5-MR center is 11.90 ppm. The shielding toward the 6-MR and the deshielding toward the 5-MR effects inside the cage cancel each other. The random orientation of the helium atoms inside C_{60} makes the averaged peak in the dihelium species nearly the same as that of the monohelium analogue.

The $C_{60}{}^{6-}$ has an even larger homogeneous magnetic field region. The NICS value at the cage center is −50.00 ppm. Moving from the cage center toward a 6-MR, $\delta = -50.00$ at 0.75 Å and $\delta = -49.90$ at 1.5 Å. Moving toward a 5-MR, the corresponding values are −50.00 and −50.16 ppm, respectively (Figure 9). The NICS values further toward both the 6-MR and the 5-MR are generally less shielded inside the cage. Thus, the random orientation of the pair of helium atoms causes the dihelium species to shift downfield. The above theoretical predictions were verified experimentally by comparing the helium chemical shifts in mono- and dihelium endohedral complexes.

Figure 9. NICS variation with distance from the cage center through the five- and 6-MR middle points for C_{60} and $C_{60}{}^{6-}$. Panels b and c are with a larger scale to show the subtle NICS changes near the cage center.

The fullerene C_{70} is ellipsoidal rather than spherical and has a much higher aromatic character than C_{60}. The NICS (at GIAO-B3LYP/6-31G*//B3LYP/6-31G*) at the cage center is −27.20 ppm. The NICS values become slightly more negative toward the polar 5-MR. However, toward the polar 6-MR in the pole, the NICS values become less shielded with larger magnitudes than the shielding effect following the C_5 axis (Figure 10). When two helium atoms are constrained in the cage, they will mainly reside at the narrow poles of the cavity, i.e., toward 5-MR A and 6-MR B. Thus, these two helium atoms can sense the small gradient in the magnitude of the magnetic field toward the polar region. Experimentally, the ^{3}He chemical shift in He$_2$@C_{70} is slightly shifted downfield as compared with that in He@C_{70}: −28.807 (He$_2$@C_{70})
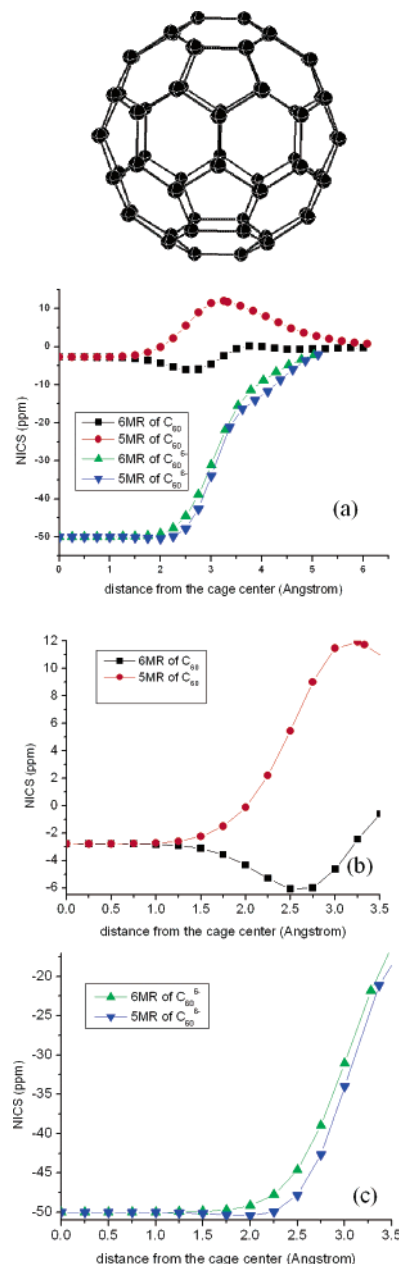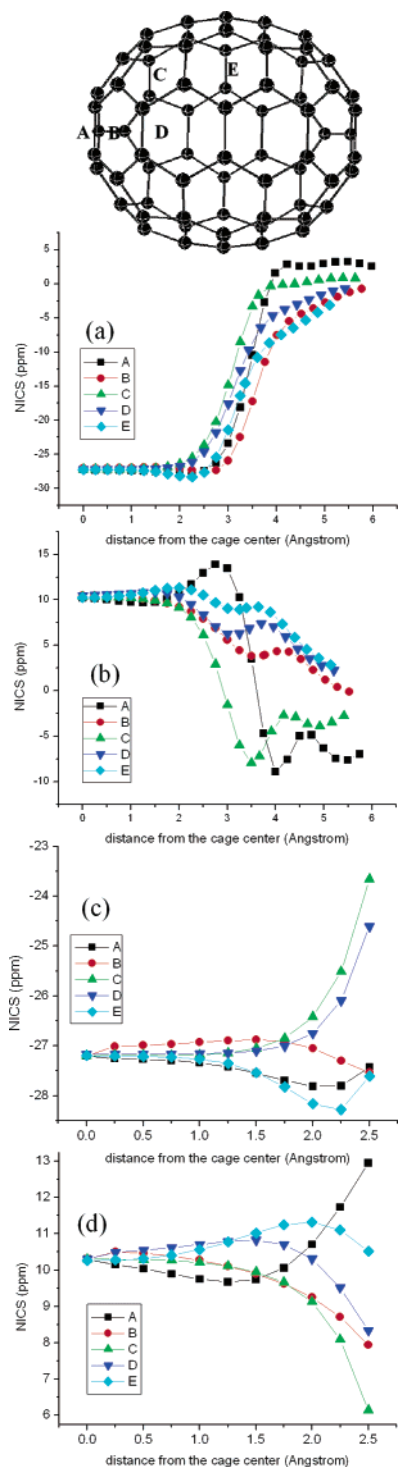
Figure 10. NICS variation with distance from the cage center through the five- and 6-MR middle points for (a) C_{70} and for (b) C_{70}^{6-}. Panels c and d are on a larger scale to show the subtle NICS changes near the cage center for C_{70} and C_{70}^{6-}, respectively.

Table 2. NICS Values at the Ring Centers and 1 Å out of the Ring Plane in C_{60}, C_{70}, and Their Hexaanions (at GIAO-B3LYP/6-31G*//B3LYP/6-31G*)

C_{60}	NICS (0)	NICS (1)	C_{60}^{6-}	NICS (0)	NICS (1)
6MR	−2.5	−0.4	6MR	−21.8	−6.8
5MR	11.7	6.3	5MR	−21.1	−8.8

C_{70}	NICS (0)	NICS (1)	C_{70}^{6-}	NICS (0)	NICS (1)
A	1.6	2.9	A	−8.9	−4.9
B	−11.5	−3.6	B	3.9	3.5
C	−1.7	0.2	C	−7.2	−2.9
D	−9.7	−3.1	D	6.8	5.9
E	−14.5	−6.5	E	9.1	7.4

field inside C_{70} was also detected in its exohedral derivatives, $He_2@C_{70}R_x$.[53]

The reduction of C_{70} to its hexaanion clearly increases and reverses the magnetic field intensity gradient along the longer axis. The computed NICS (at GIAO-B3LYP/6-31G*) at the cage center is 10.3 ppm, suggesting its antiaromatic character. The magnetic field gradient decreases toward the polar 5-MR up to the point 1.25 Å away from the cage center, for example, going from the cage center to 0.75 Å along the C_5 axis in C_{70}^{6-}. The NICS changes from 10.20 to 9.89 ppm. The increased shielding of 0.31 ppm overwhelms the magnetic field gradient increase toward the 6-MR B in this region (Figure 10). Thus, using two helium atoms to probe the magnetic field gradient inside C_{70}^{6-} experimentally, the helium chemical shift in $He_2@C_{70}^{6-}$ is 0.154 ppm upfield as compared with that in $He@C_{70}^{6-}$ (8.044 ppm in $He_2@C_{70}^{6-}$ vs 8.198 ppm in $He@C_{70}^{6-}$). A 2D INADEQUATE (incredible natural abundance double quantum transfer experiment) NMR experiment shows that the added electrons in C_{70}^{6-} are mostly concentrated at the highly curved fullerene poles[56] so that the 5-MRs at the poles become highly aromatic.[57] The magnetic field gradient inside C_{70}^{6-} and the local aromaticity changes measured experimentally agree perfectly with the trend obtained using theoretical NICS probe.

According to the computed NICS values at the ring centers, the 6-MRs of C_{60} are weakly diatropic (aromatic), while the 5-MRs are paratropic (antiaromatic) (Table 2). The 6-MRs of C_{70} are all aromatic: Equatorial ring E has the largest aromaticity (NICS −14.5 ppm), followed by ring B (−11.5 ppm) and ring D (−9.7), while the 5-MRs are not aromatic. The HOMA (harmonic oscillator model of aromaticity), possibly the most reliable structural aromaticity index,[58] and the para delocalization index (PDI),[59] which is defined as the average of all of the Bader delocalization indices between para-related carbon atoms in 6-MRs, gave the same aromaticity sequence for the 6-MRs in C_{70}.[60] PDI analysis also shows that the local electron delocalization per carbon in C_{60} is lower than that in benzene and naphthalene. However, C_{60} presents a global electron delocalization per carbon atom that is almost the same as that of clearly aromatic systems such as benzene or naphthalene.[61]

Adding six electrons to the π-systems enhances the aromaticity. Thus, 6-MRs and 5-MRs in C_{60}^{6-} are significantly diatropic with NICS values of −21.8 and −21.1 ppm at the ring centers. However, the extra

vs −28.821 ppm ($He@C_{70}$). Such a difference indicates that the magnetic field intensity is subtly lower at the center considering that the two helium atoms will be separated by ∼1.5 Å. However, note that the downfield shift of helium in $He_2@C_{70}$ is not solely due to the magnetic field gradient change along the C_5 axis but represents an averaged effect for the gradient change in the eclipsed region toward 5-MR A and 6-MR B. The apparent inhomogeneity of the magnetic

electrons convert the aromatic C_{70} to antiaromatic C_{70}^{6-}. The local ring currents also change dramatically. For example, 5-MR A at the pole is the most aromatic ring (NICS -8.9 ppm), instead of nonaromatic as in the neutral C_{70}. Furthermore, the ring E is the most antiaromatic (NICS 9.1 ppm) in C_{70},$^{6-}$ while in C_{70} this equatorial 6-MR is the most aromatic.

3.1.2. External Probes: ^{1}H NMR Chemical Shifts

Proton chemical shifts are perhaps the most often used criteria for characterizing aromaticity and antiaromaticity. In this connection, ^{1}H NMR studies on suitably designed fullerene derivatives provide useful information on the electron delocalization in fullerenes and their hexaanions.

In the bridged fullerenes **1**−**5** (Figure 11), the protons are located above the centers of rings of the fullerene skeleton, either above two 6-MRs ([6,6]) or one above a 5-MR and the other above a 6-MR ([5,6]). These methylene bridge protons serve as sensors of the local aromaticity of each ring below.[62] Examination of the ^{1}H NMR chemical shifts allows assessment of the changes of the local ring current of each ring (Table 3). Of particular use is a comparison of the ^{1}H NMR chemical shifts of the neutral fullerenes with those of their hexaanions.

The extra electrons in the hexaanions convert the antiaromatic 5-MR in C_{60} and that at the C_{70} pole to aromatic rings. The diamagnetic ring currents in the 5-MRs of C_{60}^{6-} and C_{70}^{6-} can be measured by external ^{1}H NMR chemical shifts in bridged fullerenes.
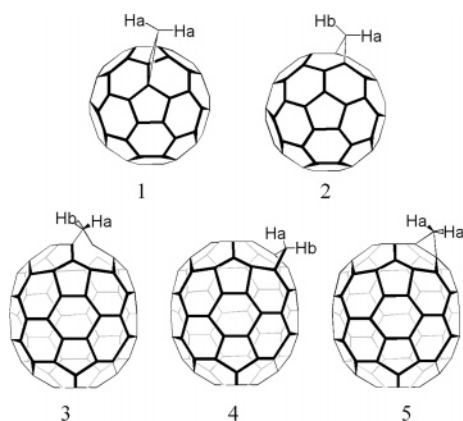

Figure 11. Structures of the bridged C_{60} and C_{70}.

Table 3. Proton NMR Spectra of Methanofullerenes

	δHa	δHb	J_{CHa}	J_{CHb}
[6,6]$C_{61}H_2$ (**1**)	3.93^a		166.5^a	
[6,6]$C_{61}H_2^{6-}$ (**1**$^{6-}$)	2.33^f		130	
[5,6]$C_{61}H_2$ (**2**)	2.87^a	6.35^b	145.0^b	147.8^b
[5,6]$C_{61}H_2^{6-}$ (**2**$^{6-}$)	2.74^a	1.34^c	133.3	130
[5,6]$C_{71}H_2$ (major) (**3**)	2.95^a	6.52^d	150.2^d	145.7^d
[5,6]$C_{71}H_2^{6-}$ (major) (**3**$^{6-}$)	2.27^a	-0.255^e	132^e	129^e
[5,6]$C_{71}H_2$ (minor) (**4**)	2.78^d	5.23^d	149.8^d	146.4^d
[5,6]$C_{71}H_2^{6-}$ (minor) (**4**$^{6-}$)	2.34^e	3.6^e	139^e	
[6,6]$C_{71}H_2$ (**5**)	2.88^e		168.0^e	
[6,6]$C_{71}H_2^{6-}$ (**5**$^{6-}$)	2.77^f		127.9	

^{a} Taken from ref 62a. ^{b} Taken from ref 62b. ^{c} Taken from ref 62c. ^{d} Taken from ref 62d. ^{e} Taken from ref 62e. ^{f} Taken from ref 62f.

In [6,6]$C_{61}H_2$ (**1** in Figure 11), the two protons reside over equivalent rings on the fullerene. The ^{1}H NMR spectrum of **1**$^{6-}$ (Table 3) contains one singlet at 2.33 ppm, which is shielded by 1.6 ppm as compared to the signal of the neutral compound. The high-field shift in the ^{1}H NMR spectrum of **1**$^{6-}$ indicates that the 6-MRs at the base of the bridge become highly conjugated in **1**$^{6-}$ and thus more aromatic than those in neutral **1**. [5,6]$C_{61}H_2$ (**2**) and its hexaanion (**2**$^{6-}$) have nearly the same ^{1}H NMR signals for Ha, the hydrogen atom residing above a 6-MR, indicating that the local aromaticity hardly changes upon reduction. However, the signal for Hb, the hydrogen residing over the 5-MR, moves upfield dramatically (from 6.35 ppm in **2** to 1.34 in **2**$^{6-}$), indicating that the added electrons are located mainly in the 5-MRs. This converts the 5-MRs from paratropic to diatropic rings. However, the ring currents of the 6-MRs experience little influence.

For $C_{71}H_2$(**3**−**5**), the H atoms over the 6-MRs (Ha) are also not influenced much. However, the H atoms over the 5-MRs (Hb) are significantly shielded after reduction, rendering the 5-MRs diatropic, especially in the polar region (as in **3**$^{6-}$). This arises from the lower symmetry of C_{70}^{6-} with respect to C_{60} and C_{60},$^{6-}$ which causes an asymmetrical charge distribution, with the extra charge concentrated mostly in the 5-MRs at the poles.

3.1.3. Aromatic Stabilization Energy of C_{60}

The estimate of the aromatic stabilization energy for fullerenes is not trivial. Thus, there is not a well-accepted ASE value even for the archetypal fullerene C_{60}.[63] Most recently, Cyrański et al.[64] suggested the reference systems as in eqs 7 and 8 to evaluate the extra stability of the fullerene upon sphere closure. Note that the reference systems used here have the same topology and therefore similar strain.

$$\Delta E = -9.8 \text{ kJ/mol} \tag{7}$$

$$\Delta E = -9.0 \text{ kcal/mol} \tag{8}$$
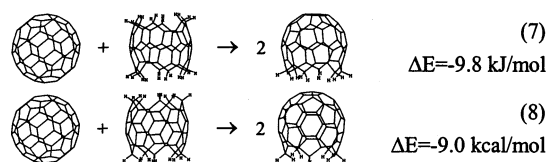
Equations 7 and 8 predict much lower destabilization of C_{60} as compared with the reference systems, namely, less than 0.2 kcal/mol per carbon (at the B3LYP/6-31G* level). This indicates that cyclic π-electron delocalization does not stabilize C_{60}; in other words, C_{60} is not π-aromatic. In this regard, the weak aromaticity of C_{60}, as indicated by a ^{3}He chemical shift of -6.4 ppm at the cage center, may be due to the σ-system. Note that the fully hydrogenated He@$C_{60}H_{60}$ and He@$C_{70}H_{60}$ also afforded a noticeable shielded endohedral helium, with $\delta(^3$He) around -5 ppm.[29a]

3.1.4. Spherical Currents of C_{60} and C_{60}^{10+}

Most recently, Sundholm and co-workers[65] pointed out that "when assessing the aromaticity of 3D pseudospherical molecules, such as fullerenes, one should primarily consider global currents, and only
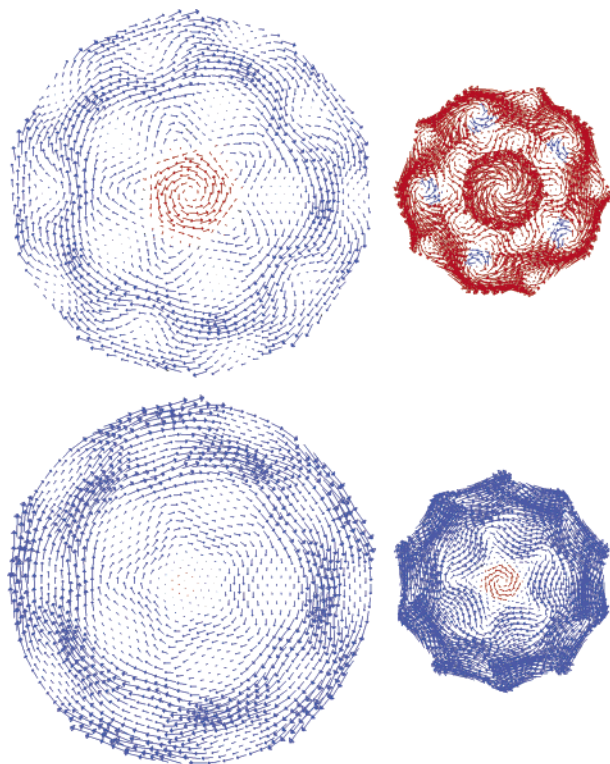
Figure 12. Induced current in neutral (top) and 10+ charged (bottom) C_{60} fullerene 1 Å above (left) and below (right) the surface. The magnetic field is directed perpendicularly out of the plane. The diamagnetic and paramagnet ring currents are represented by blue and red colors, respectively. Reprinted with permission from ref 65. Copyright 2005 Wiley.

ascribe secondary importance to local currents. These 3D sphere currents, not ring currents, define fullerene aromaticity." They plotted the spherical currents of C_{60} and C_{60}^{10+} using their newly developed gauge, including magnetically induced currents method.[66]

The currents 1 Å above and below the surfaces induced by a magnetic field are visualized in Figure 12 (top view, the magnetic field is perpendicular to the paper plane and along a pentagon ring). For both C_{60} and C_{60}^{10+}, the π-electrons move uniformly around the fullerene on both sides of the molecular surface. In C_{60}, the diamagnetic current outside the surface almost cancels the paramagnetic current on the inside completely, resulting in global nonaromaticity, if we take the total gross current as aromatic measure. Thus, the authors concluded that "contrary to common belief, the reason for the global non-aromaticity of C_{60} is not directly related to the paramagnetism of the pentagons, although they do contribute to the decrease in net current. Instead, the main reason is the oppositely directed exterior and interior sphere currents of the π-electrons."[65]

In stark contrast, the currents for C_{60}^{10+} are diamagnetic on both sides of the surface, and the magnetic shielding inside C_{60}^{10+} is quite constant, leading to a strong induced electric current around the molecule as well as a remarkably homogeneous and large endohedral magnetic shielding. Thus, the 50 π-electron C_{60}^{10+} is a true spherically aromatic fullerene gauged by its spherical current.

3.2. Aromaticity of Fullerenes beyond C_{70} and Their Hexaanions

3.2.1. Endohedral Probes: ^3He NMR Chemical Shifts

Tables 4 and 5 summarize the computed and measured ^3He chemical shifts of the higher fullerenes[29d] and their hexaanions. In addition to measuring aromaticity, ^3He chemical shifts also played an important role in the characterization of fullerenes, since each fullerene isomer has a distinctive ^3He NMR signal. Note that the theoretical characterization of C_{82} and C_{86} based on ^3He NMR agrees with that based on ^{13}C NMR.[67] The experimental ^3He NMR assignment of C_{78} isomers changed twice; the final assignment agrees with the computed values (see Table 5).

No clear correlation exists between the number of π-electrons (or carbon atoms) in fullerenes and their aromaticity. Thus, as found in many studies,[68] fullerenes with the same number of carbon atoms and the same molecular symmetry can behave differently. Chemical hardness [highest occupied molecular orbital (HOMO)–lowest unoccupied molecular orbital (LUMO) gap] was suggested to be an aromaticity measure.[69] However, there is no significant correlation between the NICS values and the HOMO–LUMO gap energies for higher fullerenes (Figure 13a), even for fullerenes of the same size (Figure 13b). Moreover, the most stable fullerene isomers do not necessarily have the largest aromaticities and vice versa. In other words, high aromaticity is not necessarily paralleled by apparent stability, since many factors affect the overall stability of a molecule (take C_{84} as an example; see Figure 13c). Thus, a critical assessment is needed if and when NICS aromaticity translates into unusual or extra stability, a connection that is intuitively made by many chemists.

The computed endohedral chemical shifts for the higher fullerenes are method- and basis set-dependent. The good agreement between the experimentally measured ^3He NMR signals and those computed at the GIAO-HF/3-21G level may be just a coincidence, since electron correlation has not been included in the Hartree–Fock method and the 3-21G basis set is rather small. Therefore, additional computations have been performed to check the basis set and electron correlation effects, as summarized in Table 5. Generally, the endohedral chemical shifts computed at the B3LYP level are less shielded, and those computed with larger basis sets are more shielded. Thus, the good agreement between the GIAO-HF/3-21G endohedral chemical shifts and the measured values for neutral higher fullerenes arise from cancellation of these two effects. However, GIAO-HF/3-21G does not give satisfactory results for the hexaanions. In particular, the endohedral chemical shifts of C_{70}^{6-} computed at the Hartree–Fock level are −10.1 and −10.4 ppm, respectively, with the 3-21G and 6-31G* basis sets, which even does not predict the correct sign (experimental value 8.3 ppm). Including electron correlation in the B3LYP method greatly improves the agreement, even with the 3-21G basis set, indicating the importance of the electron correlation effect.

Table 4. Endohedral ^{3}He Chemical Shifts (ppm) of Higher Fullerenes[a]

fullerene	isomer (symmetry)	E_{rel} (kcal/mol)	gap (eV)	NICS[b]	NICS[c]	exp. endo ^{3}He NMR
C_{60}	1 (I_h)		2.77	−8.0	−2.8	−6.3[d]
C_{70}	1 (D_{5h})		2.68	−23.1	−27.2	−28.8[d]
C_{72}	1 (D_{6d})	11.5	2.50	−15.7		
C_{72}	C_{2v}	0.0	1.47	−22.9		
C_{74}	1 (D_{3h})		0.69	−21.9		
C_{76}	1 (D_2)		1.98	−16.4	−16.2	−18.7[e]
C_{78}	1 (D_3)	9.9	1.62	−11.7	−8.3	−11.9[e], −17.6[f], −11.9[g]
C_{78}	2 (C_{2v})	6.6	2.02	−15.2	−14.3	−16.9[e], −16.9[f], −16.9[g]
C_{78}	3 (C_{2v})	0.0	1.65	−15.2	−14.9	−16.8[e], −11.9[f], −17.6[g]
C_{78}	4 (D_{3h})	24.6	2.47	−14.3		
C_{78}	5 (D_{3h})	4.5	1.54	−14.6		
C_{80}	1 (D_{5d})	2.6	0.98	−2.5		
C_{80}	2 (D_2)	0.0	1.35	−8.8		
C_{80}	3 (C_{2v})	6.7	0.80	−7.1		
C_{80}	4 (D_3)	8.9	0.74	−13.7		
C_{80}	5 (C_{2v})	8.4	0.67	−1.5		
C_{82}	1 (C_2)	7.8	1.25	−7.1		
C_{82}	2 (C_s)	6.7	1.64	−11.2		
C_{82}	3 (C_2)	0.0	1.56	−10.6		−13.05[g]
C_{82}	4 (C_s)	3.9	1.56	−10.3		
C_{82}	5 (C_2)	8.3	1.29	−7.5		
C_{82}	6 (C_s)	12.2	1.11	−3.6		
C_{82}	8 (C_{3v})	30.8	0.75	+48.3[h]		
C_{82}	9 (C_{2v})	18.3	0.75	+6.2		
C_{84}	1 (D_2)	51.8	2.37	−16.3		
C_{84}	2 (C_2)	33.3	1.95	−16.8		
C_{84}	3 (C_s)	32.3	0.79	−6.9		
C_{84}	4 (D_{2d})	15.0	2.14	−20.5		−24.35[e]
C_{84}	5 (D_2)	16.1	1.91	−16.6		
C_{84}	6 (C_{2v})	17.4	1.37	−8.6		
C_{84}	7 (C_{2v})	24.8	1.31	−6.2		
C_{84}	8 (C_2)	22.2	0.99	−8.8		
C_{84}	9 (C_2)	26.5	0.81	−2.2		
C_{84}	10 (C_s)	28.7	0.66	−4.4		
C_{84}	11 (C_2)	8.4	1.64	−9.0		
C_{84}	12 (C_1)	12.4	1.46	−7.5		
C_{84}	13 (C_2)	24.9	1.17	−3.0		
C_{84}	14 (C_s)	15.3	1.91	−11.6		
C_{84}	15 (C_s)	11.4	1.55	−9.3		
C_{84}	16 (C_s)	8.1	1.78	−10.0		
C_{84}	17 (C_{2v})	21.8	1.37	−6.4		
C_{84}	18 (C_{2v})	15.8	1.96	−10.8		
C_{84}	19 (D_{3d})	10.4	1.38	−6.9		
C_{84}	20 (T_d)	30.8	2.65	−12.6		
C_{84}	21 (D_2)	16.4	1.35	−6.4		
C_{84}	22 (D_2)	0.4	1.98	−9.6	−5.6	−8.96[e]
C_{84}	23 (D_{2d})	0.0	2.06	−9.5	−5.2	
C_{84}	24 (D_{6h})	7.2	2.34	−11.7		
C_{86}	1 (C_1)	26.2	1.14	−19.3		
C_{86}	2 (C_2)	27.2	2.12	−20.9		
C_{86}	3 (C_2)	18.6	1.17	−18.6		
C_{86}	4 (C_2)	21.3	0.88	−8.3		
C_{86}	5 (C_1)	20.3	1.01	−12.4		
C_{86}	6 (C_2)	15.3	0.97	−12.9		
C_{86}	7 (C_1)	24.4	0.87	−0.8		
C_{86}	8 (C_s)	34.7	0.85	+6.1		
C_{86}	9 (C_{2v})	40.8	0.81	+24.8[h]		
C_{86}	10 (C_{2v})	18.1	1.07	−16.6		
C_{86}	11 (C_1)	10.4	1.15	−9.6		
C_{86}	12 (C_1)	10.3	1.19	−10.3		
C_{86}	13 (C_1)	14.4	1.20	−8.2		
C_{86}	14 (C_2)	21.5	0.98	−7.0		
C_{86}	15 (C_s)	22.0	1.06	−7.7		
C_{86}	16 (C_s)	6.2	1.88	−13.8		
C_{86}	17 (C_2)	0.0	1.54	−10.9	−7.5	−10.58[f]
C_{86}	18 (C_3)	11.3	1.14	−17.0		
C_{86}	19 (D_3)	23.7	1.00	−7.5		

[a] The numbering system of fullerenes follows ref 70. [b] GIAO-SCF/3-21G//B3LYP/6-31G* level. [c] GIAO-B3LYP/6-31G*//B3LYP/6-31G*. [d] δ (^{3}He) from ref 28a. [e] δ (^{3}He) from ref 28c. [f] δ (^{3}He) from ref 28e. [g] δ (^{3}He) from ref 71. [h] Exceptionally positive NICS values of C_{82} (8) and C_{86} (9) result from the instabilities of the wave functions and are left out in the statistics in Figure 12a. Note that reliable NICS computations need stable wavefunctions.

Table 5. Endohedral ^{3}He Chemical Shifts (ppm) of Higher Fullerenes and Their Hexaanions at Different Levels (Most Computational Results Are Unpublished[72])

species	HF/3-21G	B3LYP/3-21G	HF/6-31G*	B3LYP/6-31G*	δ (^{3}He)
C_{60} (1, I_h)	−8.0	−1.9	−9.6	−2.8	−6.3[a]
C_{70} (1, D_{5h})	−23.1	−22.1	−27.6	−27.2	−28.2[a]
C_{76} (1, D_2)	−16.4	−13.0	−19.6	−16.2	−18.7[c]
C_{78} (1, D_3)	−11.7	−6.2	−14.2	−8.3	−11.9[c]
C_{78} (2, C_{2v})	−15.2	−11.5	−18.1	−14.3	−16.9[c]
C_{78} (3, C_{2v})	−15.2	−11.9	−18.4	−14.9	−16.8[c]
C_{84} (22, D_2)	−9.6	−4.2	−11.5	−5.6	−9.0[c]
C_{84} (23, D_{2d})	−9.5	−3.9	−11.4	−5.2	−7.5[d]
C_{86} (17, C_2)	−10.9	−5.8	−13.1	−7.5	−10.6[d,f]
$C_{60}{}^{6-}$ (1, I_h)	−55.6	−43.0	−64.2	−50.0	−48.7[b]
$C_{70}{}^{6-}$ (1, D_{5h})	−10.1	8.3	−10.4	10.3	8.3[b]
$C_{76}{}^{6-}$ (1, D_2)	−25.2	−15.1	−28.3	−18.2	−20.6[e]
$C_{78}{}^{6-}$ (1, D_3)	−29.8	−24.9	−34.4	−30.1	−32.4[e]
$C_{78}{}^{6-}$ (2, C_{2v})	−19.4	−4.4	−21.8	−5.3	−10.0[e]
$C_{78}{}^{6-}$ (3, C_{2v})	−24.3	−11.8	−27.0	−12.5	−13.5[e]
$C_{84}{}^{6-}$ (22, D_2)	−28.5	−16.9	−32.0	−20.1	−22.1[e,f]
$C_{84}{}^{6-}$ (23, D_{2d})	−28.9	−17.8	−32.6	−21.1	−22.8[e,f]
$C_{86}{}^{6-}$ (17, C_2)	−26.7	−15.2	−30.3	−18.6	

[a] Ref 28a. [b] Ref 28d. [c] Ref 28c. [d] Ref 28e. [e] Ref 71. [f] Our theoretical assignment.

Among C_{60} and its higher analogues, C_{60} and C_{70} are the two extremes in the aromaticity scale of neutral fullerenes: C_{60} is the least aromatic, while C_{70} is the most aromatic (Table 4). Adding electrons dramatically changes the magnetic properties. Reduction of C_{60} and C_{70} to their hexaanions inverts their aromatic character. With six additional electrons, the diatropicity of C_{60} is dramatically enhanced; however, $C_{70}{}^{6-}$ shows a much reduced diatropicity as compared with C_{70}. Higher fullerenes have "intermediate" aromatic character. Calculations predict that the magnetic properties of the higher fullerenes should depend on their reduction state.[73]

An important characteristic of the π-systems of fullerenes is their ability to accept a relatively large number of electrons,[74] as shown by their electrochemistry.[75] This arises from the availability of low-lying unoccupied MOs,[76] which results in high electron affinities.[77] Although several reduction waves, generally six, have been observed in electrochemical studies conducted on many higher fullerenes,[78] the definitive ^{13}C NMR characterization of the hexaanions of higher fullerenes was achieved only in 2003.[79]

Rabinovitz et al. successfully reduced higher fullerenes (C_{76}, D_2; C_{78}, C_{2v}; C_{78}, D_3; C_{84}, D_2; and C_{84}, D_{2d}) to their hexaanions and used endohedral ^{3}He NMR to probe the aromaticity of higher fullerene anions. The measured ^{3}He NMR data and the computed endohedal chemical shifts are summarized in Table 5.

The measured ^{3}He NMR chemical shifts of all of the higher fullerene anions occur between two extremes, namely, the high-field shift of He@$C_{60}{}^{6-}$ and the low-field shift of He@$C_{70}{}^{6-}$. Thus, the "aromaticity scale" of the fullerene anions can be suggested as follows: $C_{60}{}^{6-}$ > $C_{78}{}^{6-}$ (1, D_3) > $C_{84}{}^{6-}$ (22, D_2; and 23, D_{2d}) > $C_{76}{}^{6-}$ > $C_{78}{}^{6-}$ (3, C_{2v}) > $C_{78}{}^{6-}$ (2, C_{2v}) > $C_{70}{}^{6-}$. This aromaticity scale also agrees well with the computed endohedral chemical shifts as well as magnetic susceptibility calculations.[73b]

Comparison between the ^{3}He NMR chemical shifts of the neutral fullerenes and their anions (Table 5) shows that the changes in the chemical shifts differ
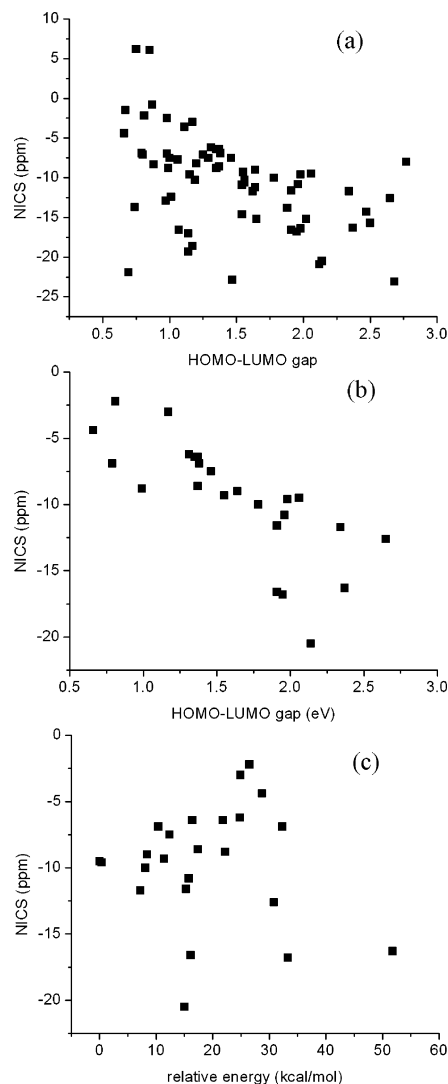

Figure 13. Correlation between HOMO−LUMO gap (eV) and NICS (ppm) (a) for higher fullerenes (summarized in Table 4) and (b) for C_{84} isomers as well as (c) the correlation between the relative stability (kcal/mol) vs NICS (ppm) for C_{84} isomers.

from one fullerene to another. While the ^{3}He signals of C_{78} (D_3), C_{84}, and C_{76} are shifted to higher field as a result of their reduction, the two isomers of C_{78} (C_{2v}) are shifted to lower field. These changes indicate an increase or decrease, respectively, in the aromaticity of the fullerenes. These two opposite trends were observed in the reduction of C_{60} and C_{70} but in a much more dramatic manner.

The magnetic properties of fullerenes and their anions are not simply related to the number of carbon atoms or the number of electrons in the π-system. This is demonstrated by the three C_{78} isomers, which behave quite differently. The aromatic character of C_{78} (D_3) increases when reduced. Thus, $C_{78}{}^{6-}$ (D_3) is highly aromatic. However, the aromaticity of the two C_{2v} isomers of C_{78} decreases when reduced, and their anions show lower aromatic character than the anion of the D_3 isomer.

3.3. Aromaticity of Smaller Fullerenes

Isolable smaller fullerenes have been long sought since the discovery of C_{60}. However, fullerenes smaller than C_{60} unavoidably have adjacent pentagons (APs) thereby violating the isolated pentagon rule (IPR)[80] governing fullerene stabilities. Consequently, smaller fullerenes have much higher strain energy in the carbon surface and are highly reactive.

Although smaller fullerenes can be generated in trace amounts by the traditional Kratschmer–Hoffman method,[81] in which graphite rods are vaporized by arc discharge under a low-pressure inert gas atmosphere, they have not been extracted from the raw soot. The high reactivity also precludes their more conventional chemical syntheses using procedures that give C_{60}.[82]

In 2000, Prinzbach et al. produced C_{20} (**6**) in the gas phase and detected its fleeting existence by anion photoelectron spectroscopy.[83] In 2001, a C_{20} crystallized solid was prepared in the ultrahigh molecular weight polyethylene samples during Ar^+ ion beam irradiation. However, no structure information other than its hexagonal symmetry is available.[84a] The computations show that the most stable C_{20} solid has a compressed body-centered cubic structure and is a semiconductor.[84b] This is still awaiting experimental confirmation.

6,$C_{20}(C_2)$ **7**, $C_{36}(D_{6h})$ **8**,$C_{50}Cl_{10}$ (D_{6h})

9,C_{50} (D_3) **10**,$C_{50}(D_{5h})$ **11**,$C_{32}(D_3)$
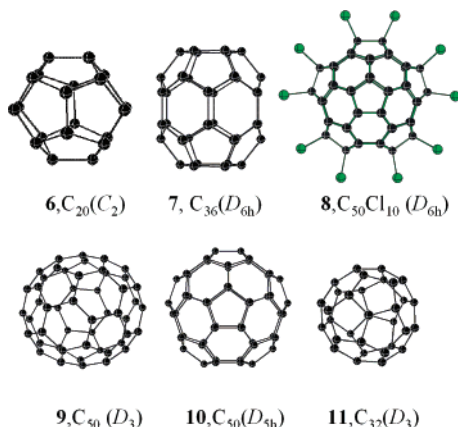
Production of the smaller fullerene, C_{36} (**7**, D_{6h}), in macroscopic quantities by DC arc discharge has been

claimed, and a fullerene-like C_{36} cage was suggested to exist as a covalently bonded cluster assembly in the solid state.[85] However, definitive characterization of a C_{36}-based solid is in doubt since no sp^3 carbon signals were found in the ^{13}C NMR spectrum. Various attempts to reproduce the production of C_{36} by arc discharge have not been successful. The synthesis, purification, and identification of $C_{36}H_6$ and $C_{36}H_6O$ have also been reported, but the detailed structures are still not clear.[86]

The most promising isolable smaller fullerene has long been considered to be C_{50}. In this connection, C_{50} was observed as a magic cluster with enhanced intensity in mass spectra as early as 1985, when C_{60} was discovered. C_{50} is the smallest carbon cage without three directly or sequentially fused pentagons and should have less strain energy than other smaller fullerenes.[87] Moreover, according to the Hirsch $2(N + 1)^2$ rule, C_{50} has a completely filled electron shell (i.e., filled S, P, D, F, and G MOs) and is therefore expected to be highly aromatic. This expected high aromaticity and smaller strain energy distinguish C_{50} from other smaller fullerenes. The expected enhanced abundance of C_{50} has been confirmed experimentally in the gas phase by mass spectroscopy.[88] However, the expected higher strain energy still makes it unlikely that the parent C_{50} will be isolated. Thus, it appears that partial saturation of the most strained carbon sites is still necessary to get an isolable C_{50} derivative. Using a modified graphite arc discharge method,[89] Xie et al.[90] successfully prepared in milligram quantities and fully characterized the first stable smaller fullerene derivative, namely, decachlorofullerene[50], $C_{50}Cl_{10}$ (**8**, D_{5h}). Note that the C_{50} (**9**, D_3) is more aromatic and less strained than C_{50} (**10**, D_{5h}), thus, lower in energy.[91]

The scarcity of free smaller fullerenes or their stable derivatives makes it very difficult to investigate their aromaticity. We have to rely heavily on the theoretical probes, mainly NICS, to characterize their aromaticity (Table 6). Readers interested in smaller fullerene chemistry are encouraged to read the review authored by Lu and Chen[92] in this thematic issue.

In 2000, Hirsch proposed the $2(N + 1)^2$ electron-counting rule[95] to explain the aromaticity of I_h symmetrical fullerenes. This rule represents the spherical analogy to the $4N + 2$ rule for annulene systems and demonstrated that the aromaticity and cluster distortions of the fullerenes depend on the number of delocalized π-electrons in the valence shell. The Hückel $4N + 2$ rule can be used, e.g., for less symmetrical heteroaromatic compounds. The same is true for the Hirsch $2(N + 1)^2$ rule, which is also applicable for a number of less symmetrical fullerenes,[96] as long as their orbitals remain closely related to those of I_h fullerenes and they retain the corresponding subshell structure despite the reduced symmetry. The NICS data for charged carbon clusters with $2(N + 1)^2$ π-electrons, ranging from $C_{16}{}^{8+}$ ($N = 1$) to $C_{80}{}^{8+}$ ($N = 5$), are summarized in Table 7. Together with Table 6, these data clearly show that carbon clusters with $2(N + 1)^2$ π-electrons, either

Table 6. Endohedral Chemical Shifts (ppm) of Smaller Fullerenes[a] at Different Levels

fullerene	isomer (symmetry)	NICS[b]	NICS[c]	NICS[d]	fullerene	isomer (symmetry)	NICS[b]	NICS[c]	NICS[d]
C_{20}	1 (C_2)[e]	−36.7	−19.2		C_{42}	33 (C_1)			−3.2
C_{24}	1 (D_6)[f]	15.6	37.7		C_{42}	45 (D_3)			−6.4
C_{26}	1 (D_{3h})[g]				C_{44}	69 (C_1)			−7.2
C_{28}	1 (D_2)	2.8	14.9		C_{44}	72 (D_{3h})			−26.0
C_{28}	2 (T_d)	−13.0	3.8		C_{44}	75 (D_2)			−7.7
C_{30}	1 (C_{2v})[h]	−23.5	−11.7		C_{44}	89 (D_2)			−7.3
C_{30}	2 (C_{2v})	−37.8	−33.0		C_{46}	86 (C_1)			−17.9
C_{30}	3 (C_{2v})	−22.1	−11.4		C_{46}	88 (C_1)			−29.7
C_{32}	1 (C_2)	−22.9	−7.8		C_{46}	90 (C_1)			−22.9
C_{32}	2 (D_2)	−24.2	−16.8		C_{46}	99 (C_s)			−31.9
C_{32}	3 (D_{3d})	−39.3	−22.8		C_{46}	101 (C_1)			−32.4
C_{32}	4 (C_2)	−48.8	−43.8		C_{46}	103 (C_1)			−20.8
C_{32}	5 (D_{3h})	−37.9	−29.7		C_{46}	107 (C_s)			−18.8
C_{32}	6 (D_3)	−53.2	−48.1		C_{46}	108 (C_s)			−14.2
C_{34}	1 (C_2)	−16.9	−2.6		C_{46}	109 (C_2)			−11.4
C_{34}	2 (C_s)	−21.7	−9.8		C_{46}	110 (C_1)			−22.2
C_{34}	3 (C_s)	−30.0	−13.6		C_{46}	114 (C_1)			−17.1
C_{34}	4 (C_2)	−26.5	−22.3		C_{46}	116 (C_2)			−24.7
C_{34}	5 (C_2)	−37.9	−24.5		C_{48}	138 (C_{2v})			−37.8
C_{34}	6 (C_1)[i]	−19.2	15.7		C_{48}	139 (C_1)			−36.7
C_{36}	1 (C_2)	−2.3	15.5		C_{48}	149 (C_1)			−21.8
C_{36}	2 (D_2)	−15.0	−6.3		C_{48}	150 (C_1)			−20.3
C_{36}	3 (C_1)	−8.8	6.6		C_{48}	160 (C_2)			−33.0
C_{36}	4 (C_s)	−14.0	0.2		C_{48}	161 (C_2)			−28.5
C_{36}	5 (D_2)	−24.3	−24.4		C_{48}	162 (C_1)			−38.6
C_{36}	6 (D_{2d})	−11.2	−1.3		C_{48}	163 (C_2)			−31.7
C_{36}	7 (C_1)	−15.8	−2.1		C_{48}	165 (C_1)			−36.2
C_{36}	8 (C_s)	−32.5	−24.4		C_{48}	168 (C_s)			−27.5
C_{36}	9 (C_{2v})	−17.6	−9.7		C_{48}	169 (D_2)			−28.0
C_{36}	10 (C_2)	−21.0	−16.1		C_{48}	171 (C_2)			−39.3
C_{36}	11 (C_2)	−34.2	−24.5		C_{48}	192 (C_2)			−36.3
C_{36}	12 (C_2)	−15.1	12.8		C_{48}	196 (C_1)			−29.7
C_{36}	13 (D_{3h})	−29.8	−29.6		C_{48}	197 (C_s)			−19.4
C_{36}	14 (D_{2d})	−15.4	−11.1		C_{48}	199 (C_2)			−26.5
C_{36}	15 (D_{6h})	−38.2	−27.3		C_{50}	260 (C_2)			−23.3
C_{38}	17 (C_s)			−7.3	C_{50}	262 (C_s)			−16.3
C_{40}	26 (C_1)			−21.6	C_{50}	263 (C_2)			−46.4
C_{40}	29 (C_2)			−5.3	C_{50}	264 (C_s)			−45.4
C_{40}	31 (C_s)			1.5	C_{50}	266 (C_s)			−43.8
C_{40}	38 (D_2)	4.0	−16.8	2.3	C_{50}	270 (D_3)		−40.3	−46.7
C_{40}	39 (D_{5d})	2.8	11.5	1.3	C_{50}	271 (D_{5h}) (A)[j]		−2.7	
					C_{50}	271 (D_{5h}) (B)[j]	−37.1	−32.4	−39.6

[a] The numbering system of fullerenes follows ref 70. [b] At the GIAO-SCF/6-31G*//B3LYP/6-31G* level, data were cited from ref 93. [c] At the GIAO-B3LYP/6-31G*//B3LYP/6-31G* level, data were cited from ref 93. [d] At the GIAO-SCF/6-31+G*//B3LYP/6-31G* level, data were cited from ref 94. [e] Distorted from the perfect symmetry of I_h. [f] Distorted from the perfect symmetry of D_{6d}. [g] The D_{3h} structure is not a local minimum and has wave function instability. [h] Distorted from the perfect symmetry of D_{5h}. [i] Distorted from the perfect symmetry of C_{3v}. [j] A and B are two electronic states, which can be obtained by reversing the HOMO and LUMO. Electronic state A is 3.3 kcal/mol more stable than B.

neutral or charged, are highly aromatic, and they have much more negative NICS values than their counterparts with more or fewer electrons. In this regard, the Hirsch $2(N + 1)^2$ rule persists in carbon clusters even with lower symmetries, provided that the π-electron count is correct. However, an anomaly is observed for C_{60}^{12-} (the core of $C_{60}Li_{12}$), since the t_{1g} orbitals derived from the $L = 6$ shell are lower in energy than the t_{2u} orbitals from the $L = 5$ shell. Consequently, the t_{1g} orbitals of $L = 6$ are filled before the t_{2u} orbitals of $L = 5$ shell, and C_{60}^{12-} does not have a completely filled electron shell although it has 72 π-electrons. Because of this, an endohedral chemical shift of +11.4 ppm has been computed for $C_{60}Li_{12}$ at GIAO-SCF/DZP//BP86/3-21G[97](3.9 ppm at GIAO-B3LYP/6-31G*//B3LYP/6-31G*) and energetic estimates suggest that in the bulk, $Li_{12}C_{60}$ should be unstable with respect to disproportionation into Li_6C_{60} and Li metal.[97]

Note that the highly aromatic cluster C_{32} has been experimentally confirmed as a magic cluster in the gas phase.[88] Although it is not realistic to get the bare C_{32} cage in a condensed phase, in principle, it is highly possible to isolate its derivatives in a suitable form or to get C_{32} solids.

Interestingly, Alcami et al.[99] found that C_{52}^{2+} (437, T), highly aromatic as indicated by its −46.2 ppm NICS value at the cage center, is the most stable isomer for the C_{52} dication. This finding, which apparently contradicts the pentagon adjacency penalty rule, is a consequence of complete filling of the HOMO π-shell (and the concomitant aromaticity) and the near-perfect sphericity of the most stable isomer. Alcami et al. concluded that "not only the number of APs, but also the electronic structure (closed-shell effects) and the shape of the fullerene play an important rule in the theoretical prediction of the most stable fullerene structure." Other examples

Table 7. NICS Values^a of Charged Carbon Clusters with $2(N + 1)^2$ π-Electrons

species	isomer (symmetry)	$N_e{}^b$	L^c	NICS
$C_{16}{}^{8+}$	D_{4d}	8	1	−58.6
$C_{16}{}^{2-}$	D_{4d}	18	2	−32.7
$C_{20}{}^{2+}$	1 (I_h)	18	2	−73.1
$C_{28}{}^{4-}$	1 (T_d)	32	3	−35.5
$C_{36}{}^{4+}$	14 (D_{2d})	32	3	−64.0
$C_{36}{}^{4+}$	9 (C_{2v})	32	3	−57.9
$C_{40}{}^{8+}$	38 (D_2)	32	3	−62.1
$C_{40}{}^{8+}$	39 (D_{5d})	32	3	−82.2
$C_{48}{}^{2-}$	199 (C_2)	50	4	−40.4^d
$C_{52}{}^{2+}$	437 (T)	50	4	−46.2^e
$C_{60}{}^{10+}$	I_h	50	4	−81.4^f
$C_{80}{}^{8+}$	1 (I_h)	72	5	−82.9^g
$C_{60}Li_{12}$	I_h	72	5	11.4^h

^{a} GIAO-SCF/6-31G*//B3LYP/6-31G* at the cage center from ref 96. ^{b} Number of the π-electrons. ^{c} Quantum number L for the closed shells. ^{d} GIAO-SCF/6-31+G*//B3LYP/6-31G* from ref 98. ^{e} GIAO-SCF/6-31G*//B3LYP/6-31G* from ref 99. ^{f} GIAO-SCF/3-21G//B3LYP/6-31G* from ref 95. ^{g} GIAO-SCF/3-21G//HF/6-31G* from ref 95. ^{h} GIAO-SCF/DZP//BP86/3-21G from ref 97.

supporting the above conclusion exist as follows: the non-IPR C_{72} (C_{2v}) is more stable than the IPR C_{72} (D_{6d}) isomer (Table 4) because C_{72} (C_{2v}) is of more spherical shape and is more aromatic (NICS of −22.9 ppm) than C_{72} (D_{6d}); C_{50} (D_3) with six APs is more stable than C_{50} (D_{5h}) with five APs,[91] which is also due to the same reasons.

3.4. Aromaticity of Heterofullerenes

Heterofullerenes, in which one or more cage carbons are substituted by heteroatoms, represent the third fundamental group of modified fullerenes besides exo- and endohedral derivatives. They have attracted high interest owing to their tunable chemical and physical properties for material science.[100] For example, first principles computations have demonstrated that $C_{60-n}B_n$ and $C_{60-m}N_m$ can be engineered as the acceptors and donors, respectively, needed for molecular electronics by properly controlling the dopant number n and m in C_{60}. In particular, the authors showed that the acceptor $C_{48}B_{12}$ and the donor $C_{48}N_{12}$ are promising components for carbon nanotube-based n−p−n (p−n−p) transistors and p−n junctions.[101]

Synthesis and isolation of some heterofullerenes have been reported. $C_{59}N$ and $C_{69}N$ have been identified as dimers in solution after suitable chemical modification of the parent fullerenes.[102] A key intermediate in azaheterofullerene chemistry,[103] namely, the $C_{59}N^+$ carbocation isoelectronic with C_{60}, has also been synthesized.[104] Boron-doped C_{60} thin films were synthesized by a radiofrequency plasma-assisted vapor deposition technique using C_{60} as a precursor.[105] More interestingly, $C_{48}N_{12}$, which has a completely filled electron shell with 72 π-electrons (S + P + D + F + G + H MOs), was synthesized as the core shell in cross-linked carbon nitride nanoonions.[106]

The synthesis of most heterofullerenes on a macroscopic scale is still a challenge. However, various experimental techniques, such as laser ablation, arc discharge, and fragmentation, can be used for their generation and their existence can be detected by mass spectrometry. Until now, heterofullerenes, such as $C_{60-x}B_x/C_{70-x}B_x$ ($x = 1–2$),[107] $C_{59}N/C_{69}N$,[108] $C_{58}BN$,[109] $C_{59}O$,[110] $C_{60-x}Si_x$,[111] $C_{59}Ge/C_{59}As/C_{69}As$,[112] $C_{59}P/C_{69}P$,[113] and transition metal-doped $C_{59}M/C_{69}M$ (M = Pt, Fe, Co, Ni, Rh, Ir),[114] $[C_nIr]^-$ ($n = 56–59$)[115] have been generated successfully in the gas phase. Most recently, $C_{59}Ge$ and $C_{58}Ge_2$ powders (average diameter 5−20 nm) were synthesized and the enhanced second- and third-order nonlinear optical susceptibilities were observed.[116]

Apart from the extensive experimental work, theoretical investigations into the monodoped $C_{59}B/C_{59}N$,[117] $C_{59}O$,[118] $C_{59}S$,[118d] $C_{59}Be$,[118c] $C_{59}Si$,[118c,119] $C_{59}P$,[120] $C_{59}M$ (M = Fe, Co, Ni, Rh),[114,121] $C_{69}M$ (M = Co, Rh, Ir),[122] $C_{58}(BN)$,[123] and $C_{59}B/C_{59}N$ dimer[124] have been performed. Some multiply substituted heterofullerenes, such as $C_{55}X_5$ (X = Si, Ge, Sn, B, Al, N, P, SiH, GeH, SnH) and their $\eta^5-\pi$-complexes with Li[125] and $C_{54}N_6$[126], have also been studied. The isomerism, aromaticity, and electronic properties of $C_{48}X_{12}$ (X = B, N, Si, P), especially $C_{48}N_{12}$, have probably been the most active area for computational studies on heterofullerenes in the last 3 years (see section 3.4.5 for details).

Because the number of possible isomers increases rapidly as more heteroatoms are incorporated, the isomerism of heterofullerenes, which is difficult to address experimentally, has been well-investigated theoretically. So far, the substitution pattern of polydoped fullerenes $C_{58}X_2$ (X = N, B, P),[127] $C_{68}X_2$ (X = N, B),[128] $C_{60-x}N_x/C_{60-x}B_x$ ($x = 2–8$),[129] $C_{70-x}N_x/C_{70-x}B_x/C_{70-x}P_x$ ($x = 2–10$),[130] $C_{60-2x}(BN)_x$ ($x = 1–24$),[131] $C_{60-2x}(AlN)_x$ ($x = 1–3$),[132] and $C_{70-2x}(BN)_x$ ($x = 1–3$)[133] have been studied and the electronic properties have been calculated based on the most stable isomers.

Smaller fullerenes substituted with heteroatoms have also been investigated. For example, carbon nitride nanostructures, $C_{n-x}N_x$ ($40 \leq n \leq 50$), have been produced by the arc discharge technique and analyzed by mass spectrometry.[134] However, the ground states of the heterofullerenes are still in question.[135] On the theoretical side, the symmetrical $P_8(C_2)_6$ is predicted to be a remarkably stable small heterofullerene with carbon atoms less pyramidal than in C_{60}.[136] In addition, $C_{34}X_2$, $C_{38}X_2$, $C_{48}X_2$ (X = B,N), and $C_{38}BN$ have been studied.[137]

NICSs, which have essentially the same values as the experimental ^{3}He NMR chemical shifts at the cage centers, have been computed for heterofullerenes for the purpose of assessing their aromaticity, "theoretical characterization," and assistance for future experimental ^{3}He NMR assignments.

3.4.1. Monodoped Hetero Fullerenes $C_{59}X_n$ and $C_{59}X^{(6-n)-}$ (X = B, N, P, As, Si) with 60 and 66 π-Electrons

These heterofullerenes have closed cage configurations according to B3LYP/6-31G* computations, although there is some deformation around the heterodoped position. In the C_{60} isoelectronic analogues, the deformations in $C_{59}B^-$ and $C_{59}N^+$ are far less than those in $C_{59}Si$, $C_{59}P^+$, and $C_{59}As^+$, since B

Table 8. NICS Values (ppm) at the Cage Center and Ring Centers Adjacent to the Heteroatom (GIAO/HF/3-21G//B3LYP/6-31G*)

	NICS		NICS
C_{60}	−8.0	$C_{60}{}^{6-}$	−55.6
$C_{59}N^+$	−8.3	$C_{59}N^{5-}$	−35.7
$C_{59}P^+$	−8.7	$C_{59}P^{5-}$	−14.2
$C_{59}As^+$	−8.9	$C_{59}As^{5-}$	−26.0
$C_{59}B^-$	−7.6	$C_{59}B^{7-}$	−40.7
$C_{59}Si$	−8.1	$C_{59}Si^{6-}$	−24.6

and N have a covalent radius comparable to carbon, while the other heteroatoms have larger radii. The heterofullerenes with 60 π-electrons, namely, $C_{59}B^-$, $C_{59}N^+$, $C_{59}P^+$, $C_{59}As^+$, and $C_{59}Si$, are as aromatic as the parent C_{60} on the basis of the NICS values at the cage center (Table 8). Significant effects upon doping are observed only for the rings adjacent to the heteroatom, while the perturbation in other rings is not significant. Thus, all of the 6−6 C−X bonds (shared by two 6-MRs) in these monodoped heterofullerenes are shorter than the 6−5 C−X bonds as in C_{60} and $C_{60}{}^{6-}$. However, $C_{59}N^{5-}$ is an exception since its 6−6 C−N bond is slightly longer than its 6−5 C−N bond (1.447 vs 1.428 Å).

All of the heterofullerenes with 66 π-electrons are more aromatic than their 60 π-electron analogues. However, all of their NICS values are less negative than that computed for $C_{60}{}^{6-}$, indicating their reduced aromaticity. The endohedral chemical shifts of $C_{59}N^{5-}$ and $C_{59}B^{7-}$ are much more shielded than those of $C_{59}P^{5-}$, $C_{59}Si^{6-}$, and $C_{59}As^{5-}$, which may be attributed to their more spherical geometries as discussed above. The heterofullerenes in the reduced form have distinct endohedral chemical shifts that cover a large range, varying from −14.2 ppm ($C_{59}P^{5-}$) to −40.7 ppm ($C_{59}B^{7-}$) as compared to −55.6 ppm of $C_{60}{}^{6-}$. Thus, it is possible to use the individual endohedral chemical shifts to distinguish between the different fullerene anions.

3.4.2. Monodoped Heterofullerenes $C_{59}O$, $C_{59}S$, and Their Dications and Tetraanions

Heterofullerenes are generally assumed to have trivalent heteroatoms. However, as pointed out by Wudl,[138] oxygen and sulfur doped analogously may exist not only as neutral ylide structures with formal $^-C−O^+$ and $^-C−S^+$ bonds in the closed cage forms but also as truncated quasi-fullerene structures bearing a $>C=O$ or $>C=S$ moiety in opened structures as shown in Figure 14.

At the B3LYP/6-31G* level, the most stable $C_{59}O$, $C_{59}O^{4-}$, and $C_{59}S^{4-}$ isomers (D isomers in Figure 14) exhibit cage opened structures having an eight-membered ring orifice and contain a C=O or C=S moiety and two fused 5-MRs. On the other hand, $C_{59}S$, $C_{59}S^{2+}$, and $C_{59}O^{2+}$ are cage-closed fullerenes (A isomers in Figure 14) in disagreement with the former semiempirical computational results, which show that both $C_{59}O$ and $C_{59}O$ have closed cages.

The endohedral chemical shifts of the most stable neutral and dications of oxa-fullerenes and thia-fullerenes (see Figure 15) are only slightly shielded as compared to that of C_{60} (NICS value of −8.0 ppm at the same level and experimental endohedral
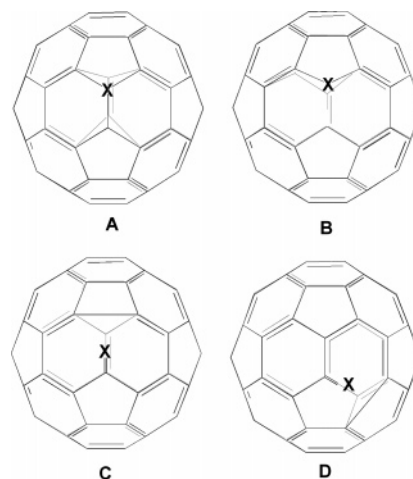
Figure 14. Possible structures for $C_{59}O/C_{59}S$ and their charged species.
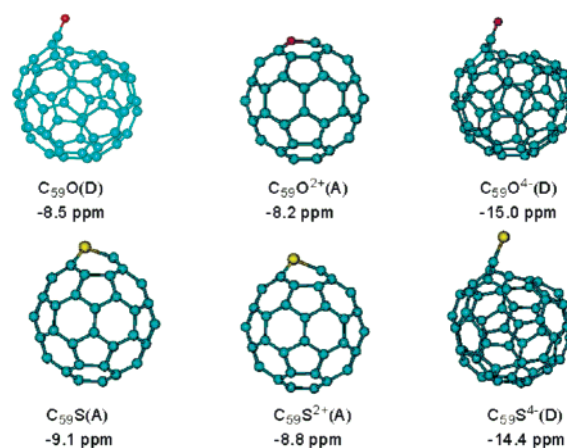
Figure 15. Most stable structure for $C_{59}O/C_{59}S$, their charged species, and computed NICS values at the cage center (ppm, at GIAO-HF/3-21G//B3LYP/6-31G*).

helium chemical shift of −6.3 ppm), indicating that there are no special effects in the doped cages. Therefore, it is less helpful to differentiate these doped fullerenes from parent C_{60} on the basis of their endohedral chemical shifts.

In contrast, large endohedral chemical shift changes have been found for the most stable tetraanions (Figure 15), which differ strongly from those of the neutral and dication species and also from that of the isoelectronic $C_{60}{}^{6-}$. For example, the NICS values of the most stable $C_{59}O^{4-}$ and $C_{59}S^{4-}$ isomers have upfield shifts of −15.0 and −14.4 ppm, as compared to those of their most stable neutral and dicationic counterparts (−8.5 and −8.2 vs −9.1 and −8.8 ppm, respectively). These changes, which are much smaller than that from C_{60} to $C_{60}{}^{6-}$ (47.6/theory and 42.4/experiment), can be used to identify the oxa- and thia-fullerenes.

3.4.3. B/N/P-Doped C_{60} and C_{70} Systems

When more than one atom in the fullerene cage is substituted by heteroatoms, an enormous number of isomers is theoretically possible.[139] This coupled with the experimental problems of purification and characterization of these doped fullerenes makes it difficult to determine the most favorable isomer.
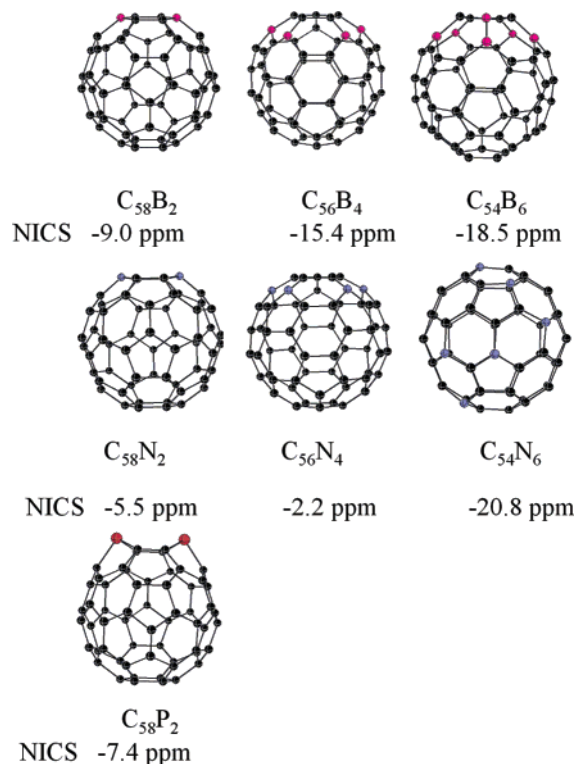
$C_{58}B_2$
NICS -9.0 ppm

$C_{56}B_4$
-15.4 ppm

$C_{54}B_6$
-18.5 ppm

$C_{58}N_2$
NICS -5.5 ppm

$C_{56}N_4$
-2.2 ppm

$C_{54}N_6$
-20.8 ppm

$C_{58}P_2$
NICS -7.4 ppm

Figure 16. Most stable structure for $C_{58}X_2$, $C_{56}X_4$, and $C_{56}X_6$ (X = B, N) and their NICS values computed NICS values at the cage center (ppm, at GIAO-B3LYP/6-31G*// B3LYP/6-31G*).

N-doped	-17.0	-16.0	-15.0
B-doped	-15.8	-13.4	-11.4
P-doped	-17.9	-16.5	-15.6

N-doped	-14.9	-11.9
B-doped	-10.1	-9.6
P-doped	-15.4	-14.0

Figure 17. Most stable structure for $C_{70-n}X_n$ (n = 2−10, X = N, B, P) and their NICS values computed NICS values at the cage center (ppm, at GIAO-HF/3-21G//MNDO).

most stable structures and their NICS values at the cage center (at GIAO-SCF/3-21G//MNDO level of theory). As compared with the endohedral chemical shift of C_{70} at the same level (−20.9 ppm; exp., −28.8 ppm), generally aromaticity decreases with increasing number of heteroatoms in the system. P-doped species are the most aromatic ones among N-, B-, and P-doped C_{70} systems, and the B-doped C_{70} exhibits the least electron delocalization.

3.4.4. BN-Doped C_{60} Systems

Among all of the 31 possible $C_{58}BN$ isomers, the lowest energy isomer has a BN edge at a hexagon−hexagon junction. The stabilities of the $C_{58}BN$ isomers decrease with increasing distance between the heteroatoms. Further computations show that N−N and B−B bonds should be avoided but that the BN unit is favorable in multiple BN-substituted fullerenes.

To study the effect of BN substitution on aromaticity, NICS values at the cage center of the BN-doped fullerenes **12**−**15** were computed (Table 9 and Figure 18). Among these, fullerenes **12** and **13** are the most stable isomers of $C_{58}BN$ and $C_{54}(BN)_3$, respectively. Compound **14** has two BN hexagons at opposite sides of C_{60}, while **15** has the maximum number of C_2 units replaced by BN units without generating direct B−B and N−N connections.

The heterofullerenes $C_{58}(BN)$ (**12**), $C_{54}(BN)_3$ (**13**), and $C_{48}(BN)_6$ (**14**) (Figure 18) are slightly more aromatic than C_{60} itself, and only $C_{12}(BN)_{24}$ (**15**) is less aromatic, as indicated by the calculated NICS values at the cage center.

Systematic theoretical studies of the hetero-fullerenes $C_{58}X_2$[127] and $C_{68}X_2$[128] (X = B, N, P) have been performed at semiempirical MNDO, AM1, and PM3 levels. For $C_{58}X_2$, the isomer corresponding to 1,4-substitution in the cyclohexatriene unit is the most stable among 23 possible isomers, and the stabilities decrease with increasing distance between the heteroatoms. Generally, the same 1,4-substitution pattern holds true for multiple substitution. According to the computed atomization energies, all of the heterofullerenes are less stable than the parent carbon fullerenes, and the stabilities decrease with increasing number of heteroatoms. Moreover, the redox characteristics of the fullerenes can be enhanced by doping. The heterofullerenes under investigation have somewhat smaller ionization potentials and bigger electron affinities relative to their all-carbon analogues thereby suggesting that it is easier to oxidize and reduce these doped fullerenes.

The most stable $C_{58}X_2$, $C_{56}X_4$, and $C_{54}X_6$ isomers are given in Figure 16, and their NICS values at the GIAO-B3LYP/6-31G*//B3LYP/6-31G* level are also given. The boron-substituted C_{60} is more aromatic than C_{60} itself. The aromaticity increases with incorporating more boron atoms into the cage, although the π-electron number decreases. For the nitrogen-substituted C_{60}, $C_{58}N_2$ is a little more aromatic than C_{60}, and $C_{56}N_4$ has the same aromatic character as C_{60}. The aromaticity of the 66 π-system $C_{54}N_6$ dramatically increases, with a NICS up to −20.8 ppm.

The 1,4-substitution pattern is also favorable energetically in B/N/P-doped C_{70} systems. Thus, para-substitution across the equatorial hexagons leads to the most stable isomers. Figure 17 summarizes the
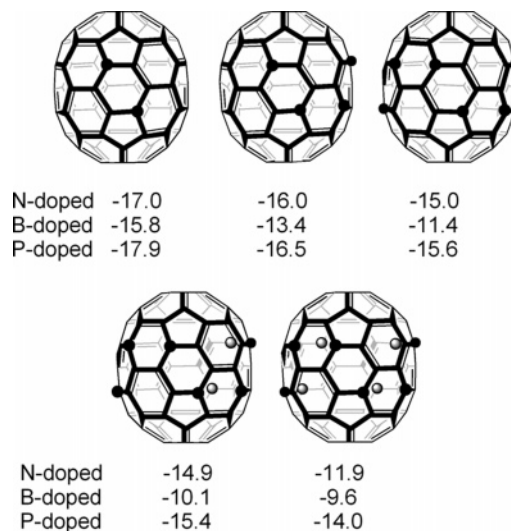
Table 9. NICS Values at the Center of BN Doped Fullerenes (at GIAO-HF/3-21G//B3LYP/6-31G*) (Experimental Helium Chemical Shifts Given in Parentheses)

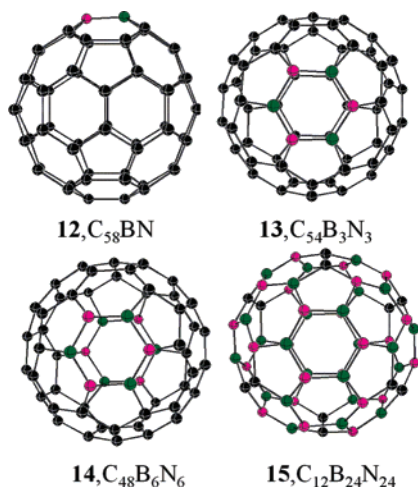| compound	NICS	compound	NICS
C_{60} (I_h)	−9.6 (−6.3)	C_{60}^{6-} (I_h)	−56.7 (−48.7)
$C_{58}BN$ (**12**, C_s)	−10.9	$C_{58}BN^{6-}$ (**12^{6-}**, C_s)	−25.3
$C_{54}(BN)_3$ (**13**, C_3)	−12.0	$C_{54}(BN)_3^{6-}$ (**13^{6-}**, C_3)	−13.1
$C_{48}(BN)_6$ (**14**, S_6)	−12.3	$C_{48}(BN)_6^{6-}$ (**14^{6-}**, S_6)	−44.1
$C_{12}(BN)_{24}$ (**15**, S_6)	−7.8	$C_{12}(BN)_{24}^{6-}$ (**15^{6-}**, S_6)	−9.0

Figure 18. B3LYP/6-31G* optimized structures of C_{60} doped with various numbers of BN units.

The NICS value of 12^{6-} is about only half that of C_{60}^{6-}, while 13^{6-} and 15^{6-} have nearly the same values as their neutral counterparts. Only 14^{6-} exhibits a highly negative NICS value in this series. This probably arises from a rather even distribution of the negative charges as for C_{60}^{6-}.

3.4.5. $C_{48}N_{12}$ and Its Analogues

Recently, a new azafullerene ($C_{48}N_{12}$) was identified, remarkably, inside an onion-structured, nitrogen-doped, fullerene-like material.[106] This preparation of $C_{48}N_{12}$ as the "soccer ball" core in cross-linked carbon nitride nanoonions is an exciting achievement owing to the implications for wear-protective coatings, displays, and other promising applications.

The form (**I**) of $C_{48}N_{12}$ (**16**) (Figure 19) has S_6 symmetry with separated and evenly spaced nitrogen atoms (i.e., one nitrogen in each pentagon and the nitrogens as far away as possible) and was first considered to be the most likely stable isomer, since repulsive nitrogen−nitrogen interactions can be minimized.[106,140] However, theoretical studies on $C_{48}N_{12}$ indicate that isomer **I** is not the most stable isomer of $C_{48}N_{12}$.[141] Thus, a second S_6 symmetrical form (**II**), $C_{48}N_{12}$ (**17**) (Figure 19), was suggested as follows: At B3LYP/6-31G*, $C_{48}N_{12}$ (**II**) is 13.2 kcal/mol lower in energy than **I** and has a much larger HOMO−LUMO energy gap (2.74 vs 1.78 eV).[142] Note that **II** also has minimized repulsion between the nitrogen atoms but to a lesser extent than in **I**.

The higher stability of isomer **II** is governed by combined local and global aromatic stabilization. Extended aromaticity is maximized in **II**, which has a structure derived from triphenylene units fused to
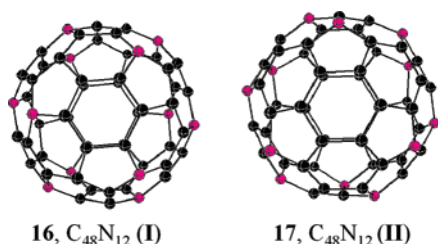
five-membered heterocycles containing one nitrogen per ring. The extended local aromaticity of the all-carbon hexagon rings in the triphenylene units and the adjacent N-substituted pentagons can be confirmed by the computed NICS values at the ring centers.[143] Moreover, $C_{48}N_{12}$ (**II**) has much stronger global aromaticity than $C_{48}N_{12}$ (**I**), as assessed by the NICS value at the cage center of −5.8 and 0.6 ppm, respectively. Thus, the decisive factor for the higher stability of **II** is not only the local aromaticity in the triphenylene units but also the global aromaticity of the whole system.

The higher aromaticity of $C_{48}N_{12}$ (**II**) is also indicated by the computed magnetizability ab initio ring current plot by Viglione and Zanasi.[144] The ring current plots show that the two isomers have a very different magnetic behavior. Thus, the thermodynamically less stable isomer (**I**) is characterized by paratropic π-electron ring currents, which largely reduce the overall molecular diamagnetism. However, the more stable isomer (**II**) is characterized by diatropic π-electron ring currents flowing on the external hexagons of each triphenylene-type unit. Despite the computed magnetizability and central magnetic shielding, **II** is found to be no more aromatic than C_{60}.

The electronic structure as well as the magnetic and optical properties of $C_{48}N_{12}$ (**II**) have been extensively studied theoretically after this more stable isomer was found.[145]

Aromaticity also stabilizes the $C_{48}X_{12}$ (X = B,[146] P, Si)[143] heterofullerenes significantly similar to $C_{48}N_{12}$. Regardless of the dopants, the global aromaticity of **II** as assessed by NICS at the cage centers is stronger than that of **I**, and **II** is more stable than **I**.

Thus, besides the principle that the repulsive interactions between heteroatoms should be minimized, the above shows that aromatic stabilization should be one factor to be considered when predicting the most stable isomers of heterofullerenes.

3.4.6. Heteroatom-Substituted Smaller Fullerenes

With 32 π-electrons, $C_{28}N_4$ (**18**, T_d) follows the $2(N + 1)^2$ rule for maximal spherical aromaticity, and its NICS value at the cage center is −27.8 ppm (at the GIAO-B3LYP/6-31G*//B3LYP/6-31G* level). Moreover, all of the 5-MRs and 6-MRs are aromatic. This suggests a high delocalization of the electrons rather than isolated electron lone pairs at the nitrogen atoms. However, its isoelectronic analogue $C_{24}P_4$ has a 9.6 ppm NICS at the cage center. This indicates $C_{24}P_4$ to be nonaromatic or weakly antiaromatic as well as localization of the phosphorus lone pairs. Because of the incomplete filling of the valence orbitals in T_d symmetry, $C_{24}B_4$ is antiaromatic (NICS 21.1 ppm at the cage center).


Figure 19. Optimized structures of isomer **I** (left) and **II** (right) of $C_{48}N_{12}$.
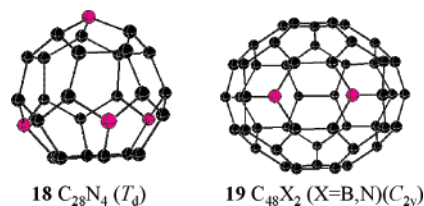
A systematic investigation on all of the possible dinitrogen/boron-substituted D_{5h} C_{50} isomers shows that the 1,4-substitution in the 6-MR located on the equator leads to the most stable isomer **19**.[137c] The NICS values at the cage center are −14.5 and −27.0 ppm for $C_{48}B_2$ and $C_{48}N_2$, respectively, at GIAO-B3LYP/6-31G*//B3LYP/6-31G* level (−14.6 and −20.8 ppm, respectively, at the GIAO-HF/3-21G//AM1 level).[137c]

4. Aromaticity of Inorganic Cages

4.1. Deltahedral Boranes and Related Boron-Based Clusters

Aromaticity is not limited to organic chemistry. For example, boron-based clusters, especially the deltahedral *closo*-boranes $B_nH_n^{2-}$ ($6 \leq n \leq 12$) and their carborane analogues (Figure 5), are accepted as aromatic.[147]

The 1,5-$X_2B_3H_3$ (X = N, CH, P, SiH, BH$^-$) members of the *closo*-borane family are unique, since both classical (localized, **20**) and nonclassical (delocalized, **21**) bonding alternatives are possible, and the form most closely approximating the true electronic nature has long been disputed.[148] Schleyer and co-workers[148] studied this problem and found that various aromaticity criteria support the nonclassical bonding description. Among the five-vertex deltahedra, $B_5H_5^{2-}$ has the most strongly diatropic NICS (−28.1 ppm) and 1,5-$N_2B_3H_3$ (−10.2 ppm) has the smallest. Besides diatropically shielded NICS values, the 3D aromaticity of the 1,5-$X_2B_3H_3$ cages is also indicated by large aromatic stabilization energies, exalted diamagnetic susceptibilities.

20   **21**

X=N,CH,P,SiH and BH$^-$
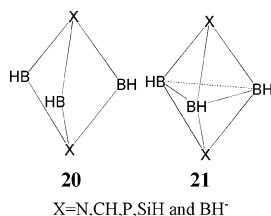
Larger *closo*-boranes and its isoelectronic analogues are also aromatic, as confirmed by highly negative NICS values at the cage centers (Figures 20 and 21 and Table 10).[149] Note that the six- and 12-vertex systems have much more negative NICS
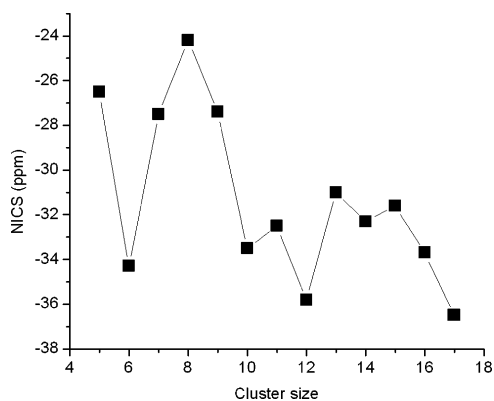

Figure 20. Plot of NICS at the center of *closo*-$B_nH_n^{2-}$ (n = 5−17) (at GIAO-HF/ 6-31+G*//B3LYP/6-31G*).
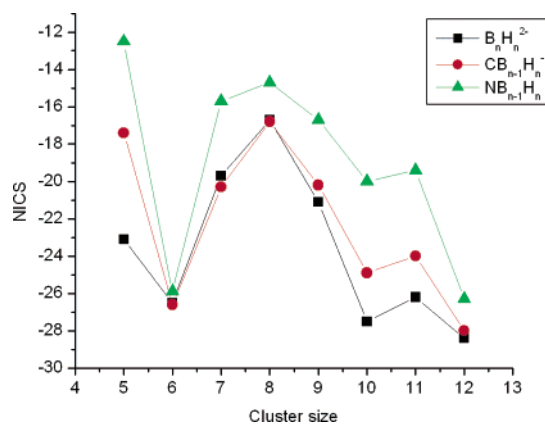

Figure 21. Plot of NICS at the center of *closo*-$B_nH_n^{2-}$ and the most stable *closo*-$CB_{n-1}H_n^-$ and *closo*-$NB_{n-1}H_n$ (from Table 10) vs cluster size.

Table 10. Nucleus Independent Chemical Shifts (NICS, ppm) of *closo*-Borane Dianions, $B_nH_n^{2-}$, the Most Stable *closo*-Monocarbaboranes, $CB_{n-1}H_n^-$, and the *closo*-Azaboranes, $NB_{n-1}H_n$ (at CSGT-B3LYP/ 6-311+G//B3LYP/6-311+G**; Also See Figures 21 and 22)**

cluster	$B_nH_n^{2-}$	$CB_{n-1}H_n^-$	$NB_{n-1}H_n$
5 vertex	−23.1	−17.4	−12.5
6 vertex	−26.5	−26.6	−25.9
7 vertex	−19.7	−20.3	−15.7
8 vertex	−16.7	−16.8	−14.7
9 vertex	−21.1	−20.2	−16.7
10 vertex	−27.5	−24.9	−20.0
11 vertex	−26.2	−24.0	−19.4
12 vertex	−28.4	−28.0	−26.3
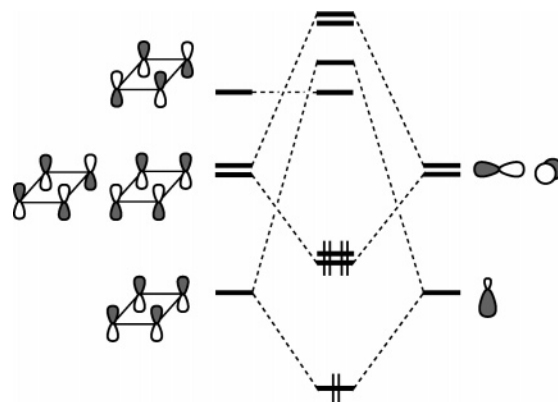
Figure 22. Qualitative MO diagram showing the origin of aromatic character: six interstitial electrons in the stabilized orbitals (a_1 and e in C_{4v} symmetry) resulting from the interaction of the ring π-orbitals with the orbitals of the capping unit. Reprinted with permission from ref 151. Copyright 2004 RSC.

values than their neighbors. This is peculiar and deserves more investigation.

Molecules in the *nido* forms can also be aromatic. In 1982, Jemmis and Schleyer proposed the "six interstitial electron" rule[150] as a 3D extension of Hückel's ($4n + 2$) π-electron rule for planar systems. The origin of aromatic character of the six interstitial electrons can be understood through the qualitative MO diagram in Figure 22, which summarizes the interactions between a C_4H_4 base and a capping atom. The cap−ring interactions result in three stabilized MOs; just as in benzene, the six electrons
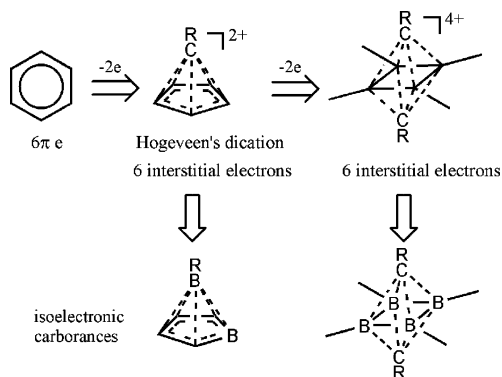
Figure 23. Procedure to transfer the six π-electron benzene to 3D molecules with six interstitial electrons.

occupying these orbitals are the "interstitial electrons".

There are many known 3D aromatics with six interstitial electrons (e.g., **22**−**25**). This "six interstitial electron" rule can also be considered as an extension of Hückel's $4N + 2$ rule. Figure 23 shows how we can transfer the six π-electron benzene to 3D molecules with six interstitial electrons. Compounds **26**−**29** are more examples, and their aromaticity is indicated by their highly negative NICS values at the cage centers.
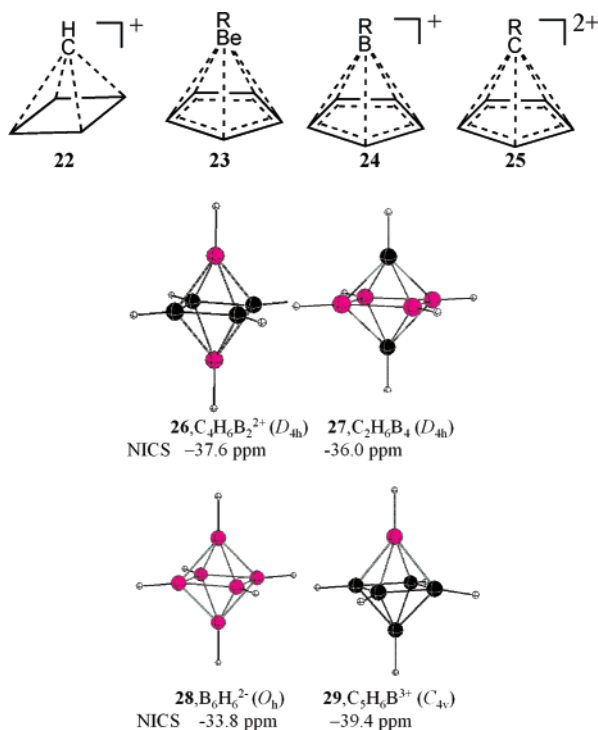

Most recently, the isoelectronic series $C_nH_nP_{5-n}^+$ as *nido* clusters are also characterized as highly delocalized systems.[151] Within isomeric *nido* clusters, a strong correlation between the total energy and the NICS indicates that 3D aromaticity plays a significant role in determining the stability of the cluster.

4.2. Some Well-Known Inorganic Clusters: Zintl Ions and Their Analogues

In 2001, Hirsch et al. successfully extended the $2(N + 1)^2$ electron-counting rule for I_h symmetrical

Table 11. Calculated NICS (ppm) Values for E$_4$ and E$_4^{4-}$ (T_d) Clusters

E$_4^a$	N$_4$	P$_4$	As$_4$	Sb$_4$	Bi$_4$
NICS^{b,c}	−71.4	−54.6	−55.3	−40.3	−37.3

E$_4^{4-}$ ^{a}	Si$_4^{4-}$	Ge$_4^{4-}$	Sn$_4^{4-}$	Pb$_4^{4-}$
NICS^{b,c}	−41.9	−39.9	−32.3	−29.1

^{a} All are energy minima. ^{b} At the cage center. ^{c} GIAO-MP2/6-31G*//MP2/6-31G* for E = N, P, As, Si and GIAO-MP2/LANL2DZp// MP2/LANL2DZp for E = Ge, Sn, Pb, Sb, Bi.
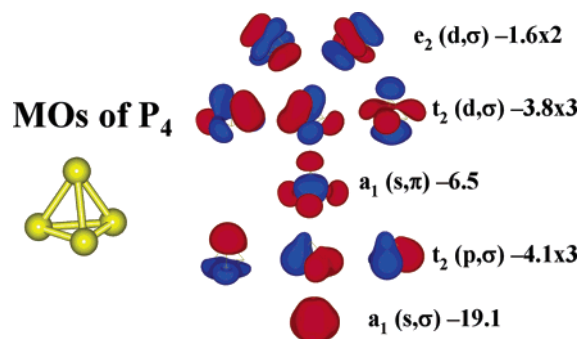

Figure 24. MO-NICS of P$_4$ GIAO-PW91/6-311+G*//B3LYP/6-311+G* level. The a$_1$ (s,π) orbital is a cluster π-orbital. The endohedral overlap of atomic p orbitals is much more pronounced than the exohedral overlap owing to the pyramidalization of the cluster atoms.

fullerene spherical systems to a set of well-known inorganic cages,[152] including the tetrahedral E$_4$ clusters (E = N, P, As, Sb, and Bi) and the isoelectronic tetrahedral cluster ions E$_4^{4-}$ (E = Si, Ge, Sn, and Pb) as well as the E$_9^{4-}$ (E = Si, Ge, Sn, Pb) and Bi$_9^{5+}$ clusters with D_{3h} and C_{4v} symmetry and the E$_9^{2-}$ (E = Ge, Sn, Pb) and Bi$_9^{7+}$ clusters with D_{3h} symmetry. Note that N$_4$ (T_d) is unstable against dissociation although it is highly aromatic, since other factors dominate its stability.

The pronounced diamagnetic ring currents in the tetrahedral clusters N$_4$, P$_4$, As$_4$, Sb$_4$, and Bi$_4$ and their isoelectronic analogues Si$_4^{4-}$, Ge$_4^{4-}$, Sn$_4^{4-}$, and Pb$_4^{4-}$ are demonstrated by the highly negative NICS values of all clusters (Table 11). To get more insight, MO-NICS analysis[153] was performed. MO-NICS dissects the total NICS into the contributions from each canonical MO. The σ-system with $2(N_\sigma + 1)^2$ σ-electrons ($N_\sigma = 2$) consists of a cluster S orbital, three degenerate cluster P orbitals, and two sets of cluster D orbitals (e and t$_2$), while the π-system contains $2(N_\pi + 1)^2$ π-electrons ($N_\pi = 0$). MO-NICS shows that all of the σ- and π-orbitals have negative NICS contributions, and the overall aromaticity of P$_4$ is dominated by σ-aromaticity (Figure 24). Thus, the angular momenta are symmetrically distributed in the complete filling of all σ- and π-shells and the clusters are characterized as doubly spherically aromatic.[154] Note that the NICS contribution decreases as the number of nodes of the MOs is increased. Thus, the lower the energies, the larger are the diamagnetic NICS contributions.

A set of less symmetrical nine-vertex Zintl ion clusters[155] (Figures 25 and Table 12) are also aromatic. The D_{3h} symmetrical *closo* cages E$_9^{4-}$ (E = Si, Ge, Sn, Pb) and Bi$_9^{5+}$, considered as energy minima,
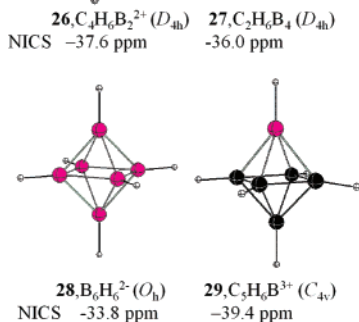
Table 12. Calculated NICS Values (δ, ppm)[a] and Relative Energies (E_{rel}, kcal/mol) for E_9^{4-} (E = Si, Ge, Sn, Pb), E_9^{2-} (E = Ge, Sn, Pb), Bi_9^{5+}, and Bi_9^{7+}

species	symmetry	NICS	E_{rel}
Si_9^{4-}	closo (D_{3h})	−87.7	0.0
	nido (C_{4v})	−86.7	1.1
Ge_9^{4-}	closo (D_{3h})	−81.0	0.0
	nido (C_{4v})	−80.3	0.8
Sn_9^{4-}	closo (D_{3h})	−68.9	0.0
	nido (C_{4v})	−68.2	0.8
Pb_9^{4-}	closo (D_{3h})	−68.9	0.0
	nido (C_{4v})	−68.3	1.0
Bi_9^{5+}	closo (D_{3h})	−28.1	0.0
	nido (C_{4v})	−28.1	0.4
Ge_9^{2-}	closo (D_{3h})	−43.0	
Sn_9^{2-}	closo (D_{3h})	−38.3	
Pb_9^{2-}	closo (D_{3h})	−39.6	
Bi_9^{7+}	closo (D_{3h})	−26.8	

[a] GIAO-MP2/6-31G*//MP2/6-31G* for E = Si and GIAO-MP2/LANL2DZp//MP2/LANL2DZp for E = Ge, Sn, Pb, Sb, Bi.
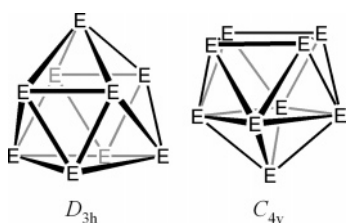
Figure 25. Frameworks of nine atom clusters with D_{3h} and C_{4v} symmetries.
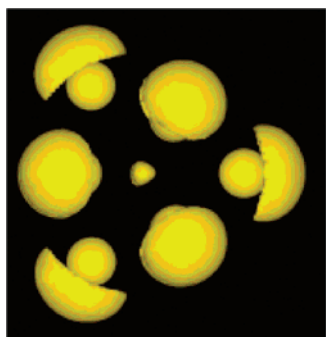
Figure 26. ELF surface ($\eta^{iso} = 0.55$) in Bi_9^{5+} (D_{3h}) looking down the 3-fold axis. The 3c−2e bond in the upper triangle is clearly displayed. Reprinted with permission from ref 157. Copyright 2001 Wiley.

do not obey the Wade rules.[156] A reason for their abnormal stability could be their double spherical aromaticity arising from 32 σ- ($N_\sigma = 3$) and eight π-electrons ($N_\pi = 1$). Unlike the T_d clusters, the MO schemes of these Zintl ions are characterized by a variety of crossovers between the subshells and a considerable decrease in orbital degeneracy of the completely filled σ (S, P, D, F)- and π (S, P)-levels. However, they still exhibit very high NICS values approaching those of some highly aromatic fullerenes with closed π-shells. The corresponding nido structures with C_{4v} symmetry are slightly less stable (Figure 25 and Table 12).

The electron delocalization in the bismuth cluster polycations $Bi_n^{(n-2)+}$, $Bi_n^{(n-4)+}$, and $Bi_n^{(n-6)+}$ has been studied. The bonding in these bismuth polycations was found to be characterized by a high degree of electron delocalization and "3D aromaticity".[157] For example, in Bi_9^{5+} (D_{3h} in Figure 25), the two three-

center two-electron (3c−2e) bonds in each of the two peripheral triangles become very distinct in the ELF (electron localization function) at $\eta^{iso} < 0.6$, as illustrated in Figure 26 ($\eta^{iso} = 0.55$) looking down the 3-fold axis. No localized regions, except for the two 3c−2e bonds of the peripheral triangles, can be seen until the η^{iso} value is very close to 0.50. Six 3c−2e bonds start to appear at $\eta^{iso} = 0.53$. Note that the ELF is normalized and runs between 0 and 1; high values of η correspond to a high degree of localization, while $\eta = 0.5$ corresponds to the perfectly delocalized homogeneous electron gas, used as a reference state.

4.3. Antiaromaticity in Bare Deltahedral Clusters

The bare clusters Si_6^{2-} (O_h) and Si_{12}^{2-} (I_h) satisfy Wade's and Hirsch's rules as isoelectronic analogues of closo $B_nH_n^{2-}$. However, Si_6^{2-} and Si_{12}^{2-} were found to be antiaromatic as indicated by comparing the computed NICS values at the cage centers of closo-$B_nH_n^{2-}$ and the corresponding Si_n^{2-} cage centers (Figure 27).[158] With some variations, the isoelectronic $B_nH_n^{2-}$ and Si_n^{2-} series have similar diatropic NICS(0) values except for two completely unexpected exceptions. Remarkably and completely different from their closo borane counterparts, the most symmetrical octahedral Si_6^{2-} and icosahedral Si_{12}^{2-} clusters exhibit paratropic NICS (0) values characteristic of antiaromaticity.

This behavior can be explained by analyzing the dissected NICS (0) contributions to the total NICS(0) values from the individual bonding MOs (Figure 28). The mixing of the external hydrogen orbitals with the symmetry adapted skeletal MOs of $B_6H_6^{2-}$ lowers their energies relative to the corresponding lone pair-dominated Si_6^{2-} MOs. This affects the magnitude of the t_{1u} orbital contributions sufficiently to change the sign of total NICS (0) from negative (diatropic) in $B_6H_6^{2-}$ to positive (paratropic) in Si_6^{2-}.

The contrast between icosahedral $B_{12}H_{12}^{2-}$ and Si_{12}^{2-} is even more pronounced: The antiaromaticity of Si_{12}^{2-} also is much greater than that of Si_6^{2-} (Figure 27). The highly paratropic 5-fold degenerate h_g MO set of Si_{12}^{2-} has a larger effect on the total NICS (0) than the 3-fold degenerate t_{1u} orbitals in Si_6^{2-}, as well as the h_g MO set of $B_{12}H_{12}^{2-}$ (Figure 28).
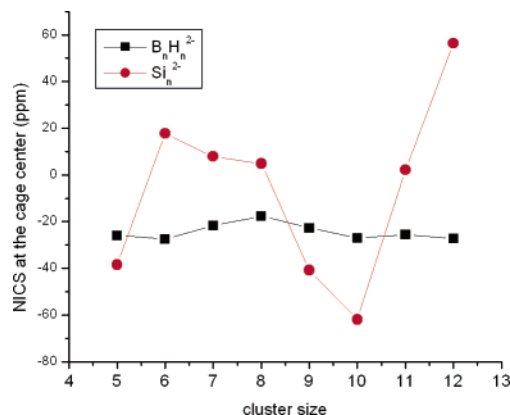
Figure 27. NICS values at the cage centers of the closo-$B_nH_n^{2-}$ and the corresponding Si_n^{2-} clusters at the GIAO-PW91/IGLOIII level with additional s and p diffuse functions for silicon.
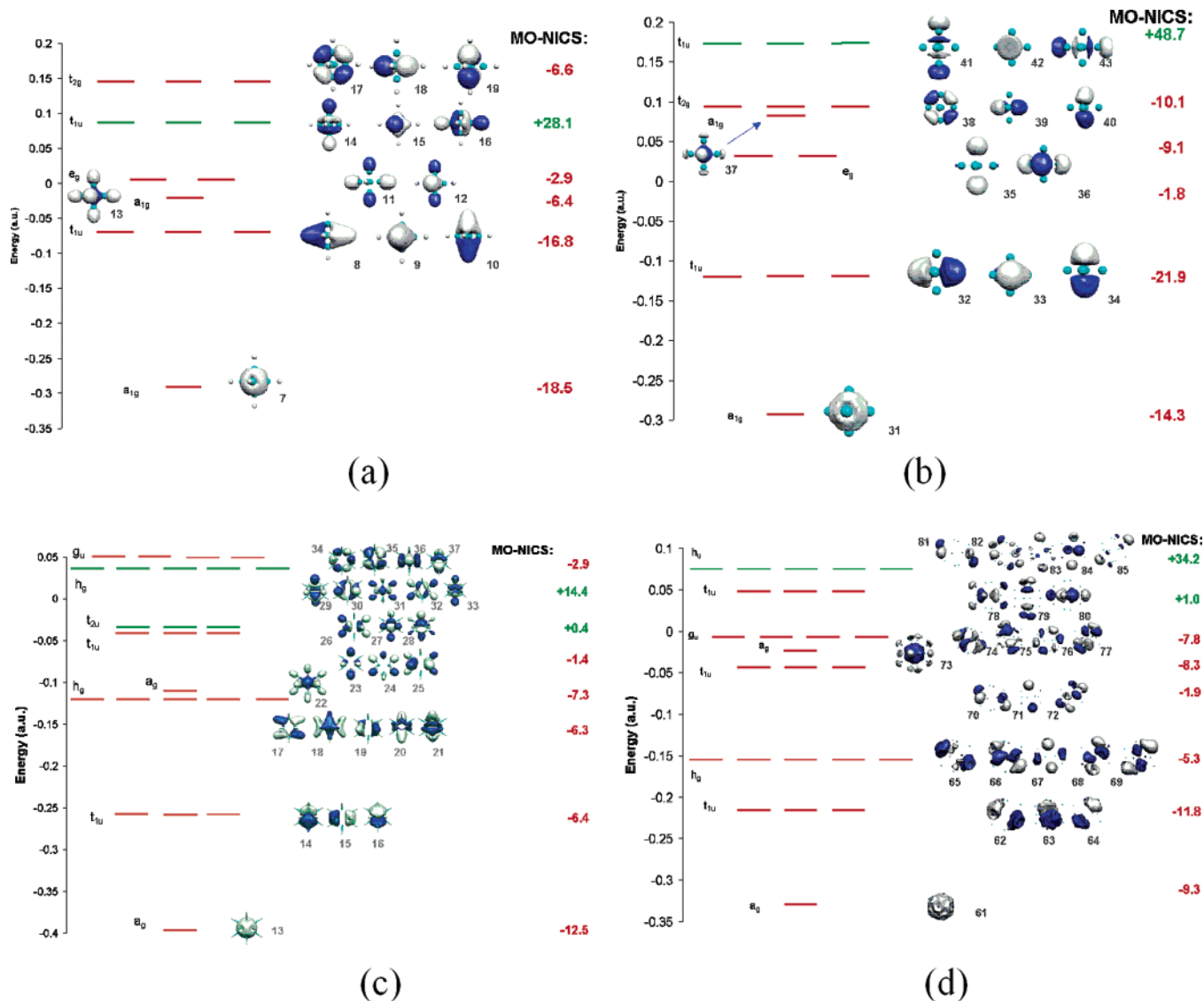
Figure 28. MO-NICS of (a) $B_6H_6^{2-}$, (b) Si_6^{2-}, (c) $B_{12}H_{12}^{2-}$, and (d) Si_{12}^{2-}.

The aromaticity of bare deltahedral group 14 clusters (E_n^{2-}, $n = 5-12$, E = Si, Ge, Sn, Pb) has also been evaluated both experimentally using an endohedral aluminum cation (Al^{3+}) in clusters with sufficiently large cavities (Sn_{10}^{2-}, Pb_{10}^{2-}, and E_{12}^{2-}) and theoretically using NICS.[159] The aromatic character of such deltahedra has direct consequences in these related endohedrally encapsulated species. A strong correlation exists between computed (anti)aromaticity and experimental abundance providing that the cavity is large enough. For example, Pb_{10}^{2-} (D_{4d}) and Pb_{12}^{2-} (I_h) are aromatic and have a cavity to accommodate a guest atom or ion. Accordingly, $AlPb_{10}^+$ (**30**) and $AlPb_{12}^+$ (**31**) were generated by Neukermans et al.[159] as magic clusters in the gas phase, and [Ni@Pb$_{10}$]$^{2-}$ (**32**) and [Pt@Pb$_{12}$]$^{2-}$ (**33**) were prepared by Eichhorn and co-workers[160] using wet chemistry. More endohedral Zintl ions can be expected by taking advantage of the aromaticity of the bare Zintl ion cages.[161] However, structural criteria are not sufficient in characterizing aromaticity for the species studied. While E_6^{2-} (O_h) is highly antiaromatic, there are no competing low energy alternatives. Therefore, the E_6^{2-} (O_h) set provides promising synthetic

targets for characterizing experimentally genuine antiaromatic metal clusters. Moreover, it strongly indicates that NICS computations not only give numbers but also are useful tools to design stable clusters.

30 AlPb$_{10}^+$ (D_{4d})   31 AlPb$_{12}^+$ (I_h)

32 [Ni@Pb$_{10}$]$^{2-}$ (D_{4d})   33 [Pt@Pb$_{12}$]$^{2-}$ (I_h)

4.4. Substituent Effects in Inorganic Cage Compounds

Most recently, King, Schleyer, and co-workers have found that substituent groups also have a significant

Figure 29. Comparison of NICS for boron clusters: top row nine vertex D_{3d} tricapped trigonal prismatic clusters; bottom row, four vertex T_d tetrahedral clusters. Reprinted with permission from ref 162. Copyright 2004 Wiley.

effect on cage compounds such as *closo*-boranes.[162] Neutral B_8Cl_8 and B_9Cl_9 are well-known,[163] but B_8H_8 and B_9H_9 have not been observed. As illustrated by the comparison below for D_{3h} B_9F_9 and $B_9H_9{}^{2-}$ (both diatropic, red dots) with B_9H_9 (paratropic, green dots), NICS shows the halo derivatives to be aromatic but the neutral hydrides to be antiaromatic (Figure 29). Tetrahedral B_4H_4 and B_4F_4 behave analogously. Despite the apparent antiaromaticity of the p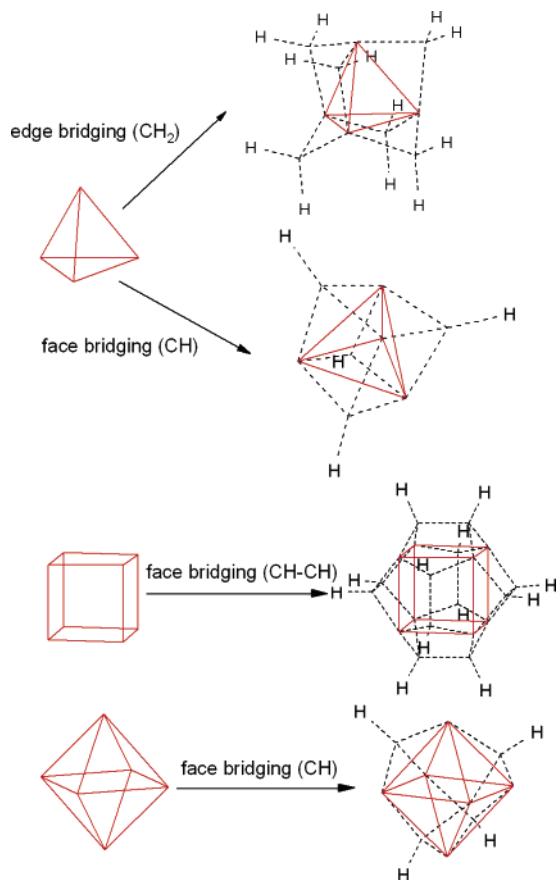arent B_4H_4 (T_d) cluster, an alkyl derivative, tetra-*tert*-butyltetraboratetrahedrane $B_4(tBu)_4$, has been reported,[164] which suggests the importance of the substituent effect.

An MO-NICS analysis reveals that some of the cage orbitals are strongly paratropic (like the HOMO of cyclobutadiene). The hydrogens of $B_{12}H_{12}{}^{2-}$ and the halogens of B_8Cl_8 and B_9Cl_9 withdraw skeletal electrons and reduce the paratropicity of these MOs substantially and selectively, thus allowing the influence of the diatropic MOs to dominate.

5. Spherical Homoaromaticity

Homoaromaticity[165] can also exist in three dimensions. Various spherical homoaromatic molecules have been designed guided by the $2(N + 1)^2$ electron-counting rule for spherical aromatic molecules.[166] The same procedure also has been applied to their sila- and germa-analogues rich in group 14 elements (Figure 30).[167]

These spherical homoaromatic systems are designed containing cubane, dodecahedrane, and adamantane frameworks and consist of two or eight mobile electrons (Figure 31). Conceptually, such systems can be constructed by alkylene bridging of smaller, highly symmetrical carbon cages. For example, adding six edge-bridging methylenes to a C_4 tetrahedron gives the adamantane framework. Removal of two electrons leads to the 1,3-dehydro-5,7-

Figure 30. Various spherical homoaromatic systems.

adamantanediyl dication ($C_{10}H_{12}{}^{2+}$, **34**) reported by Schleyer et al.[168] This system represents the 3D four-center two-electron (4c−2e) homoaromatic prototype. A series of isoelectronic charged and neutral 4c−2e species based on this framework also are homoaromatic.[169]

A peculiar feature of these novel aromatic systems is that each set has complete spherical homoaromaticity; that is, all of the sp² carbons (or Si and Ge atoms) in the highly symmetrical frameworks are separated by one or two sp³-hybridized atoms.

All of these species have significantly negative NICS values and large HOMO−LUMO gaps (see Table 13).

The homoaromatic character of 3D species arises from their closed π-electron shell structures. As an example, the closed π-shell of **44** is shown by the MO scheme in Figure 32. Incomplete filling of the shells reduces the aromatic character as in the doubly charged analogues, $C_{20}H_{12}{}^{2+}$ (D_{2h}) and $C_{20}H_{12}{}^{2-}$ (D_{2h}) (with six and 10 electrons, respectively).

According to Wade's rule, $Si_8{}^{2-}$ and $Ge_8{}^{2-}$ should adopt a bisdisphenoidal structure with D_{2d} symmetry. However, the T_d isomers, $Si_8{}^{2-}$ and $Ge_8{}^{2-}$, are more stable than the D_{2d} bisphenoid dianions as well as the dianions of the lowest energy neutral analogues. The two extra electrons in $Si_8{}^{2-}$ and $Ge_8{}^{2-}$ thus change the stability order of the neutral cluster

Figure 31. Construction principles for spherical homo-aromatics. Reprinted with permission from ref 166. Copyright 2002 Wiley.

Table 13. Homoconjugative Distances (Å), HOMO−LUMO Gaps (eV), and NICS Values (ppm) at the Cage Center of the Spherical Homoaromatic Systems (See Figure 30)[166,167]

species	X−X^a	gap^a	NICS^b
34 ($C_{10}H_{12}^{2+}$, T_d)	2.103	6.48	−46.2
35 ($C_6Si_4H_{12}^{2+}$, T_d)	2.885	4.26	−29.2
36 ($C_6Ge_4H_{12}^{2+}$, T_d)	3.012	4.39	−33.2
37 ($C_8H_4^{2+}$, T_d)	1.975	5.77	−33.4
38 ($C_4Si_4H_4^{2+}$, T_d)	2.650	3.87	−14.4
39 ($Si_8H_4^{2+}$, T_d)	3.156	3.17	−8.0
40 ($Ge_8H_4^{2+}$, T_d)	3.370	2.81	−8.8
41 (C_8^{2-}, T_d)	2.067	3.99	−33.6
42 (Si_8^{2-}, T_d)	2.819	3.25	−18.5
43 (Ge_8^{2-}, T_d)	3.050	3.19	−17.0
44 ($C_{20}H_{12}$, T_h)	2.249	2.47	−32.2
45 ($C_{12}Si_8H_{12}$, T_h)	2.991	2.05	−33.0
46 ($C_{12}Ge_8H_{12}$, T_h)	3.045	2.26	−33.7
47 ($C_{20}H_{24}$)	2.458	2.00	−15.8
48 ($C_{12}Si_8H_{24}$)	2.621	2.05	−20.3
49 ($C_{12}Ge_8H_{24}$)	2.702	3.56	−18.6
50 ($C_{10}H_4^{4+}$, T_d)	2.207	4.69	−58.6
51 ($C_4Si_6H_4^{4+}$, T_d)	3.201	1.44	−17.1
52 ($C_4Ge_6H_4^{4+}$, T_d)	3.296	2.47	−18.6
53 ($Si_{10}H_4^{4+}$, T_d)	3.759	2.55	−25.4
54 ($Ge_{10}H_4^{4+}$, T_d)	3.760	2.84	−32.9
55 ($C_6B_4H_4$, T_d)	1.871	7.28	−38.0
56 ($Si_6B_4H_4$, T_d)	2.958	3.48	−41.6
57 ($Ge_6B_4H_4$, T_d)	2.974	3.84	−42.5

^{a} At the B3LYP/6-31G* level. ^{b} At the GIAO-B3LYP/6-31G*// B3LYP/6-31G* level.

isomers. This confirms further the homoaromatic stabilization from the two new π-electrons, since the underlying skeleton is not the most stable. Thus, in
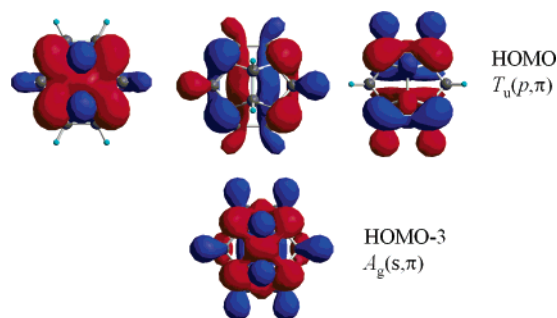

Figure 32. Representation of cluster s,π and p,π orbitals of $C_{20}H_{12}$ (T_h).

addition to the formerly used endohedrally doping strategy,[170] spherical homoaromaticity serves as another way to stabilize silicon and germanium clusters.

6. σ-Aromaticity in 3D Systems

6.1. Saturated Hydrocarbons

Aromaticity also governs the stability of systems with only σ-electrons, although to much lesser extent. One well-known example is cyclopropane, which is stabilized both by σ-aromaticity[171] involving the six electrons in its strained C−C bonds and by C−H bond strengthening, owing to the sp²-like carbon hybridization. The σ-aromaticity stabilization energy is computed to be 11.3 kcal/mol[172] as compared with 33.2 kcal/mol for benzene.[173]

Most recently, cyclobutane is characterized as σ-antiaromatic by its large and paratropic NICS contribution from the CC(σ) bonds (+15.2 ppm).[174] The diatropic ring current in the three-membered ring and the paratropic ring current in the four-membered ring persist in the cage hydrocarbons. For example, with four fused cyclopropane rings, tetrahedrane (**58**) is super σ-aromatic, with very large NICS (0) (at the cage center) and CC(σ) (−48.3 and −37.2, respectively). However, cubane (**59**) with six fused cyclobutane rings is highly anti-σ-aromatic,

58, C_4H_4 (T_d)   **59**, C_8H_8 (O_h)

60, Au_{20} (T_d)   **61**, Au_{32} (I_h)
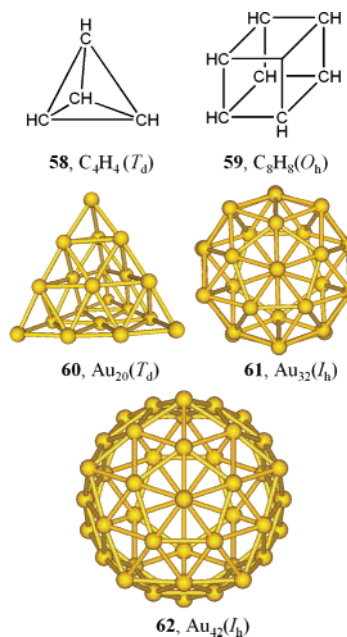

62, Au_{42} (I_h)

Table 14. Bond Length (*R*, Å), Number of Imaginary Frequencies (NImag), and NICS Values (ppm)^{a,b} of nearly Spherical Hydrogen and Lithium Clusters (Unpublished Results)

species	symmetry	NImag	R	NICS (0)
H_4^{2+}	T_d	3	1.257	−27.0
H_6^{2-}	O_h	9	1.417	−57.7
H_8	O_h	3	1.141	−65.3
H_{12}^{4+}	I_h	19	1.581	−49.9
H_{20}^{2+}	I_h	8	1.172	−79.2
H_{32}	I_h	40	1.299	−132.3
Li_4^{2+}	T_d	0	3.426	−11.5
Li_6^{2-}	O_h	2	2.987	−17.3
Li_8	O_h	6	2.811	−25.6
Li_{12}^{4+}	I_h	12	3.711	−19.4
Li_{20}^{2+}	I_h	24	2.882	−34.0
Li_{32}	I_h	11	3.066	−53.8

^{a} At GIAO-B3LYP/6-311++G(d,3pd)//B3LYP/6-311++G-(d,3pd) for H_n (n < 20); at GIAO-B3LYP/6-31G**//B3LYP/6-31G** for H_n (n ≥ 20). ^{b} At GIAO-B3LYP/6-311+G*//B3LYP/6-311+G* for Li_n (n < 20); at GIAO-B3LYP/6-31G*//B3LYP/6-31G* for Li_n (n ≥ 20).

with a NICS (0) of +23.1 ppm at the cage center, of which 21.6 ppm arises from the CC(σ) contributions. The strong face-localized paratropic ring currents in cubane are also found by Fowler et al.[175] using the current density plots.

6.2. Hydrogen and Lithium Clusters

Three-dimensional hydrogen clusters, e.g., the T_d symmetrical H_4^{2+} and the O_h symmetrical H_8 and H_6^{2-} clusters in which the valence shells are fully occupied by two and eight σ-electrons, respectively, have been studied. The aromaticity of these clusters has previously been characterized by the computed diamagnetic susceptibility exaltations[15] and is now confirmed by the highly negative NICS values in the cluster centers (Table 14).

The T_d symmetrical H_4^{2+} and Li_4^{2+} are the smallest possible 3D σ-electron systems. Because H_4^{2+} and Li_4^{2+} have two σ-electrons and can follow the $4N + 2$ Hückel rule, one may expect that they prefer the planar D_{4h} symmetrical square. However, computations show that the T_d structures are more favorable, by 20.1 and 13.4 kcal/mol for H_4^{2+} and Li_4^{2+}, respectively. Moreover, despite the large Coulomb repulsion, Li_4^{2+} (T_d) is confirmed to be a true local minimum. The pronounced negative NICS values at the center of the H_4^{2+} and Li_4^{2+} cages, namely, −27.0 and −11.3 ppm, respectively, indicate their remarkable aromaticity. Recently, Boldyrev et al.[176] showed that a quite high resonance energy exists for Li_4^{2+} (T_d), and the aromaticity of H_4^{2+} (T_d) has previously been characterized by the computed diamagnetic susceptibility exaltations ($\Lambda = -15.6$ ppm cgs), higher stability, and magnetic properties.[177]

The higher analogues are computed to be higher saddle points. However, their notably negative NICS values at the cage centers clearly show their strong aromaticity.

6.3. Gold Clusters

Gold often shows unusual and sometimes surprising chemical and physical properties as compared to
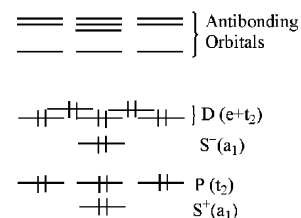
Figure 33. MO energy levels in an Au_{20} tetrahedron showing both the spherical harmonic and the group theoretical labels for the bonding orbitals.

the lighter group 11 elements (gold anomaly), since its properties are strongly influenced by relativistic effects.[178] Gold nanomaterials have recently attracted much attention owing to their promising applications.[179]

The gold cluster Au_{20} was recently discovered[17] by means of laser vaporization of a pure gold target with a helium carrier gas, analogous to the well-known preparation of C_{60}. Relativistic density functional calculations favor a tetrahedral structure for Au_{20}.

Besides the relativistic effect, aromaticity is one important factor in stabilizing the spherical structure of Au_{20}. The MO pattern of the simplest M_{20} (**60**, T_d) is $(a_1) (t_2)^3 (a_1) (t_2)^3 (e)^2$ (Figure 33). The spherical harmonic pattern of Au_{20} (T_d) is similar to that in other deltahedral clusters exhibiting spherical aromaticity.[180]

Most recently, the icosahedral "golden" fullerene Au_{32} (**61**) was computed as the first all-gold fullerenic species.[181] The structure of Au_{32} consists of a network of triangles with icosahedral symmetry making a nearly perfect rhombic triacontahedron. Each atom binds to either five or six neighboring gold atoms. Thus, this polyhedron computed for Au_{32} is the dual of the C_{60} polyhedron. With 32 σ-electrons, Au_{32} satisfies the Hirsch $2(N + 1)^2$ electron-counting rule for spherical aromaticity and is highly aromatic, as indicated by the record NICS value at its center of −100 ppm as compared with the corresponding NICS value of −36 ppm for T_d Au_{20}.

Most recently, an alternative icosahedral golden fullerene cage, Au_{42} (**62**), was computed.[182] However, unlike the known gold fullerene Au_{32}, Au_{42} (I_h) does not satisfy the $2(N + 1)^2$ rule, and its rather positive NICS value at the cage center indicates its antiaromatic character. Not surprisingly, Au_{42} is higher in energy than the most stable compact-filling isomers and definitely not a global minimum; moreover, Au_{42} has a small HOMO−LUMO gap (0.4 and 0.9 eV, respectively, at BP86/Lanl2DZ and B3LYP/Lanl2DZ levels of theory). Nevertheless, Au_{42} was suggested to serve as a golden cage to accommodate interstitial atoms or molecules or as structural motifs to build highly stable core−shell nanoclusters.

7. Closing Remarks

In recent years, immense efforts have been made to develop various criteria of aromaticity and these criteria have been used not only to explain the available experimental observations but also to design novel aromatics. Extending the aromaticity concept from the classical 2D annulenes to spherical (or, more generally, 3D) species opens a new exciting

research area as summarized in this review with particular emphasis on fullerenes and *closo*-boranes. In the next few years, many new interesting spherical molecules related to those discussed in this review will undoubtedly be synthesized and isolated. For example, various heterofullerenes can now be separated from complex mixtures using modern high-performance liquid chromatography methods.

The world of 3D aromaticity is considerably more complicated than the "flatland" of the more familiar 2D planar aromatics of which benzene is the prototype. For this reason, the understanding of spherical aromaticity is still far from complete. Thus, Bühl and Hirsch in their 2001 review conclude that "qualitative relations between spherical aromaticity and electronic structure are only beginning to emerge."[31] The $2(N + 1)^2$ rule proposed by Hirsch in 2000[95] serves as the 3D analogue of the $4N + 2$ rule for planar systems proposed by Hückel in 1931.[30] The $2(N + 1)^2$ rule has so far been successfully applied to design various novel aromatic compounds. However, deviations from this simple rule are found indicating the need for further refinement.

8. Acknowledgments

9. References

(1) (a) Minkin, V. I.; Glukhovtsev, M. N.; Simkin, B. Y. *Aromaticity and Antiaromaticity. Electronic and Structural Aspects*; John Wiley & Sons: New York, 1994. (b) Schleyer, P. v. R.; Jiao, H. *Pure Appl. Chem.* **1996**, *68*, 209. (c) Krygowski, T. M.; Cyrañski, M. K.; Czarnocki, Z.; Hafelinger, G.; Katritzky, A. R. *Tetrahedron* **2000**, *56*, 1783. (d) *Chem. Rev.* **2001**, *5*.
(2) (a) Bird, C. W. *Tetrahedron* **1998**, *54*, 10179. (b) Katritzky, A. R.; Jug, K.; Oniciu, D. C. *Chem. Rev.* **2001**, *101*, 1421. (c) Balaban, A. T.; Oniciu, D. C.; Katritzky, A. R. *Chem. Rev.* **2004**, *104*, 2777.
(3) Fokin, A. A.; Jiao, H.; Schleyer, P. v. R. *J. Am. Chem. Soc.* **1998**, *120*, 9364.
(4) Jiao, H.; Schleyer, P. v. R. *J. Phys. Org. Chem.* **1998**, *11*, 655.
(5) (a) Mauksch, M.; Gogonea, V.; Jiao, H.; Schleyer, P. v. R. *Angew. Chem., Int. Ed.* **1998**, *37*, 2395. (b) Ajami, D.; Oeckler, O.; Simon, A.; Herges, R. *Nature* **2003**, *426*, 819.
(6) Gogonea, V.; Schleyer, P. v. R.; Schreiner, P. R. *Angew. Chem., Int. Ed.* **1998**, *37*, 1945.
(7) (a) Masui, H. *Coord. Chem. Rev.* **2001**, *219*, 957. (b) Bleek, J. R. *Chem. Rev.* **2001**, *101*, 1205.
(8) Schleyer, P. v. R.; Kiran, B.; Simion, D. V.; Sorensen, T. S. *J. Am. Chem. Soc.* **2000**, *122*, 510.
(9) Urnezius, E.; Brennessel, W. W.; Cramer, C. J.; Ellis, J. E.; Schleyer, P. v. R. *Science* **2002**, *295*, 832.
(10) (a) King, R. B. *Chem. Rev.* **2001**, *101*, 1119. (b) Zhai, H. J.; Kiran, B.; Li, J.; Wang, L. S. *Nat. Mater.* **2003**, *2*, 827.
(11) See the review on aromaticity of metal clusters: Boldyrev, A. I.; Wang, L. S. *Chem. Rev.* **2005**, *10*, 3716.
(12) Kuznetsov, A. E.; Corbett, J. D.; Wang, L. S.; Boldyrev, A. I. *Angew. Chem., Int. Ed.* **2001**, *40*, 3369.
(13) Li, X. W.; Pennington, W. T.; Robinson, G. H. *J. Am. Chem. Soc.* **1995**, *117*, 7578.
(14) Li, X.; Kuznetsov, A. E.; Zhang, H. F.; Boldyrev, A. I.; Wang, L. S. *Science* **2001**, *291*, 859.
(15) Jiao, H.; Schleyer, P. v. R.; Glukhovtsev, M. N. *J. Phys. Chem.* **1996**, *100*, 12299.
(16) Tanaka, H.; Neukermans, S.; Janssens, E.; Silverans, R. E.; Lievens, P. *J. Am. Chem. Soc.* **2003**, *125*, 2862.
(17) (a) Li, J.; Li, X.; Zhai, H. J.; Wang, L. S. *Science* **2003**, *299*, 864. (b) Zhang, H. F.; Stender, M.; Zhang, R.; Wang, C.; Li, J.; Wang, L. S. *J. Phys. Chem. B* **2004**, *108*, 12259.
(18) Kuznetsov, A. E.; Birch, K. A.; Boldyrev, A. I.; Li, X.; Zhai, H. J.; Wang, L. S. *Science* **2003**, *300*, 622.
(19) Chen, Z.; Corminboeuf, C.; Heine, T.; Bohmann, J.; Schleyer, P. v. R. *J. Am. Chem. Soc.* **2003**, *125*, 13930.
(20) Kroto, H. W.; Heath, J. R.; O'Brien, S. C.; Curl, R. F.; Smalley, R. E. *Nature* **1985**, *318*, 162.
(21) Iijima, S. *Nature* **1991**, *354*, 56.
(22) Lipscomb, W. N. *J. Am. Chem. Soc.* **1959**, *81*, 5833.
(23) Yoneda, S. *Coll. Eng., Kyoto Univ., Kyoto, Japan. Kagaku Sosetsu* **1977**, *15*, 36.
(24) Aihara, J. *J. Am. Chem. Soc.* **1978**, *100*, 3339.
(25) Zdetsis, A. D. *Phys. Rev. A* **2001**, *64*, 23202.
(26) Schleyer, P. v. R.; Maerker, C.; Dransfeld, A.; Jiao, H.; Hommes, N. J. R.v. E. *J. Am. Chem. Soc.* **1996**, *118*, 6317.
(27) See reviews: (a) Chen, Z.; Heine, T.; Schleyer, P. v. R.; Sundholmd, D. In *Calculation of NMR and EPR Parameters. Theory and Applications*; Kaupp, M., Bühl, M., Malkin, V. G., Eds.; Wiley-VCH: New York, 2004; p 395. (b) Chen, Z.; Wannere, C. S.; Corminboeuf, C.; Puchta, R.; Schleyer, P. v. R. *Chem. Rev.* **2005**, *10*, 3842.
(28) For examples: (a) Saunders, M.; Jiménez-Vázquez, H. A.; Cross, R. J.; Mroczkowski, S.; Freedberg, D. L.; Anet, F. A. L. *Nature* **1994**, *367*, 256. (b) Saunders, M.; Cross, R. J.; Jiménez-Vázquez, H. A.; Shimshi, R.; Khong, A. *Science* **1996**, *271*, 1693. (c) Saunders, M.; Jimenez-Vazquez, H. A.; Cross, R. J.; Billups, W. E.; Gesenberg, C.; Gonzalez, A.; Luo, W.; Haddon, R. C.; Diederich, F.; Herrmann, A. *J. Am. Chem. Soc.* **1995**, *117*, 9305. (d) Shabtai, E.; Weitz, A.; Haddon, R. C.; Hoffman, R. E.; Rabinovitz, M.; Khong, A.; Cross, R. J.; Saunders, M.; Cheng, P. C.; Scott, L. T. *J. Am. Chem. Soc.* **1998**, *120*, 6389. (e) Wang, G. W.; Saunders, M.; Khong, A.; Cross, R. J. *J. Am. Chem. Soc.* **2000**, *122*, 3216.
(29) For example: (a) Bühl, M.; Thiel, W.; Jiao, H.; Schleyer, P. v. R.; Saunders, M.; Anet, F. A. L. *J. Am. Chem. Soc.* **1994**, *116*, 6005. (b) Bühl, M. *Chem. Eur. J.* **1998**, *4*, 734. (c) Chen, Z.; Cioslowski, J.; Rao, N.; Moncrieff, D.; Bühl, M.; Hirsch, A.; Thiel, W. *Theor. Chem. Acc.* **2001**, *106*, 364.
(30) (a) Hückel, E. *Z. Phys.* **1931**, *70*, 204. (b) Hückel, E. *Z. Phys.* **1931**, *72*, 310. (c) Hückel, E. *Z. Phys.* **1932**, *76*, 628.
(31) Bühl, M.; Hirsch, A. *Chem. Rev.* **2001**, *101*, 1153.
(32) Most likely, the term spherical aromaticity was first used by Aihara in the paper titled "Spherical aromaticity of buckminsterfullerene"; see Aihara, J.; Hosoya, H. *Bull. Chem. Soc. Jpn.* **1988**, *61*, 2657. However, in 1986, Haddon et al. suggested that "C_{60} may be the first example of a spherical aromatic molecule"; see Haddon, R. C.; Brus, L. E.; Raghavachari, K. *Chem. Phys. Lett.* **1986**, *125*, 459. Much earlier, "3D aromaticity", close in meaning to spherical aromaticity, was used by Aihara in a paper titled "Three-dimensional aromaticity of polyhedral boranes"; see Aihara, J. *J. Am. Chem. Soc.* **1978**, *100*, 3339. However, as early as 1970, Osawa proposed the structure of C_{60} but used superaromatic to rationalize its aromatic character; see Osawa, E. *Kagaku (Chemistry)* **1970**, *25*, 854 (in Japanese); for its English version, see Osawa, E. *Philos. Trans. R. Soc. London A* **1993**, *343*, 1.
(33) Reiher, M.; Hirsch, A. *Chem. Eur. J.* **2003**, *9*, 5442.
(34) Mizerogi, N.; Kiuchi, M.; Tanaka, K.; Sekine, R.; Aihara, J.-i. *Chem. Phys. Lett.* **2003**, *378*, 598.
(35) Byerly, W. E. *An Elementary Treatise on Fourier's Series and Spherical, Cylindrical, and Ellipsoidal Harmonics*; Dover: New York, 1959 (reprinted from the 1893 edition published by Ginn and Company).
(36) King, R. B. *J. Chem. Educ.* **1996**, *73*, 993.
(37) Tang, A. C.; Huang, F. Q.; Li, Q. S.; Liu, R. Z. *Chem. Phys. Lett.* **1994**, *227*, 579.
(38) King, R. B. *Mol. Phys.* **1997**, *92*, 293.
(39) King, R. B. *J. Phys. Chem.* **1997**, *101*, 4653.
(40) Stone, A. J. *Inorg. Chem.* **1981**, *20*, 563.
(41) Stone, A. J. *Mol. Phys.* **1980**, *41*, 1339.
(42) Stone, A. J.; Alderton, M. J. *Inorg. Chem.* **1982**, *21*, 2297.
(43) Stone, A. J. *Polyhedron* **1984**, *3*, 1299.
(44) Bicerano, J.; Marynick, D. S.; Lipscomb, W. N. *Inorg. Chem.* **1978**, *17*, 3443.
(45) (a) Fowler, P. W. *Polyhedron* **1985**, *4*, 2051. (b) Fowler, P. W.; Lazzeretti, P.; Zanasi, R. *Inorg. Chem.* **1988**, *27*, 1298.
(46) Fowler, P. W.; Lazzeretti, P.; Zanasi, R. *Inorg. Chem.* **1988**, *27*, 1298.
(47) Battye, R. A.; Sutcliffe, P. M. *Phys. Rev. Lett.* **1997**, *79*, 363.
(48) Battye, R. A.; Sutcliffe, P. M. *Phys. Lett. B* **1998**, *416*, 385.
(49) Battye, R. A.; Sutcliffe, P. M. *Phys. Rev. Lett.* **2001**, *86*, 3989.
(50) King, R. B. *Collect. Czech. Chem. Commun.* **2002**, *67*, 751.
(51) King, R. B. *Chem. Phys. Lett.* **2001**, *338*, 237.
(52) King, R. B. In *Topology in Chemistry*; Rouvray, D. H., King, R. B., Eds.; Horwood Publishing Ltd.: Chichester, 2002; p 361.
(53) Khong, A.; Jiménez-Vázquez, H. A.; Saunders, M.; Cross, R. J.; Laskin, J.; Peres, T.; Lifshitz, C.; Strongin, R.; Smith, A. B., III. *J. Am. Chem. Soc.* **1998**, *120*, 6380.

(54) Sternfeld, T.; Hoffman, R. E.; Saunders, M.; Cross, R. J.; Syamala, M. S.; Rabinovitz, M. *J. Am. Chem. Soc.* **2002**, *124*, 8786.

(55) Bühl, M.; Wüllen, C. V. *Chem. Phys. Lett.* **1995**, *247*, 63.

(56) Sternfeld, T.; Hoffman, R. E.; Aprahamian, I.; Rabinovitz, M. *Angew. Chem., Int. Ed.* **2001**, *40*, 455.

(57) Sternfeld, T.; Hoffman, R. E.; Thilgen, C.; Diederich, F.; Rabinovitz, M. *J. Am. Chem. Soc.* **2000**, *122*, 9038.

(58) (a) Kruszewski, J.; Krygowski, T. M. *Tetrahedron Lett.* **1972**, 3839. (b) Krygowski, T. M. *J. Chem. Inf. Comput. Sci.* **1993**, *33*, 70. (c) Krygowski, T. M.; Cyranski, M. K. *Tetrahedron* **1996**, *52*, 1713. (d) See review: Krygowski, T. M.; Cyranski, M. K. *Chem. Rev.* **2001**, *101*, 1385.

(59) Poater, J.; Fradera, X.; Duran, M.; Solá, M. *Chem. Eur. J.* **2003**, *9*, 400.

(60) Poater, J.; Fradera, X.; Duran, M.; Solá, M. *Chem. Eur. J.* **2003**, *9*, 1113.

(61) Poater, J.; Duran, M.; Solá, M. *Int. J. Quantum Chem.* **2004**, *98*, 361.

(62) (a) Smith, A. B., III; Strongin, R. M.; Brard, L.; Furst, G. T.; Romanow, W. J.; Owens, K. G.; King, R. C. *J. Am. Chem. Soc.* **1993**, *115*, 5829. (b) Suzuki, T.; Li, Q.; Khemani, K. C.; Wudl, F. *J. Am. Chem. Soc.* **1992**, *114*, 7301. (c) Sternfeld, T.; Wudl, F.; Hummelen, K.; Weitz, A.; Haddon, R. C.; Rabinovitz, M. *Chem. Commun.* **1999**, 2411. (d) Smith, A. B., III; Strongin, R. M.; Brard, L.; Furst, G. T.; Romanow, W. J.; Owens, K. G.; Goldschmidt, R. J.; King, R. C. *J. Am. Chem. Soc.* **1995**, *117*, 5492. (e) Sternfeld, T.; Hoffman, R. E.; Thilgen, C.; Diederich, F.; Rabinovitz, M. *J. Am. Chem. Soc.* **2000**, *122*, 9038. (f) Sternfeld, T.; Thilgen, C.; Hoffman, R. E.; Heras, M. d. R. C.; Diederich, F.; Wudl, F.; Scott, L. T.; Mack, J.; Rabinovitz, M. *J. Am. Chem. Soc.* **2002**, *124*, 5734.

(63) Slayden, S. W.; Liebman, J. E. *Chem. Rev.* **2001**, *101*, 1541.

(64) Cyrański, M. K.; Howard, S. T.; Chodkiewicz, M. L. *Chem. Commun.* **2004**, 2458.

(65) Johansson, M. P.; Jusélius, J.; Sundholm, D. *Angew. Chem., Int. Ed.* **2005**, *44*, 1843.

(66) Jusélius, J.; Sundholm, D.; Gauss, J. *J. Chem. Phys.* **2004**, *121*, 3952.

(67) (a) Sun, G.; Kertesz, M. *J. Phys. Chem. A* **2001**, *105*, 5468. (b) Sun, G.; Kertesz, M. *Chem. Phys.* **2002**, *276*, 107.

(68) For example: Knupfer, M.; Knauff, O.; Golden, M. S.; Fink, J.; Bürk, M.; Fuchs, D.; Schuppler, S.; Michel, R. H.; Kappes, M. M. *Chem. Phys. Lett.* **1996**, *258*, 513.

(69) (a) Zhou, Z.; Parr, R. G.; Garst, J. F. *Tetrahedron Lett.* **1988**, *29*, 4843. (b) Zhou, Z.; Parr, R. G. *J. Am. Chem. Soc.* **1989**, *111*, 7371. (c) Zhou, Z.; Navangul, H. V. *J. Phys. Org. Chem.* **1990**, *3*, 784. (d) Zhou, Z. *J. Phys. Org. Chem.* **1995**, *8*, 103. (e) Bird, C. W. *Tetrahedron* **1997**, *53*, 3319. (f) De Proft, F.; Geerling, P. *Phys. Chem. Chem. Phys.* **2004**, *6*, 242. (g) See review: De Proft, F.; Geerling, P. *Chem. Rev.* **2001**, *101*, 1451.

(70) Fowler, P. W.; Manolopoulos, D. E. *An Atlas of Fullerenes*; Clarendon: Oxford, 1995.

(71) Sternfeld, T.; Saunders, M.; Cross, R. J.; Rabinovitz, M. *Angew. Chem., Int. Ed.* **2003**, *42*, 3136.

(72) Most are unpublished computational results by Chen, Z., Thiel, W., and Schleyer, P. v. R.

(73) (a) Haddon, R. C.; Cockayne, E.; Elser, V. *Synth. Met.* **1993**, *59*, 369. (b) Haddon, R. C.; Pasquarello, A. *Phys. Rev. B* **1994**, *50*, 16459.

(74) Reed, C. A.; Bolskar, R. B. *Chem. Rev.* **2000**, *100*, 1075 and references therein.

(75) Echegoyen, L.; Echegoyen, L. E. *Acc. Chem. Res.* **1998**, *31*, 593 and references therein.

(76) (a) Fowler, P. W.; Woolrich, J. *Chem. Phys. Lett.* **1986**, *127*, 78. (b) Saito, S.; Okada, S.; Sawada, S.; Hamada, N. *Phys. Rev. Lett.* **1995**, *75*, 685. (c) Azamar-Barrios, J. A.; Dennis, T. J. S.; Sadhukan, S.; Shinohara, H.; Scuseria, G. E.; Pénicaud, A. *J. Phys. Chem. A* **2001**, *105*, 4627.

(77) (a) Boltalina, O. V.; Sidorov, L. N.; Borshchevsky, A. Ya.; Sukhanova, E. V.; Skokan, E. V. *Rapid Commun. Mass. Spectrom.* **1993**, *7*, 1009. (b) Sidorov, L. N.; Boltalina, O. V.; Borshchevsky, A. Y. *Rapid Commun. Mass Spectrom.* **1997**, *11*, 662.

(78) (a) Boudon, C.; Gisselbrecht, J.-P.; Gross, M.; Herrmann, A.; Rüttimann, M.; Crassous, J.; Cardullo, F.; Echegoyen, L.; Diederich, F. *J. Am. Chem. Soc.* **1998**, *120*, 7860. (b) Boulas, P. L.; Jones, M. T.; Ruoff, R. S.; Lorents, D. C.; Malhorta, R.; Tse, D. S.; Kadish, K. M. *J. Phys. Chem.* **1996**, *100*, 7573.

(79) Sternfeld, T.; Thilgen, C.; Chen, Z.; Siefken, S.; Schleyer, P. v. R.; Thiel, W.; Diederich, F.; Rabinovitz, M. *J. Org. Chem.* **2003**, *68*, 4850.

(80) Schmalz, T. G.; Seitz, W. A.; Klein, D. J.; Hite, G. E. *J. Am. Chem. Soc.* **1988**, *110*, 1113.

(81) Kratschmer, W.; Lamb, L. D.; Fostiropoulos, K.; Hoffman, D. R. *Nature* **1990**, *347*, 354.

(82) Scott, L. T.; Boorum, M. M.; McMahon, B. J.; Hagen, S.; Mack, J.; Blank, J.; Wegner, H.; de Meijere, A. *Science* **2002**, *295*, 1500.

(83) Prinzbach, H.; Weller, A.; Landenberger, P.; Wahl, F.; Worth, J.; Scott, L. T.; Gelmont, M.; Olevano, D.; Issendorff, B, v. *Nature* **2000**, *407*, 60.

(84) (a) Wang, Z.; Ke, X.; Zhu, Z.; Zhu, F.; Ruan, M.; Chen, H.; Huang, R.; Zheng, L. *Phys. Lett. A* **2001**, *280*, 351. (b) Chen, Z.; Heine, T.; Jiao, H.; Hirsch, A.; Thiel, W.; Schleyer, P. v. R. *Chem. Eur. J.* **2004**, *10*, 963.

(85) Piskoti, C.; Yarger, J.; Zettl, A. *Nature* **1998**, *393*, 771.

(86) (a) Koshio, A.; Inakuma, M.; Sugai, T.; Shinohara, H. *J. Am. Chem. Soc.* **2000**, *122*, 398. (b) Koshio, A.; Inakuma, M.; Wang, Z. W.; Sugia, T.; Shinohara, H. *J. Phys. Chem. B* **2000**, *104*, 7908.

(87) Kroto, H. W. *Nature* **1987**, *329*, 529.

(88) For example: Kietzmann, H.; Rochow, R.; Ganteför, G.; Eberhardt, W.; Vietze, K.; Seifert, G.; Fowler, P. W. *Phys. Rev. Lett.* **1998**, *81*, 5378.

(89) Gao, F.; Xie, S. Y.; Huang, R. B.; Zheng, L. S. *Chem. Commun.* **2003**, 2676.

(90) (a) Xie, S. Y.; Gao, F.; Lu, X.; Huang, R. B.; Wang, C. R.; Zhang, X.; Liu, M. L.; Deng, S. L.; Zheng, L. S. *Science* **2004**, *304*, 699. (b) Highlighted by Chen, Z. *Angew. Chem., Int. Ed.* **2004**, *43*, 4690.

(91) Lu, X.; Chen, Z.; Thiel, W.; Schleyer, P. v. R.; Huang, R. B.; Zheng, L. S. *J. Am. Chem. Soc.* **2004**, *126*, 14871.

(92) Lu, X.; Chen, Z. *Chem. Rev.* **2005**, *10*, 3643.

(93) (a) Chen, Z.; Thiel, W. *Chem. Phys. Lett.* **2003**, *367*, 15. (b) Chen, Z.; Jiao, H.; Bühl, M.; Hirsch, A.; Thiel, W. *Theor. Chem. Acc.* **2001**, *106*, 352.

(94) Sun, G.; Nicklaus, M. C.; Xie, R. H. *J. Phys. Chem. A* **2005**, *109*, 4617.

(95) Hirsch, A.; Chen, Z.; Jiao, H. *Angew. Chem., Int. Ed.* **2000**, *39*, 3915.

(96) Chen, Z.; Jiao, H.; Hirsch, A.; Thiel, W. *J. Mol. Mod.* **2001**, *7*, 161.

(97) Bühl, M. *Z. Anorg. Allg. Chem.* **2000**, *626*, 332.

(98) Wu, H. S.; Xu, X. H.; Jiao, H. *J. Phys. Chem. A* **2004**, *108*, 3813.

(99) Diaz-Tendero, S.; Martin, F.; Alcami, M. *ChemPhysChem* **2005**, *6*, 92.

(100) (a) Tenne, R. *Adv. Mater.* **1995**, *7*, 965. (b) Hummelen, J. C.; Bellavia-Lund, C.; Wudl, F. *Top Curr. Chem.* **1999**, *199*, 93. (c) Hirsch, A.; Nuber, B. *Acc. Chem. Res.* **1999**, *32*, 795. (d) Reuther, U.; Hirsch, A. *Carbon* **2000**, *38*, 1539.

(101) Xie, R. H.; Bryant, G. W.; Zhao, J.; Smith, V. H., Jr.; Di Carlo, A.; Pecchia, A. *Phys. Rev. Lett.* **2003**, *90*, 206602.

(102) (a) Hummelen, J. C.; Knight, B.; Pavlovich, J.; Gonzalez, R.; Wudl, F. *Science* **1995**, *269*, 1554. (b) Nuber, B.; Hirsch, A. *Chem Commun* **1996**, 1421. (c) Tagmatarchis, N.; Okada, K.; Tomiyama, T.; Shinohara, H. *Synlett* **2000**, 1761.

(103) Hauke, F.; Hirsch, A. *Tetrahedron* **2001**, *57*, 3697.

(104) Kim, K. C.; Hauke, F.; Hirsch, A.; Boyd, P. D. W.; Carter, E.; Armstrong, R. S.; Lay, P. A.; Reed, C. A. *J. Am. Chem. Soc.* **2003**, *125*, 4024.

(105) Zou, Y. J.; Zhang, X. W.; Li, Y. L.; Wang, B.; Yan, H.; Cui, J. Z.; Liu, L. M.; Da, D. A. *J. Mater. Sci.* **2002**, *37*, 1043.

(106) Hultman, I.; Stafström, S.; Czigány, Z.; Neidhardt, J.; Hellgren, N.; Brunell, I. F.; Suenaga, K.; Colliex, C. *Phys. Rev. Lett.* **2001**, *87*, 225503.

(107) (a) Guo, T.; Jin, C.; Smalley, R. E. *J. Phys. Chem.* **1991**, *95*, 4948. (b) Muhr, H. J.; Nesper, R.; Schnyder, B.; Kötz, R. *Chem. Phys. Lett.* **1996**, *249*, 399. (c) Cao, B.; Zhou, X.; Shi, Z.; Jin, Z.; Gu, Z.; Xiao, H.; Wang, J. *Acta Phys. Chim. Sin.* **1997**, *13*, 204. (d) Cao, B.; Zhou, X.; Shi, Z.; Gu, Z.; Xiao, H.; Wang, J. *Fullerene Sci. Technol.* **1998**, *6*, 639. (e) Nakamura, T.; Ishikawa, K.; Yamamoto, K.; Ohana, T.; Fujiwara, S.; Koga, Y. *Phys. Chem. Phys.* **1999**, *1*, 2631.

(108) (a) Pradeep, T.; Vijayakrishnan, V.; Santra, A. K.; Rao, C. N. R. *J. Phys. Chem.* **1991**, *95*, 10564. (b) Averdung, J.; Luftmann, H.; Schlachter, I.; Mattay, J. *Tetrahedron* **1995**, *51*, 6977. (c) Lamparth, I.; Nuber, B.; Schick, G.; Skiebe, A.; Grösser, T.; Hirsch, A. *Angew. Chem. Int. Ed. Engl.* **1995**, *34*, 2257. (d) Yu, R.; Zhan, M.; Cheng, D.; Yang, S.; Liu, Z.; Zheng, L. *J. Phys. Chem.* **1995**, *99*, 1818. (e) Bellavia-Lund, C.; Wudl, F. *J. Am. Chem. Soc.* **1997**, *119*, 943. (f) Ying, Z. C.; Hettich, R. L.; Compton, R. N.; Haufler, R. E. *J. Phys. B: At., Mol. Opt. Phys.* **1996**, *29*, 4935. (g) Clipston, N. L.; Brown, T.; Vasil'ev, Y. Y.; Barrow, M. P.; Herzschuh, R.; Reuther, U.; Hirsch, A.; Drewello, T. *J. Phys. Chem. A* **2000**, *104*, 9171.

(109) (a) Piechota, J.; Byszewski, P.; Jablonski, R.; Antonova, K. *Fullerene Sci. Technol.* **1996**, *4*, 491. (b) Antonova, K.; Byshewski, P.; Zhizhin, G.; Piechota, J.; Marhevka, M. *Microchim. Acta* (*Suppl.*) **1997**, *14*, 271. (c) Nakamura, T.; Ishikawa, K.; Goto, A.; Ishihara, M.; Ohana, T.; Koga, Y. *Diamond Relat. Mater.* **2001**, *10*, 1228. (d) Nakamura, T.; Ishikawa, K.; Goto, A.; Ishihara, M.; Ohana, T.; Koga, Y. *Diamond Relat. Mater.* **2003**, *12*, 1908.

(110) (a) Stry, J. J.; Garvey, J. F. *Chem. Phys. Lett.* **1995**, *243*, 199. (b) Christian, J. F.; Wan, Z.; Anderson, S. L. *Chem. Phys. Lett.* **1992**, *199*, 373.

(111) (a) Kimura, T.; Sugai, T.; Shinohara, H. *Chem. Phys. Lett.* **1996**, *256*, 269. (b) Fye, J. L.; Jarrold, M. *J. Phys. Chem.* **1997**, *101*,

1836. (c) Pellarin, M.; Ray, C.; Melinon, P.; Lerme, J.; Vialle, J. L.; Keghelian, P.; Perez, A.; Broyer, M. *Chem. Phys. Lett.* **1997**, *277*, 96. (d) Ray, C.; Pellarin, M.; Lerme, J.; Vialle, J. L.; Broyer, M.; Blasé, X.; Melinon, P.; Keghelian, P.; Perez, A. *Phys. Rev. Lett.* **1998**, *80*, 5365. (e) Cao, B.; Zhou, X.; Shi, Z.; Gu, Z.; Xiao, H.; Wang, J. *Chem. Lett.* **1998**, 735. (f) Pellarin, M.; Ray, C.; Lerme, J.; Vialle, J. L.; Broyer, M.; Blasé, X.; Keghelian, P.; Melinon, P.; Perez, A. *J. Chem. Phys.* **1999**, *110*, 6927. (g) Pellarin, M.; Ray, C.; Lerme, J.; Vialle, J. L.; Broyer, M.; Blasé, X.; Keghelian, P.; Melinon, P.; Perez, A. *Eur. Phys. J. D* **1999**, *9*, 49. (h) Billas, I. M. L.; Branz, W.; Malinowski, N.; Tast, F.; Heinebrodt, M.; Martin, T. P.; Massobrio, C.; Boero, M.; Parrinello, M. *Nanostruct. Mater.* **1999**, *12*, 1071. (i) Billas, I. M. L.; Tast, F.; Branz, W.; Malinowski, N.; Heinebrodt, M.; Martin, T. P.; Boero, M.; Massobrio, C.; Parrinello, M. *Eur. Phys. J. D* **1999**, *9*, 337.

(112) Ohtsuki, T.; Ohno, K.; Shina, K.; Kawazoe, Y.; Maruyama, Y.; Masumoto, K. *Phys. Rev. B* **1999**, *60*, 1531.

(113) Möschel, C.; Jansen, M. *Z. Anorg. Allg. Chem* **1999**, *625*, 175.

(114) (a) Branz, W.; Billas, I. M. L.; Malinowski, N.; Tast, F.; Heinebrodt, M.; Martin, T. P. *J. Chem. Phys.* **1998**, *109*, 3425. (b) Poblet, J. M.; Munoz, J.; Winkler, K.; Cancilla, M.; Hayashi, A.; Lebrilla, C. B.; Balch, A. L.; Winkler, K. *Chem. Commun.* **1999**, 493.

(115) Hayashi, A.; Xie, Y.; Poblet, J. M.; Campanera, J. M.; Lebrilla, C. L.; Balch, A. L. *J. Phys. Chem. A* **2004**, *108*, 2192.

(116) Kityk, I. V.; Takahira, P. *Mater. Lett.* **2004**, *58*, 1553.

(117) (a) Kurita, N.; Koboyyashi, K.; Kumabora, H.; Tago, K.; Ozawa, K. *Chem. Phys. Lett.* **1992**, *198*, 95. (b) Liu, J.; Gu, B.; Han, R. *Solid State Commun.* **1992**, *84*, 807. (c) Andreoni, W.; Gygi, F.; Parrinello, M. *Chem. Phys. Lett.* **1992**, *190*, 159. (d) Chen, F.; Singh, D.; Jansen, S. *J. Phys. Chem.* **1993**, *97*, 10958. (e) Jiang, J.; Dong, J.; Xu, Q.; Xing, D. Y. *Z. Phys. D: At. Mol. Clusters* **1996**, *37*, 341.

(118) (a) Ren, A.; Feng, J.; Tian, W.; Sun, X.; Sun, C. *Chem. J. Chin. Univ.* **1998**, *19*, 288. (b) Lu, J.; Zhang, S.; Zhang, X.; Zhao, X. *Solid State Commun.* **2001**, *118*, 247. (c) Lu, J.; Zhang, X.; Zhao, X. *Mod. Phys. Lett. B* **2000**, *14*, 23. (d) Jiao, H.; Chen, Z.; Hirsch, A.; Thiel, W. *Phys. Chem. Chem. Phys.* **2002**, *4*, 4916.

(119) (a) Chen, Z.; Ma, K.; Pan, Y.; Zhao, X.; Tang, A. *Acta Chim. Sin.* **1999**, *57*, 712. (b) Billas, I. M. L.; Massobrio, C.; Boero, M.; Parrinello, M.; Branz, W.; Tast, F.; Malinowski, N.; Heinebrodt, M.; Martin, T. P. *J. Chem. Phys.* **1999**, *111*, 6787. (c) Guirado-Lopez, R. *Phys. Rev. B* **2002**, *65*, 165421. (d) Lu, J.; Luo, Y.; Huang, Y.; Zhang, X.; Zhao, X. *Solid State Commun.* **2001**, *118*, 309. (e) Cheng, W. D.; Wu, D. S.; Zhang, H.; Chen, J. T.; Wang, H. X. *Phys. Rev. B* **2002**, *66*, 085422. (f) Fuks, I.; Kityk, I. V.; Kasperczyk, J.; Berdowski, J.; Schirmer, I. *Chem. Phys. Lett.* **2002**, *353*, 7.

(120) Lu, J.; Zhou, Y.; Luo, Y.; Huang, Y.; Zhang, X.; Zhao, X. *Mol. Phys.* **2002**, *99*, 1203.

(121) (a) Ding, C.; Yang, J.; Cui, X.; Chan, C. T. *J. Chem. Phys.* **1999**, *111*, 8481. (b) Billas, I. M. L.; Massobrio, C.; Boero, M.; Parrinello, M.; Branz, W.; Tast, F.; Malinowski, N.; Heinebrodt, M.; Martin, T. P. *Comput. Mater. Sci.* **2000**, *17*, 191.

(122) Ding, C.; Yang, J.; Han, R.; Wang, K. *Phys. Rev. A* **2001**, *64*, 43201.

(123) (a) Kurita, N.; Kobayashi, K.; Kumahora, H.; Tago, K. *Fullerene Sci. Technol.* **1993**, *1*, 319. (b) Esfarjani, K.; Ohmo, K.; Kawazoe, Y. *Phys. Rev. B* **1994**, *50*, 17830. (c) Esfarjani, K.; Ohno, K.; Kawazoe, Y.; Gu, B. *Solid State Commun.* **1996**, *97*, 539. (d) Esfarjani, K.; Ohno, K.; Kawazoe, Y. *Surf. Rev. Lett.* **1996**, *3*, 747. (e) Piechota, J.; Byszewski, P. *Z. Phys. Chem.* **1997**, *200*, 147. (f) Chen, Z.; Ma, K.; Zhao, H.; Pan, Y.; Zhao, X.; Tang, A.; Feng, J. *J. Mol. Struct. (THEOCHEM)* **1999**, *466*, 127. (g) Batirev, I. G.; Lee, K. H.; Leiro, J. A. *J. Phys. Chem. Solids* **2000**, *61*, 695.

(124) Ren, A.; Feng, J.; Sun, X.; Li, W.; Tian, W.; Sun, C.; Zheng, X.; Zerner, M. C. *Int. J. Quantum Chem.* **2000**, *78*, 422.

(125) Chistyakov, A. L.; Stankevich, I. V. *Inorg. Chim. Acta* **1998**, *280*, 219.

(126) Bühl, M. *Chem. Phys. Lett.* **1995**, *242*, 580.

(127) (a) Chen, Z.; Ma, K.; Pan, Y.; Zhao, X.; Tang, A.; Feng, J. *J. Chem. Soc., Faraday Trans.* **1998**, *94*, 2269. (b) Chen, Z.; Ma, K.; Pan, Y.; Zhao, X.; Tang, A. *Chem. J. Chin. Univ.* **1999**, *20*, 1921.

(128) Chen, Z.; Ma, K.; Pan, Y.; Zhao, X.; Tang, A. *Can. J. Chem.* **1999**, *77*, 291.

(129) Chen, Z.; Zhao, X.; Tang, A. *J. Phys. Chem. A* **1999**, *103*, 10961.

(130) (a) Chen, Z.; Reuther, U.; Hirsch, A.; Thiel, W. *J. Phys. Chem. A* **2001**, *105*, 8105. (b) Chen, Z.; Wang, G.; Zhao, X.; Tang, A. *J. Mol. Model.* **2002**, *8*, 223.

(131) (a) Pattanayak, J.; Kar, T.; Scheiner, S. *J. Phys. Chem. A* **2001**, *105*, 8376. (b) Pattanayak, J.; Kar, T.; Scheiner, S. *J. Phys. Chem. A* **2002**, *106*, 2970.

(132) Pattanayak, J.; Kar, T.; Scheiner, S. *J. Phys. Chem. A* **2003**, *107*, 4056.

(133) Chen, Z.; Ma, K.; Pan, Y.; Zhao, X.; Tang, A. *J. Mol. Struct. (THEOCHEM)* **1999**, *490*, 61.

(134) Schultz, D.; Droppa, R., Jr.; Alvarez, F.; dos Santos, M. C. *Phys. Rev. Lett.* **2003**, *90*, 015501.

(135) Sun, G.; Xie, R.; Nicklaus, M. C. *Los Alamos National Laboratory, Preprint Archive, Condensed Matter* **2003**, *1*; arXiv: cond-mat/0301494. http://xxx.lanl.gov/pdf/cond-mat/0301494.

(136) Alder, R. W.; Harvey, J. N.; Schleyer, P. v. R.; Moran, D. *Org. Lett.* **2001**, *3*, 3233.

(137) (a) Yang, Z.; Xu, X.; Wang, G.; Shang, Z.; Cai, Z.; Pan, Y.; Zhao, X. *THEOCHEM* **2002**, *618*, 191. (b) Yang, X.; Wang, G.; Shang, Z.; Pan, Y.; Cai, Z.; Zhao, X. *Phys. Chem. Chem. Phys.* **2002**, *4*, 2546. (c) Xu, X.; Xing, Y.; Shang, Z.; Wang, G.; Cai, Z.; Pan, Y.; Zhao, X. *Chem. Phys.* **2003**, *287*, 317.

(138) Hummelen, J. C.; Bellavia-Lund, C.; Wudl, F. *Top. Curr. Chem.* **1999**, *199*, 93.

(139) Balasubramanian, K. *J. Phys. Chem.* **1993**, *97*, 6990.

(140) Stafström, S.; Hultman, L.; Hellgren, N. *Chem. Phys. Lett.* **2001**, *340*, 227.

(141) For example: (a) Xie, R. H.; Bryant, G. W.; Smith, V. H., Jr. *Chem. Phys. Lett.* **2003**, *368*, 486. (b) Xie, R. H.; Bryant, G. W.; Jensen, L.; Zhao, J.; Smith, V. H., Jr. *J. Chem. Phys.* **2003**, *118*, 8621. (c) Xie, R. H.; Bryant, G. W.; Smith, V. H., Jr. *Phys. Rev. B* **2003**, *67*, 155404. (d) Schimmelpfennig, B.; Ågren, H.; Csillag, S. *Synth. Met.* **2003**, *132*, 265.

(142) Manaa, M. R.; Sprehn, D. W.; Ichord, H. A. *J. Am. Chem. Soc.* **2002**, *124*, 13990.

(143) Chen, Z.; Jiao, H.; Moran, D.; Hirsch, A.; Thiel, W.; Schleyer, P. v. R. *J. Phys. Org. Chem.* **2003**, *16*, 726.

(144) Viglione, R. G.; Zanasi, R. *Phys. Chem. Chem. Phys.* **2004**, *6*, 295.

(145) (a) Emanuele, E.; Negri, F.; Orlandi, G. *Chem. Phys.* **2004**, *306*, 315. (b) Brena, B.; Luo, Y. *J. Chem. Phys.* **2003**, *119*, 7139. (c) Balasubramanian, K. *Chem. Phys. Lett.* **2004**, *391*, 69. (d) Balasubramanian, K. *Chem. Phys. Lett.* **2004**, *391*, 64. (e) Gu, F. L.; Chen, Z.; Jiao, H.; Tian, W. Q.; Aoki, Y.; Thiel, W.; Schleyer, P. v. R. *Phys. Chem. Chem. Phys.* **2004**, *6*, 4566.

(146) Manaa, R. M.; Ichord, H. A.; Sprehn, D. W. *Chem. Phys. Lett.* **2003**, *378*, 449.

(147) King, R. B. *Chem. Rev.* **2001**, *101*, 1119.

(148) Schleyer, P. v. R.; Subramanian, G.; Dransfeld, A. *J. Am. Chem. Soc.* **1996**, *118*, 9988 and literatures therein.

(149) (a) Schleyer, P. v. R.; Najafian, K. *Inorg. Chem.* **1998**, *37*, 3454. (b) Schleyer, P. v. R.; Najafian, K.; Mebel, A. M. *Inorg. Chem.* **1998**, *37*, 6765. (c) Najafian, K.; Schleyer, P. v. R.; Tidwell, T. T. *Inorg. Chem.* **2003**, *42*, 4190.

(150) (a) Jemmis, E. D.; Schleyer, P. v. R. *J. Am. Chem. Soc.* **1982**, *104*, 4781. (b) Jemmis, E. D. *J. Am. Chem. Soc.* **1982**, *104*, 7071.

(151) Pantazis, D. A.; McGrady, J. E.; Lynam, J. M.; Russell, C. A. Green M. *Dalton Trans* **2004**, *14*, 2080.

(152) Hirsch, A.; Chen, Z.; Jiao, H. *Angew. Chem, Int. Ed.* **2001**, *40*, 2834.

(153) (a) Corminboeuf, C.; Heine, T.; Weber, J. *Phys. Chem. Chem. Phys.* **2003**, *5*, 246. (b) *J. Phys. Chem. A* **2003**, *107*, 6470. (c) Corminboeuf, C.; Heine, T.; Seifert, G.; Schleyer, P. v. R.; Weber, J. *Phem. Chem. Chem. Phys.* **2004**, *6*, 273.

(154) Double aromaticity for planar systems, see Schleyer, P. v. R.; Jiao, H.; Glukhovtsev, M. N.; Chandrasekhar, J.; Kraka, E. Double aromaticity in the 3,5-dehydrophenyl cation and in cyclo-[6]carbon, *J. Am. Chem. Soc.* **1994**, *116*, 10129.

(155) For some recent reviews, see Corbett, J. D. *Angew. Chem., Int. Ed.* **2000**, *39*, 670.

(156) (a) Wade, K. *Chem. Commun.* **1971**, 792. (b) Wade, K. *Adv. Inorg. Chem. Radiochem.* **1976**, *18*, 1. (c) Wade, K. *Inorg. Nucl. Chem. Lett.* **1972**, *8*, 563.

(157) Kuznetsov, A. N.; Kloo, L.; Lindsjö, M.; Rosdahl, J.; Stoll, H. *Chem. Eur. J.* **2001**, 7, 2821.

(158) King, R. B.; Heine, T.; Corminboeuf, C.; Schleyer, P. v. R. *J Am. Chem. Soc.* **2004**, *126*, 430.

(159) (a) Neukermans, S.; Janssens, E.; Chen, Z.; Silverans, R. E.; Schleyer, P. v. E.; Lievens, P. *Phys. Rev. Lett.* **2004**, *92*, 163401. (b) Chen, Z.; Neukermans, S.; Wang, X.; Janssens, E.; Silverans, R. E.; King, R. B.; Schleyer, P. v. R.; Lievens, P. Manuscript to be submitted.

(160) (a) Esenturk, E. N.; Fettinger, J.; Lam, Y. F.; Eichhorn, B. *Angew. Chem., Int. Ed.* **2004**, *43*, 2132. (b) Esenturk, E. N.; Fettinger, J.; Eichhorn, B. *Chem. Comm.* **2005**, 247.

(161) (a) Fässler, T. F.; Hoffmann, S. D. *Angew. Chem., Int. Ed.* **2004**, *43*, 6242. (b) Janssens, E.; Neukermans, S.; Lievens, P. *Curr. Opin. Solid State Mater. Sci.* **2004**, *8*, 185.

(162) King, R. B.; Schleyer, P. v. R. Theory and concepts in main-group cluster chemistry. In *Molecular Clusters of the Main Group Elements*; Driess, M., Nöth, H., Eds.; Wiley-VCH: New York, **2004**; pp 1−33.

(163) Hönle, W.; Grin, Y.; Burckhardt, A.; Wedig, U.; Schultheiss, M.; von Schnering, H. G.; Kallner, R.; Binder, H. *J. Solid State Chem.* **1997**, *133*, 59.

(164) Mennekes, T.; Paetzold, P.; Boese, R. B. *Angew. Chem., Int. Ed.* **1991**, *30*, 173.

(165) The latest review on homoaromaticity: Williams, R. V. *Chem. Rev.* **2001**, *101*, 1185 and references therein.

(166) Chen, Z.; Jiao, H.; Hirsch, A.; Schleyer, P. v. R. *Angew. Chem., Int. Ed.* **2002**, *41*, 4309.
(167) Chen, A.; Hirsch, A.; Nagase, S.; Thiel, W.; Schleyer, P. v. R. *J. Am. Chem. Soc.* **2003**, *125*, 15507.
(168) Bremer, M.; Schleyer, P. v. R.; Schoetz, K.; Kausch, M.; Schindler, M. *Angew. Chem., Int. Ed. Engl.* **1987**, *26*, 761.
(169) (a) Chan, M. S. W.; Arnold, D. R. *Can. J. Chem.* **1997**, *75*, 192. (b) Fokin, A. A.; Kiran, B.; Bremer, M.; Yang, X.; Jiao, H.; Schleyer, P. v. R.; Schreiner, P. R. *Chem. Eur. J.* **2000**, *6*, 1615. (c) Olah, G. A.; Rasul, G.; Prakash, G. K. S. *J. Org. Chem.* **2000**, *65*, 5956.
(170) Recent experiment, see Hiura, H.; Miyazaki, T.; Kanayama, T. *Phys. Rev. Lett.* **2001**, *86*, 1733. Recent theoretical studies, see (a) Kumar, V.; Kawazoe, Y. *Phys. Rev. Lett.* **2001**, *87*, 45503. (b) Kumar, V.; Kawazoe, Y. *Appl. Phys. Lett.* **2002**, *80*, 859. (c) Khanna, S. N.; Rao, B. K.; Jena, P. *Phys. Rev. Lett.* **2002**, *89*, 16803. (d) Kumar, V.; Kawazoe, Y. *Phys. Rev. Lett.* **2002**, *88*, 235504. (e) Kumar, V.; Majumder, C.; Kawazoe, Y.; *Chem. Phys. Lett.* **2002**, *363*, 319. (f) Lu, J.; Nagase, S. *Phys. Rev. Lett.* **2003**, *90*, 115506. (g) Lu, J.; Nagase, S. *Chem. Phys. Lett.* **2003**, 372. (h) Kumar, V.; Kawazoe, Y. *Phys. Rev. Lett.* **2003**, *90*, 55502. (i) Kumar, V. *Bull. Mater. Sci.* **2003**, *26*, 109. (j) Miyazaki, T.; Hiura, H.; Kanayama, T. *Phys. Rev. B.* **2002**, *66*, 121403. (k) Sun, Q.; Wang, Q.; Briere, T. M.; Kumar, V.; Kawazoe, Y.; Jena, P. *Phys. Rev. B* **2002**, *65*, 235417. (l) Sun, Q.; Wang, Q.; Jena, P.; Rao, B. K.; Kawazoe, Y. *Phys. Rev. Lett.* **2003**, *90*, 135503.
(171) (a) Dewar, M. J. S. *J. Am. Chem. Soc.* **1984**, *106*, 669. (b) Cremer, D.; Gauss, J. *J. Am. Chem. Soc.* **1986**, *108*, 7467.
(172) Exner, K.; Schleyer, P. v. R. *J. Phys. Chem. A* **2001**, *105*, 3407.
(173) Schleyer, P. v. R.; Puhlhofer, F. *Org. Lett.* **2002**, *4*, 2873.
(174) Moran, D.; Manoharan, M.; Heine, T.; Schleyer, P. v. R. *Org. Lett.* **2003**, *5*, 23 and references therein.
(175) Havenith, R. W. A.; Fowler, P. W.; Steiner, E. *Chem. Phys. Lett.* **2003**, *371*, 276.
(176) Alexandrova, A. N.; Boldyrev, A. I. *J. Phys. Chem. A* **2003**, *107*, 554−560.
(177) (a) Jursic, B. S. *J. Mol. Struct. (THEOCHEM)* **1999**, *490*, 81. (b) Jursic, B. S. *Int. J. Quantum Chem.* **1998**, *69*, 679. (c) Jursic, B. S. *Int. J. Quantum Chem.* **1999**, *73*, 451. (d) Jursic, B. S. *J. Mol. Struct. (THEOCHEM)* **2000**, *498*, 159.
(178) Recent reviews, see (a) Pyykkö, P. *Angew. Chem. Int. Ed.* **2002**, *41*, 3573. (b) Schwerdtfeger, P. *Heteroat. Chem.* **2002**, *13*, 578. (c) Pyykkö, P. *Angew. Chem., Int. Ed.* **2004**, *43*, 4412.
(179) Schwerdtfeger, P. *Angew. Chem., Int. Ed.* **2003**, *42*, 1892.
(180) King, R. B.; Chen, Z.; Schleyer, P. v. R. *Inorg. Chem.* **2004**, *43*, 4564.
(181) Johansson, M. P.; Sundholm, D.; Vaara, J. *Angew. Chem., Int. Ed.* **2004**, *43*, 2678.
(182) Gao, Y.; Zeng, X. C. *J. Am. Chem. Soc.* **2005**, *127*, 3698.